APPLICATION OF LUBRICANTS IN THE AH-64D HELICOPTER GEARBOXES FOR
IMPROVEMENT OF CONDITION-BASED MAINTENANCE PRACTICES

by

Kareem Moustafa Gouda

Bachelor of Science
Higher Technological Institute, 2006

Master of Engineering
University of South Carolina, 2014

Submitted in Partial Fulfillment of the Requirements

for the Degree of Doctor of Philosophy in

Mechanical Engineering

College of Engineering and Computing

University of South Carolina

2015

Accepted by:

Abdel-Moez E. Bayoumi, Major Professor

Jeff Morehouse, Committee Member

Joshua Tarbutton, Committee Member

Richard Robinson, Committee Member

Lacy Ford, Vice Provost and Dean of Graduate Studies

Dedication

To my wonderful parents, Moustafa and Omaima. I am blessed with an unparalleled foundation built by these two individuals. Thank you for implanting within me the value of hard work and for motivating me to pursue my academic goal. Without you, this work wouldn't have been possible

Acknowledgments

It is a pleasure to acknowledge the people who helped me to complete this degree.

Words cannot express gratitude to my advisor, Dr.Abdel-Moez E. Bayoumi, whom I'm indebted to for his support, dedication, guidance, and being a mentor throughout my graduate school years. I am very fortunate for the opportunity to work with a caliber like himself. I will be forever thankful for his commitment and time to his students. I would also like to thank Drs.Joshua Tarbutton, Jeff Morehouse, and Richard Robinson for serving on my dissertation committee. I would like to extend my gratitude in particular to Dr.Tarbutton for his teaching approach in graduate courses of signal processing basics that helped in completing this work.

I sincerely thank my brother, Ameen, for his understanding and support. I would like to thank the undergraduate students, and fellow graduate students who work at the condition-based maintenance research (CBM) center for their help in the experiments needed for this dissertation. The long hours of testing and changing hardware could not have been accomplished without this team effort. I would also like to thank Mr.Alex Cao, Research Engineer at CBM for his insightful technical comments and Dr.Mostafa M. Elag for his writing tips that helped in this work. Finally, I wish to thank Dr.Mohsen Nikkhoo, and Mr.Steve Marcous for their significant contribution on the third chapter of this dissertation.

I acknowledge the South Carolina Army National Guarad, AMCOM-AED and the US Army Aviation and Missile Command for funding the CBM research center for more than a decade.

ABSTRACT

This dissertation aims to develop new condition-based maintenance (CBM) tools for increasing performance of Apache helicopter drivetrain gearboxes, through lubrication and signal analysis. An extensive consumer of CBM is the Apache helicopter that involves testing critical components to demonstrate reliability and performance, measured through data-driven condition indicators (CIs). These indicators provide vital information about the condition of a mechanical component and are derived from onboard sensors using signal processing methods. A challenge known among researchers in the Apache community is leakage of grease lubricant from drivetrain gearboxes with performance of some CIs unachieved. Although extensive maintenance operations are used in the field to minimize this effect by ground inspections, failure of grease lubricant still occurs due to heavy loads. Based on this motivation, oil nanofluids are presented here as a new lubricant approach for the intermediate gearbox (IGB) of the Apache helicopter. Furthermore, a signal-based approach utilizing wavelet analysis is adapted to develop a new CI. The goal of this work can be achieved through addressing the following research studies.

The first study qualifies the improved thermophysical properties of two turbine jet oil nanofluid samples and eight Mobil Aviation Gear Lubricant (AGL) oil nanofluid samples with different particle concentrations and chemical compositions. Numerous fluid properties such as thermal conductivity, dynamic viscosity, and viscosity index are measured using off-line experimental tools. Based on the experimental results, four AGL oils with graphite nanoparticles have displayed excellent thermophysical properties and are used as prospective lubricants for mechanical testing in the IGB.

Then, this study investigates key nanoparticle mechanisms to provide a better understanding of the nanofluids through developing a new nanofluid model using the effective medium approach. It is found that experimental results closely agree with theoretical predictions (eg. $R^2 =0.988$). Experimental data and existing models from the literature are also used to validate the accuracy of the proposed model. Results help in improving model predictions and conclude that the flake-like morphology of the nanoparticles as well as its dynamic behavior in the fluid contribute significantly to increasing thermophysical properties.

The second study investigates the impact of nanolubricants in an actual IGB. Two Apache helicopter drivetrain test stands at the CBM research center, University of South Carolina are presented to optimize performance of the lubricant. First, preliminary testing is performed on a drivetrain test stand with no load being applied. The four selected samples: 1%, 1.5%, 2% and 2.5% graphite-based AGL additives, against a control AGL sample are tested as gearbox lubricants. Preliminary condition monitoring results show that the 2% sample demonstrates optimum gearbox performance with the lowest temperature and vibration responses, compared to all tested lubricants. This improvement can be attributed to the capability of the nanolubricant in obtaining an effective fluid film between gear surfaces, absorbing load, heat, and friction. The highest concentration of 2.5% graphite additive fails to make an impact and yields the worst gearbox performance due to possible rheological changes in oil. Second, full-load mechanical testing on the tail rotor drivetrain test stand is demonstrated. The 2% nanofluid sample, along with base oil, are tested in the IGB. Vibration results based on spectral and wavelet analysis demonstrate promising attributes of this new lubrication approach. A key finding from this study is the improvement of temperature-based CI due to the incorporation of nanolubricants with approximately $40°F$-$50°F$ lower response, compared to that of base AGL.

The third study presents a new CI using wavelet analysis for the purpose of fault detection in an AH-64 gearbox. Historically, vibration-based CIs from employed component monitoring equipment are derived from both temporal and spectral domain analysis. However, these indicators failed to accurately capture high order correlations for the gearbox study addressed. An improved approach is necessary to overcome limitations of traditional vibrational monitoring techniques. The proposed condition indicator is derived from the Morlet continuous wavelet transform. The power spectra obtained from the wavelet transform coefficients at a certain scale or frequency are added together and then are normalised to one composite signal, denoted by a numeric index. Concepts of the wavelet index (WI) are discussed. This index is applied using real-world vibration data from a tail rotor gearbox with an output seal leak as part of CBM practices. Results demonstrate potential of the proposed WI to more effectively capture the fault when compared to gearbox CIs. Statistical analysis is demonstrated using a wavelet denoising thresholding approach to reduce redundancy in the data. Predicted results yielded significant improvement in WI with less variability. Finally, a statistical test with an 85% confidence interval is applied on different wavelet power distribution samples. WI results from these samples are found to be statistically valid.

Research results described in this dissertation establish a step forward towards the development of new CBM tools in system-based applications. This work ends with conclusions and recommendations for future research.

Table of Contents

LIST OF TABLES

LIST OF FIGURES

xiv

CHAPTER 1

INTRODUCTION

1.1 MAINTENANCE STRATEGIES

Mechanical systems are subject to different failure mechanisms, whether it is in the form of excessive vibration, fatigue, friction, or thermal shock. In many applications where the design of a system cannot be fully optimized to minimize or prevent all failures, it is necessary to take robust maintenance actions so that the system can be in a functional state. There exists a wide variety of maintenance methods that can be applied on a system, which encompass activities of testing, inspections, measurements, and component replacements(Mobley, 2002).

In his work, Mobley proposed three essential approaches that remain to date the backbone of the maintenance strategy: run-to-failure, preventive maintenance, and predictive maintenance, which is known as condition-based maintenance or CBM (Figure 1.1). Run-to-failure is a reactive form of maintenance and is the most traditional maintenance method where machines simply run until failure. The unexpected breakdown of a component until failure can lead to longer downtime for major repairs. Preventive maintenance is a scheduled approach where actions on a system are taken on regular basis; usage-based or time-based. An oil change in a car that would take place every 3 months or 3000 miles is a good example of preventive maintenance. Despite the ability to reduce catastrophic failures by planning ahead in advance for a given system, the major disadvantage of preventive maintenance can be costly, especially if excessive and redundant maintenance actions are taken.
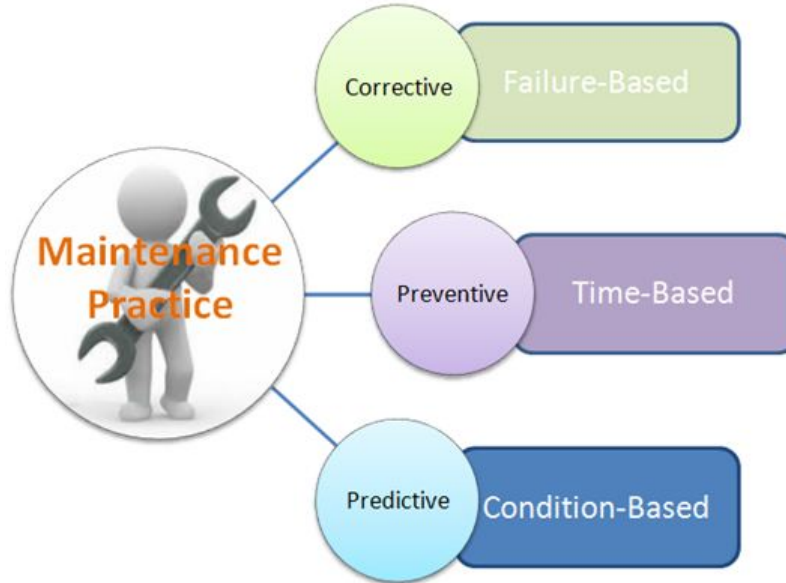
Figure 1.1: Different maintenance strategies

CBM is a state of the art proactive form of maintenance that is implemented in the field and employs advanced component monitoring equipment to detect signs of failures and enable targeted maintenance based upon evidence. The predominant benefit of CBM is the cost-savings it allows over reactive maintenance by maximizing the component life, minimizing risk and coast. A toolbox that uses different qualitative and quantitative data from different sources for the accurate monitoring of components and its diagnostics.

Applying CBM is a powerful approach in pointing out faults that are almost always pertained to decisions affecting the characteristics of the system, which can include structure, material, and performance: dynamics, vibrations, gear pitting, corrosion and tribology. Fortunately, the US Army has successfully implemented a CBM program on different aircrafts where advanced condition monitoring equipment are employed, known as health and usage monitoring system (HUMS). HUMS is the diagnostic on-board system installed on numerous military aircraft platforms including, but not limited to, AH-64 Apache and the UH-60 Black hawk helicopters (Dempsey et al., 2008).

1.2 Fundamentals of Condition Monitoring

Condition monitoring is the foundational element of CBM. There are numerous condition monitoring methods and tools used to diagnose faults in mechanical systems(Randall, 2011). The most common techniques include: vibration analysis, oil analysis, acoustic emission and thermography. Oil analysis is an offline method used to monitor debris particles within a lubricant, which can be connected to the condition of a gear or bearing. Acoustic emission is used to detect cracks in structures or shock pulses from rotating machinery. Thermography is used to detect mechanical or thermal defects in electrical equipment like generators or misaligned couplings. To date, vibration analysis is still the basic component used in condition monitoring of rotating machinery because of its important dynamic information needed for feature extraction.(Girondin et al., 2013).

All rotating machinery produce different vibration signatures that carry important feature information. If a rotating component is operating with imbalance conditions, reaction forces are produced, and this vibrational energy is transferred to the non-rotating part of the system. For example, a misaligned gearbox that produces vibrations due to reaction forces leads to the development of free vibrations in the structures that are excited as a result of energy dissipation from the forced vibration. The former are governed by the fundamental properties of mass, stiffness, and damping, which tend to be constant regardless of the speed of the system.

There are different ways to measure vibrations that include: displacement, velocity or acceleration in a three-dimensional axis or six degrees of freedom. Most often, the frequency bandwidth of the system under study is the key point to choose the appropriate methods of measurement. For rotating machinery, accelerometers are the commonly used tools to monitor vibration due to their high frequency range. Furthermore, the structural asymmetry of machines makes the vibration signals in the axial, radial and vertical directions to be significantly different. Where possible,

3

a three-dimensional sensor can be used to pick up these different signals, however, in practice only two axis sensors are likely to be used that are mounted perpendicularly to each other in both radial and axial directions of the rotating component. Despite the inherent complexity of the vibration monitoring tool as previously mentioned, it is still the common condition monitoring method and the most used practice in any CBM industry, compared to other techniques. Vibration is produced by different sources in the system, such as the applied load or torque of the rotating part to the deflections of the surrounding structures. The produced vibration signature can be challenging with the analysis and interpretation to isolate the problem, especially when it comes to a mechanical system with vibration and noise from different sources.

A key step in condition monitoring is feature extraction using vibration analysis methods. In CBM for rotorcraft, vibration signals are collected using onboard sensors,attached to critical components. The signals are then processed using different signal processing algorithms to calculate features known as condition indicators (CIs). These CIs are developed from controlled ground field data. They are model-based and sensitive to faults, as they attempt to extract information about a particular physical process or event, such as shock impulses, gear meshing, friction or temperature. A single component can have multiple CIs; a single fault can affect multiple CIs and multiple faults can affect a single CI. Numerous CI functions are applied to various domains to produce normalized single-valued metrics, which are compared to well-known established thresholds such as 'healthy', 'caution', and 'exceed' created from the benchmark testing on healthy and faulted components. Maintainers rely on these values in their decision-making process.

Raw vibration data is typically sampled at some sampling period, and thus it is known as time-series or time-domain. These signals are quit complex, as the extracted features or CIs like peak-to-peak, root-mean square (RMS) kurtosis or skewness do not provide all important information on the condition of the part which is rotat-

ing and only provides a quick estimation of changes in the overall signal stemming from imminent failure (Figure 1.2). Therefore, it is often necessary to map the data into another domain, which is more relevant to condition monitoring applications being sought, and this is typically done by transformation into the frequency-domain through a Discrete Fourier transform using the Fast Fourier Transform (FFT) algorithm (Figure 1.3). The analysis in this domain is more suitable for the diagnostics of rotating components, because metrics extracted can be directly related to the frequency of the rotating component. The detailed mathematical description from Lebold et al. discuss the classical signal processing techniques to compute these CIs that include: raw data preprocessing, time synchronous averaging, filtering, and spectral analysis. (Lebold et al., 2000).
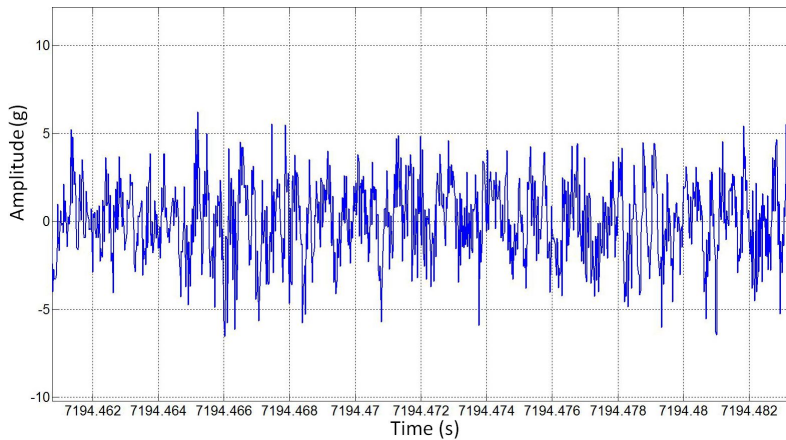
Figure 1.2: Example of vibration signal in time-domain

1.3 CBM Testing at the University of South Carolina

Over more than a decade, the University of South Carolina (USC) has been collaborating with the Army Engineering Directorate (AED) through the South Carolina Army National Guard. All of the efforts expanded into a fully matured CBM research center test stand at USC, which hosts actual military aircraft hardware. The goal of this project is to achieve CBM objectives within the US Army through monitoring
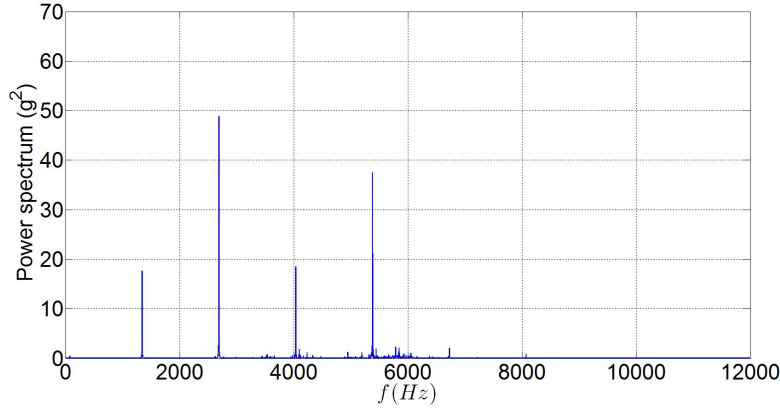
Figure 1.3: Example of vibration signal in frequency-domain

critical aircraft components and to provide a scientific understanding of the AH-64D helicopter component conditions, as they relate to vibration signals and other qualitative maintenance data. This scientific knowledge is achieved through component testing, which is a key concept to achieve an integrated CBM.

Testing is an important component of a CBM program to validate certain concepts that are unsafe to study on actual aircrafts. As CBM involves gathering experimental data from mechanical systems on test stands using different sensors,it is powerful for diagnostic purposes in its ability to validate or improve exiting CIs and even produce new ones based on vibration, temperature or friction.

The CBM research center has a full-scale AH-64 tail rotor drivetrain (TRDT) and main rotor swashplate test sands, which are designed to emulate flight regimes as on an actual helicopter (Figure 1.4). The TRDT is a constant-speed and dynamic-loading power transmission system, starting from the main transmission tail rotor take-off to the tail rotor swashplate (TRSP) assembly. Furthermore, the stand is configured with an 800 hp motor, which is the prime mover of the drivetrain controlled by a variable frequency drive that spins the shafts at 101% of the operating speed (4863 RPM) . An absorption motor similar to the prime mover creates the braking torque required and acts as a regenerative system to save energy. These two motors are also capable of exceeding 150% of the actual drivetrain loading. The components

or articles subject to testing on the drivetrain include: forward hanger bearing (FHB), aft. hanger bearing (AHB), intermediate gearbox (IGB), tail rotor gearbox (TGB) and the TRSP. The drivetrain consists of a total of four shafts, which are purposely misaligned within the acceptable safe limits of 2 degrees for radial loading on the bearings. Three of the shafts have the FHB, AHB and IGB components pass through them. The fourth shaft is on a vertical stabilizer between both IGB and TGB. The configuration, instrumentation, stiffness, and structure comply with military standards(Nooli, 2011).

Figure 1.4: TRDT/MRSP in actual AH-64D (Top) and TRDT/MRSP test stands at USC (Bottom)

The TRDT employs two data acquisition systems (DAQs) for the collection of vibration,temperature and other data from the drive-train components. The first is known as Modernized Signal Processing Unit (MSPU): a vibration acquisition tool , which is a major component used in HUMS (Figure 1.5). The MSPU is optimized to acquire data from sensors and to generate the CIs from the vibration-based methods.

The data is processed through filtering, preprocessing, ensemble averaging, spectral analysis, and other convolution functions built in MSPU. It is a vital link between information gathered from a lab setting and on helicopters in the field.

The second is a National Instruments (NI) DAQ that operates in parallel to MSPU and it collects raw vibration data. The purpose of the NI-DAQ is to help in providing complete information on the health of the gearbox and to validate test stand results with MSPU-CI data of the actual airframe. NI-DAQ runs with a custom written code using LABVIEW software and is responsible for controlling the test stand operations that include speed and load profiles. Detailed data description used in this dissertation with sensor locations are elaborated in chapter 5.

Figure 1.5: Example of MSPU used on AH-64 (Intelligent Automation Corporation: VMEP Crew Member Information Guide

1.4 LUBRICATION AND TRIBOLOGICAL CHARACTERISTICS IN ROTATING MACHINERY

Lubricants play a key role in mechanical components. The primary function of lubricants is to provide a fluid film layer between moving components for minimizing friction, wear and heat generation. A secondary function is to remove this generated heat through a heat transfer process. If the fluid film is broken due to applied load, friction can be one of the main contributors that lead to lubricant failure and

leakage (Bartelmus, 2014). There are different lubrication and friction mechanisms in machine elements that include: hydrodynamic lubrication, elasto-hydrodynamic lubrication (EHL), and boundary lubrication (Figure 1.6). For gears and bearings applications, the EHL is the dominant lubrication mechanism considered (Zhu et al., 2013; Hamrock et al., 1999).
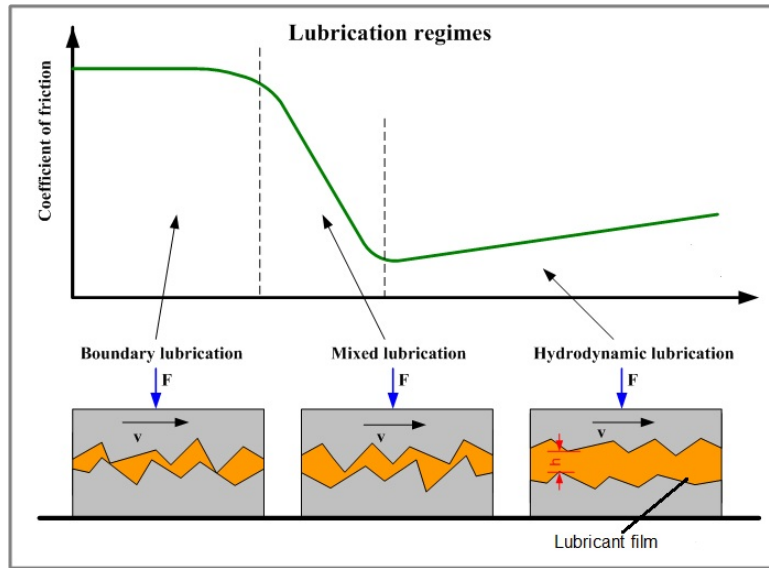
Figure 1.6: Lubrication regimes between sliding contacts

The early work of Dyson, Crook, and Archard investigated the tribological effect of different lubricants in the EHL regime between sliding contacts (Archard, 1957; Crook, 1961; Dyson, 1970). All the efforts established the significance of a direct empirical correlation between friction and thermophysical properties of the lubricant.

During gearbox operation in the EHL regime, the applied load is carried by pressure within the fluid lubricant film between the meshing gears. The bulk thermophysical properties of the lubricant become crucial, where friction is generated due to shearing with dependence on the thermophysical characteristics of the lubricant film. This means that an adequately selected lubricant for rotating machinery is an important factor that can significantly increase the performance of the system. Despite not being a primary tool for determining the condition of machinery directly,

advancements in lubrication through improving tribological, thermal, and rheological properties is a key step for CBM, where machinery diagnosis can be improved from the results of lubrication.

In this dissertation, the focus is limited to lubricant studies and applications for both IGB and TGB that constitute critical components of the AH-64D helicopter.

1.5 MOTIVATION

Both IGB and TGB have an important function of transmitting torque to the blades and are supported with a set of duplex and roller bearings. These gearboxes are grease lubricated that is commercially known as NS-4405-FG. It is most commonly used in rotating machinery components that involve heavy loads. Typically, grease is a shear-thinning fluid, and its main advantage over oil is its ability to act as a sealant, minimizing leakage effects, and at the same time acts as a lubricant when exposed to shearing(Toms and Toms, 2008).

Unfortunately, on the AH-64 helicopter, grease leaking from drivetrain gearboxes is a pressing challenge, represented in different forms of faults, such as leaks from an IGB breather port (Figure 1.7). These naturally-occurring field faults have negatively impacted the availability of the aircraft and present a serious inconvenience to maintenance crews. To date, grease leakage is the leading cause of drivetrain gearbox failure that requires extensive maintenance procedures and part removals (Abdel Bayoumi and McVay, 2012). Where these ongoing efforts are successful to minimize leakage, the main problem over time is the failure of grease lubricant due to the applied load.

Increases in peak temperatures can be attained instantaneously between different regions of the gearbox, without being detected by the aircraft. Grease loses its ability as an efficient lubricant and does not maintain a stable film between meshing gears and other components, and after a long period of operation, excessive vibration, wear

and friction can be experienced, leading to gearbox failure. Ongoing research efforts in this area are vital to increase performance of the gearbox lubricant, having more efficient CIs, so that the aircraft can operate in a normal and safe manner.
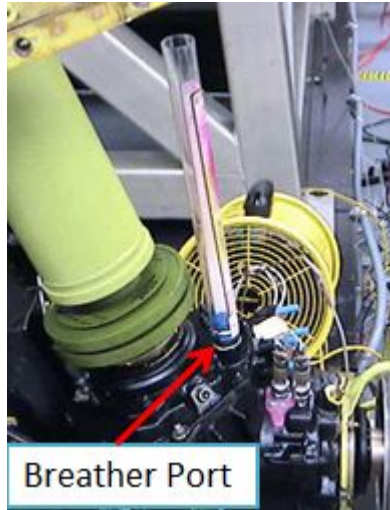
Figure 1.7: Grease leaks from IGB breather port

Numerous grease lubricant studies have been conducted at CBM. Goodman et al. performed a 500 hrs TGB grease lubrication experiment on three different gearboxes for the purpose of demonstrating its performance under seeded fault conditions (Goodman et al., 2009). A previously unknown grease movement between the two compartments of the gearbox was a major discovery. During testing, lubricant and temperature issues began to rise that led to over-heating above the specified maximum operational temperature limit of the gearbox. Furthermore, different vibration-based CIs were unsuccessful in detecting a fault in the gearbox. One major conclusion from the study was that changes in the lubricant properties affected vibration responses of the TGB. Another grease performance study was investigated in the IGB (Goodman, 2011). During the course of the experiment, an unexpected change of gearbox over-temperature occurred and the test stand was shutdown. A physical investigation of the IGB components through a tear down analysis was performed,where there was no indication of actual damage. It was theorized that the reason for this heat generation

was not due to mechanical phenomena such as friction or wear, but rather due to the chemical degradation of the grease lubricant.

Oil is a Newtonian fluid; viscosity is independent of shear rate and is still desired for high speed machinery applications for its ability to act as both a lubricant and coolant. Furthermore, it has long been discussed among AED community, the necessity to switch to oil instead of grease as a lubricant in the AH-64 drivetrain gearboxes. An IGB study was investigated using Mobil aviation gear lubricant (AGL) oil as its lubricant (Abdel Bayoumi and McVay, 2012). The main purpose of this experiment was to test the gearbox with AGL and to compare its performance with a conventional grease lubricated IGB as baseline. Oil was found to show promise with lower operating temperature and better cooling capabilities than grease, however, vibration results were inconclusive with no obvious differences between both lubricant types.

Therefore, as previously mentioned , it is crucial to improve the existing conditions of lubricant that would lead to better CI performance in drivetrain gearboxes. This dissertation picks up from previous work performed at CBM and attempts to close the loop of poor lubrication performance in gearboxes. Nanofluids or nanolubricants is presented as a new approach for a potential lubricant in the AH-64D gearbox. Furthermore, an advanced signal processing tool based on wavelet analysis is adapted to investigate the impact of different lubricants on CI performance. In chapter 2, a detailed literature review of these techniques is introduced.

Advantages of using nanofluids include:

- Improvement of thermophysical properties of the lubricant.

- Improvement of tribological characteristics with less metal-to-metal contact between sliding surfaces.

- Improvement of heat transfer characteristics.

Advantages of using wavelet analysis is extracting transient characteristics from vibration signals that are buried in noise. Unfortunately, the classical signal processing methods deployed on the helicopter inherently assume a distribution of stationary signals that don't allow transient characteristic extraction from vibration signals. Several signal processing methods, such as time-frequency and wavelets are capable of extracting transient characteristics. These transients may appear in the form of impulses as high frequency harmonics, produced if a rotating component develops a fault and have to be detected. The use of a signal processing tool in the helicopter is necessary to overcome these challenges to improve CI performance during lubrication conditions.

Motivated by the advantages mentioned above, the overarching goal of this dissertation is to leverage new approaches in a system-based application for better gearbox performance that may be deployed as CBM tools to extend time between overhauls.

1.6 Research Objectives

The following research objectives are addressed:

- Investigation of prospective aircraft oil nanolubricants for IGB using off-line analysis by measuring important thermophysical properties such as thermal conductivity and viscosity.

- Testing nanolubricants in an actual IGB and investigating the dynamic responses obtained.

- Optimization of nanofluids as a new lubrication approach for the commercial readiness in a real-life helicopter gearbox.

- Proposing a new CI based on wavelet analysis for Apache drivetrain gearboxes, applied to different lubrication conditions

- Developing accurate diagnostic information from machinery lubrication conditions, leading to a simple-to-use wavelet tool for CBM applications.

1.7 Organization of The Dissertation

The remaining of this dissertation is organized as follows. In chapter 2, I introduce a literature review of the subjects of nanofluids and wavelets, addressing the basics of experimental and theoretical investigations of nanofluids, as well as, adaptation of different signal processing techniques, and the advantage of using wavelets as a tool in the addressed application. This will facilitate an understanding for the following chapters that encompass the outcomes of nanolubricant optimization in the gearbox and the development of a signal processing tool as a new CI based on wavelet analysis. Furthermore, this chapter discusses the most common deployed CI algorithms used for gearbox diagnostics.

In chapter 3, a comprehensive experimental and theoretical investigation of different aircraft nanolubricant oils are studied as candidates for the IGB. Different off-line analysis tools are utilized that include a transient method for thermal conductivity(K) measurement, capillary tube viscometer for viscosity index (VI) measurement, and rheometer for dynamic viscosity (μ) measurement through different ranges of shear-rate effects. Then, a nanofluid model is proposed using the effective approach for a fundamental understanding of the dynamic behavior of NP interactions in the oil.

In chapter 4, wavelet analysis is presented as a possible new tool in a system-based application. This chapter discusses the detailed mathematical theory of deriving a new wavelet index for gearbox feature extraction. Moreover, a wavelet denoising approach based on thresholding is presented to improve wavelet results. Then, a statistical test based on the wavelet power and gaussian white noise sampling distributions are applied with an 85% confidence level, to point out actual wavelet features

representing the system. To illustrate effectiveness of this wavelet approach, application of wavelet index is demonstrated using IGB and TGB vibration data, presented in chapters 5 and 6.

In chapter 5, a proof-of-concept study is demonstrated to experimentally investigate the impact of nanolubricants on the IGB. Different system dynamics, such as, temperature and vibration are investigated to represent key performance characteristics for CI improvements. Also, wavelet index is applied on IGB to investigate the impact of nanolubricants on vibration responses, compared to base oil responses.

In chapter 6, the proposed wavelet index is presented as a new CI for a TGB during lubrication starvation. It is compared to the classical deployed MSPU CIs and is found to detect failure of gear wear more effectively. Overall, this index advances CI performance by capturing more information from high frequencies, without the need of adding more sensors to the component. The chapter ends with statistical analysis for feature selection on wavelet results. First, a wavelet denoising method based on thresholding on different observations of gearbox data is undertaken. Wavelet results illustrate excellent denoising attributes. Finally, a statistical test using an established null hypothesis is applied on the wavelet index. Results on tested samples are statistically valid and have succeeded to distinguish real wavelet properties from noise using an 85% confidence interval.

Summary, conclusions and recommendations of the dissertation are presented in chapter 7.

Chapter 2

Background

This chapter starts with a detailed mathematical description of the most common used CI algorithms for the deployed Apache gearbox. This is followed by a literature review for the approaches proposed as CBM candidates. Sections 2.1 and 3.3 were previously summarized in (Gouda et al., 2015).

2.1 Gearbox Condition Indicators

As briefly mentioned in chapter 1, CIs refer to vibration due to mechanical behavior. This section presents a theoretical background of the most common MSPU deployed CIs for the addressed gearbox that include: RMS, energy ratio (ER), zero-order figure of merit (FM0), and sideband level factor (SLF) (Grabill et al., 2002; Večeř et al., 2005).

Threshold limits for the CI algorithms are listed in Table 2.1. These limits are set based on engineering judgment and statistical analysis of available data from both the fleet and ground tests. The majority of the CIs are set subjectively high, and still hold true to date, until enough fault cases from the aircraft are collected by which to realistically set them. Then, the limits would be lowered based on its field data vs. the fleet, which have not yet been fully optimized.

RMS is a good indicator in tracking the overall noise level and is a measure of the power content in the signal. RMS is given by:

$$RMS(x_n) = \sqrt{\frac{1}{N} \sum_{n=1}^{n} x_n^2} \qquad (2.1)$$

where x_n is the data series of length N.

The FM0 is defined as the peak-to-peak of the time signal average (TSA) normalized by the sum of gear mesh frequency and its harmonics (Figure 2.1):

$$FM0 = \frac{max(x) - min(x)}{\sum\limits_{i=1}^{n} A(f_i)} \tag{2.2}$$

where x is the TSA signal and $A(f_i)$ is the sum of amplitudes of the i-th harmonic of the GMF.
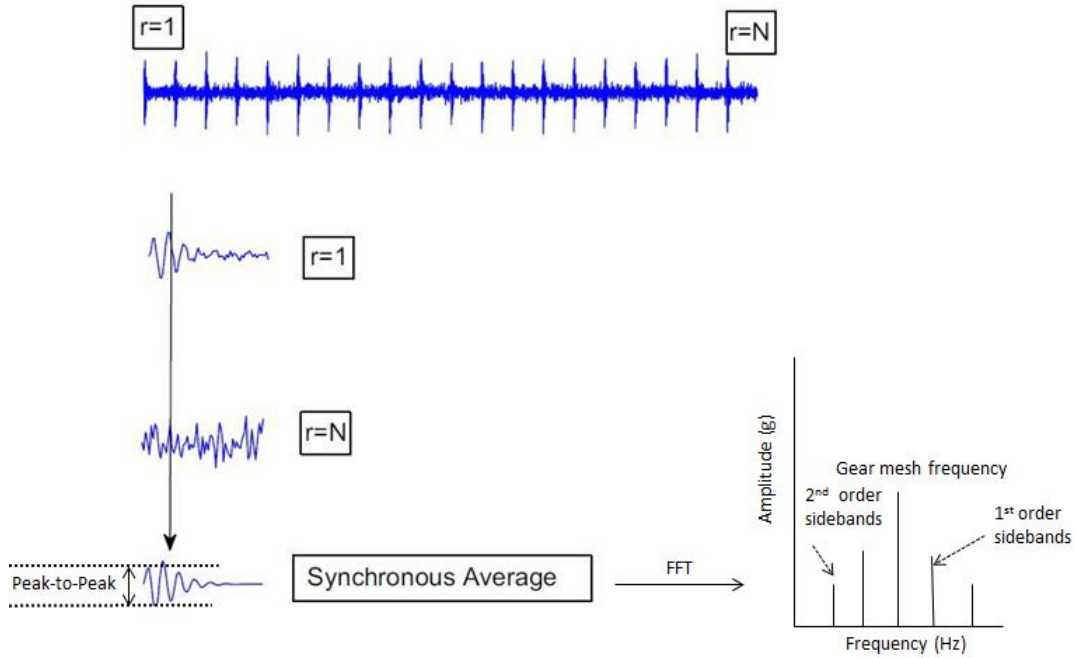
Figure 2.1: Schematic example of TSA and gearbox FFT

FM0 is a robust condition indicator, which is sensitive to major faults in gear meshes such as tooth breakage and uniform wear (Lebold et al., 2000).In case of uniform wear, the peak-to-peak does not change appreciably, but the meshing frequencies decrease and the energy is redistributed from the gear mesh frequency to the modulating sidebands. This results in increase of FM0 values in which the meshing surface is affected and degrades significantly.

Regular, difference and and residual signal CIs

The regular signal (r) represents the difference between the original signal (x) and the energies of only the primary meshing components with the first order sidebands included.

$$r = F^{-1}[A(x)_{sh} + A(x)_g + A(x)_{sb}] \tag{2.3}$$

where A is the FFT amplitude and the subscripts sh, g, sb are the shaft, gear and sidebands respectively and F^{-1} is the inverse Fourier transform.

The difference signal (d) is defined as the difference between the original signal (x) and energies of all regular meshing components (r) that include the shaft frequency, gear mesh frequency and its harmonics. While the residual signal (s) is the difference between the original signal and the energies of only the primary meshing components with the first order sidebands included. In summary, the difference signal is the same as the residual signal, excluding all first order sidebands of the primary meshing components.

$$x(d) = x - r \tag{2.4}$$

$$s = x - F^{-1}[A(x)_{sh} + A(x)_g] \tag{2.5}$$

The RMS of the difference signal x (d) and x(s) can then be computed . It is important to state that the RMS of the original signal and the RMS of the residual signal are labelled as diagnostic algorithm 1 (DA1)and diagnostic algorithm 2 (DA2), respectively in the MSPU.

$$RMS(x_d) = \sqrt{\frac{1}{N}\sum_{n=1}^{n} X_d^2} \tag{2.6}$$

$$RMS(x_r) = \sqrt{\frac{1}{N}\sum_{n=1}^{n} X_s^2} \tag{2.7}$$

ER is a CI that detects heavy uniform wear and is defined as the RMS of the difference signal normalized by the RMS of the regular signal (Večeř et al., 2005).

$$ER = \frac{RMS(d)}{RMS(r)} \tag{2.8}$$

For a gearbox in healthy condition, the majority of the vibrational energy is located at the gear mesh frequency (or regular signal). However, as wear develops energy is redistributed and transferred to the difference signal.

SLF is defined in equation [2.9] as the ratio between the first order sidebands of the gear mesh frequency and the RMS of the average signal. SLF is a coarse indicator that is sensitive to tooth damage in gear (Zakrajsek, 1989).

$$SLF = \frac{A(x_{sb})^{1,-1} + A(x_{sb})^{1,+1}}{RMS(x_n)} \tag{2.9}$$

In probability and statistics, Kurtosis is a measure of peak width in a distribution and is mathematically defined as follows:

$$K = \frac{1}{N} \sum_{i=1}^{N} (x_i - x_a)^4 \tag{2.10}$$

where x_i is the original TSA signal and x_a is the mean of the signal.

As a metric, it can be sensitive to major peaks in the data. However, as previously discussed with time-domain metrics, it might not be very accurate. So, a normalized kurtosis (FM4)is derived instead.

FM4 is a CI that was developed to overcome some of the limitations of the FM0, it is sensitive to localized faults in gear teeth, such as cracks or spalling. Mathematically, it is defined as the absolute kurtosis of the difference signal normalized by the square of variance of the difference signal.

$$FM4 = \frac{AK(d)}{[\sigma^2]^2} \tag{2.11}$$

where $AK(d)$ is the fourth statistical moment or the absolute kurtosis.

Table 2.1: Threshold levels of some condition indicator algorithms implemented in MSPU

Algorithm Name	Caution Limit	Exceedance Limit
FM0	100	200
FM4	5	8
DA1	100	200
DA2	100	200
ER	100	200
SLF	5	8

2.2 Nanofluids

Nanofluids have captured huge attention in the past decade as a new class of heat transfer material with excellent cooling capabilities for a variety of applications such as aerospace, microelectronics, transportation, solar energy, biomedical, and thermal management for efficient heat transfer devices (Taylor et al., 2013). Nanofluids are colloidal suspension of sub-micron or nano-sized solid NPs in the fluid forming a two phase solid-liquid mixture (Figure 2.2). These NP additives are thoroughly dispersed in the liquid phase and are intended to boost the thermophysical properties of the base fluid, yielding increases in K with minimum impact on μ. The incorporation of NP additives in fluids will also increase μ due to Brownian and hydrodynamic interactions that are responsible for particle-particle and particle-liquid interactions, and if applied in machinery lubricants (e.g.gearbox), would yield a strong film between moving surfaces, and reduce metal-to-metal contact (friction). However, major increases or decreases in μ should be minimized to avoid energy consumptions due to friction. Moreover, the distinctive high surface-area-to volume ratio of the NPs enhances surface functionality, resulting in nanofluids with superior heat transfer characteristics

when compared to the conventional fluids with no additives. All these attributes make nanofluid a serious candidate to meet aircraft demands and specifications of extremely high loads.
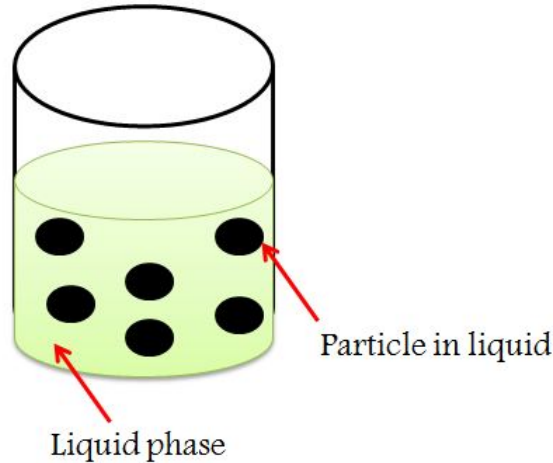
Figure 2.2: Schematic example of nanofluid dispersion

Numerous studies of nanofluids in the review of literature have been investigated where the focus is on synthesis, characterization and computational modelling. Song et al. determined experimentally the rheological properties of different concentrations of nanofluids or nanolubricants using aircraft grease, concluding the major impact the NPs have on the lubricant where more shear-thinning behavior of the nanofluid was observed than that of the base grease with no NPs (Song et al., 2010). Other groups were interested in understanding the underlying mechanism behavior of particle interaction in nanofluids and nanolubricants. Three different mechanisms are widely proposed in the literature for alleviating friction and wear between moving parts. Eastman and Rapoport presented the 'ball bearing mechanism' where the nanoparticles act as clusters or aggregates of a third body between asperities of moving parts, preserving their shape (Eastman et al., 2004; Rapoport et al., 2003). Schwarz et al. showed that the nanofluids are subjected to very high loads, leading to the formation of a protective sheet, having a particle-liquid interface or layer at surface of particles

with extremely large thermal properties(Schwarz et al., 2002). The third mechanism addressed by Liu et al. is governed by a surface engineering point of view, where NPs have Brownian motion and hydrodynamic interactions that help in an efficient heat transfer process (Liu et al., 2004).

Yu et al. measured experimentally the thermal conductivity and dynamic viscosity of aluminum oxide nanoparticles in engine polyalphaolefin oil (Yu et al., 2012). A substantial increase in these lubricant properties was reported. Koo and Rizvi developed new models to predict the effective thermal conductivity and effective viscosity of nanofluids, taking into account different parameters that include: the interfacial nano-layer,particle size, volume fraction, Brownian motion, and temperature. (Koo and Kleinstreuer, 2004; Rizvi et al., 2013). The results were in agreement with available experimental data found in the literature. The tribological effect of the nanotribology was also an interest to several researchers. Peng et al. studied experimentally the tribological behavior of diamond nanoparticles in liquid paraffin using instruments like tribometer, scanning electron microscope (SEM) and Fourier transform infrared spectrum. Results have shown outstanding promising behavior of NPs to improve tribological properties (Peng et al., 2009). The cursory overview of this literature suggest that the incorporation of NPs in fluids are expected to increase thermal, rheological, and tribological properties of lubricants, and ultimately improving the performance of the system.

Although these scientific efforts have achieved advancements in different areas of nanofluid research, its application in complex mechanical systems remain limited and is yet to be explored.

2.3 Wavelets

The most famous signal processing techniques to detect transient characteristics are time-frequency and wavelets (Staszewski et al., 1997; Coats et al., 2011; Wang et al., 2013). Unlike time-frequency analysis, wavelet analysis has the flexibility to apply a movable window with variable-sized regions for the investigation of high and low frequency components. This is a key aspect making wavelets favorable for feature extraction in mechanical system applications that involve multi-component signals.

Wavelets discriminate in both time and frequency domains. This is performed by mapping a one-dimensional input time signal to a two-dimensional time-scale plane. The output at a given position in this plane is known as the wavelet transform coefficient. This coefficient is obtained from the convolution of a given input signal with a wavelet function called the 'mother wavelet'. The mother wavelet generates a series of other wavelet functions at various scales and shifts in time to compute all the wavelet coefficients. As a result, the signal is transformed into its constituent wavelets (Figure 2.3). Proper selection of the mother wavelet function is vital to provide a good filtering performance.
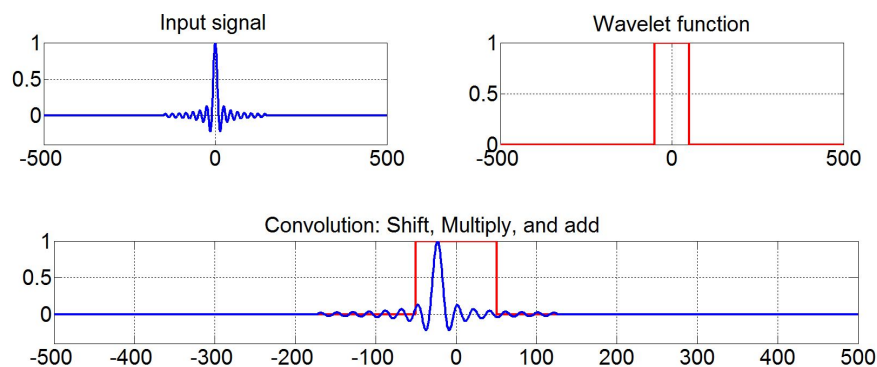
Figure 2.3: Example of convolution process between an input signal and impulse response

There exists a variety of wavelet functions to be used with different transforms. For example, orthogonal wavelets are mainly used with the discrete wavelet transforms

(DWT). These orthogonal wavelets have the capability to reduce redundancy from the transform through an orthonormal basis. DWT is used with different applications, which include image de-noising and compression. However, there are major challenges when applying DWT in mechanical diagnostics. DWT has stringent requirements to obtain the output of the transform through the choice of the correct orthogonal wavelets with alias cancellation capabilities, perfect reconstruction and the number of vanishing moments Fugal (2009). Furthermore, the scales in DWT are slightly sparse due to dyadic discretization. This means features in signals might not be accurately detected. On the other hand, non-orthogonal wavelets are mainly used with continuous wavelet transform (CWT). CWT is still the preferred transform for signal identification and feature extraction in rotating machinery, since discretization is across all possible integers when applied with non-orthogonal wavelets (Boulahbal et al., 1999; Lin and Zuo, 2003; Lokesha et al., 2011). Abundant research in the review of wavelet literature proposed robust metrics for diagnosis of several rotating machinery components such as bearings and gearbox. (Ren et al., 2006; Kankar et al., 2011; Gao and Yan, 2006; Wang et al., 2009; Bendjama et al., 2012; Chen et al., 2012; Lim and Leong, 2013).

Where these scientific efforts have achieved significant advancements in condition monitoring, the findings were exclusively applied on component-based test rig experiments and were not accurately comparable to actual CIs from aircraft monitoring systems. This dissertation proposes a new CI based on wavelet analysis using real-world data that would represent naturally occurring field-faults

CHAPTER 3

EXPERIMENTAL INVESTIGATION OF NANOPARTICLE ADDITIVES IN OIL USING OFF-LINE ANALYSIS

3.1 INTRODUCTION

The purpose of this fluid study is to test the hypothesis of improved thermophysical properties of ten nanofluid samples and to select optimum samples for gearbox testing based on oil analysis measurements. In this work, two types of synthetic gear oils are investigated as potential lubricants in the IGB, Turbine Jet oil and AGL. Both are common oils that are widely used as lubricants and coolants in a variety of military applications. The nanofluid dispersions were prepared by CBM's industrial partner using high shear mixing after ultrasonic processing or thermochemical exfoliation. The chemical compositions of the solid NPs incorporated in the base fluid are boron nitride (BN) and graphite. These samples contain different particle concentrations ranging from 0.5%-2.5% by volume (Table 3.1). Numerous thermophysical properties including K, μ, and VI are the measured from the experiments. Also, SEM micrographs in Figure 3.1 reveal the characteristics of particles. This flake-like morphology is attributed to the graphite and BN precursors, where the particle size distribution of the NPs are expected to be within ranges of nanometer size.

The upcoming sections explain the detailed methodology, experimental set up, results and discussion. Moreover in this chapter, a new nanofluid model is developed based on effective medium theory (EMT); a theoretical approach that predicts dispersion of particles in fluids, as a one phase system. Nanofluid model results are a key

step towards a better understanding of NPs mechanism and the dynamic behavior of these particles in oil. Results are connected with the interpretation of IGB online results presented in chapter 5.

Table 3.1: Nanofluid samples investigated

Base Oil	Chemical Composition	Concentration (vol%)
Turbine Jet Oil	BN	0.5
Turbine Jet Oil	BN	1
AGL	BN	1.5
AGL	BN	1
AGL	BN	2
AGL	Graphite	0.5
AGL	Graphite	1
AGL	Graphite	1.5
AGL	Graphite	2
AGL	Graphite	2.5
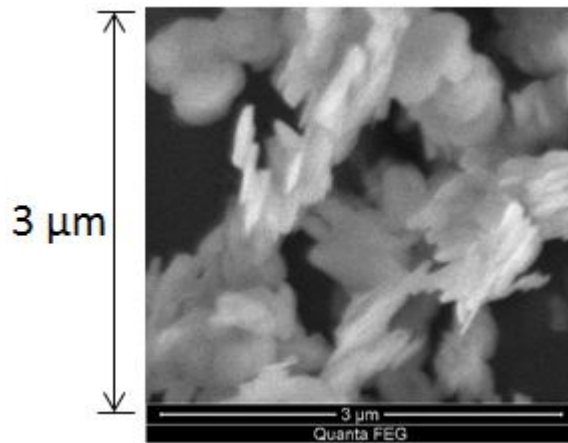
Figure 3.1: Example of SEM micrograph of graphite nanoparticles

3.2 Thermal Conductivity Measurement: A Transient Method

The purpose of this experiment is to determine the K value for the nanofluids under stationary conditions using a transient method (Figures 3.2). K is an important lubricant property that indicates the ability of material to conduct heat. This experimental approach is similar to the well-established hot wire method (Xie et al., 2006). In this experiment, an oil sample is injected at the center of a test tube and placed in a constant temperature bath that acts as the uniform heat generation source. A thermocouple sensor is vertically inserted in the test sample. It is gradually heated and temperature values at the radial position are measured and recorded using the sensor until reaching equilibrium with the bath temperature. Then, the thermal properties of the fluid can be calculated from the temperature data using equation [3.1]. This equation represents the governing mathematical model for the approach and is derived from the Fourier's law for one-dimensional transient heat conduction with the assumption of having heat transfer by conduction alone and uniform temperature across a long thin tube.
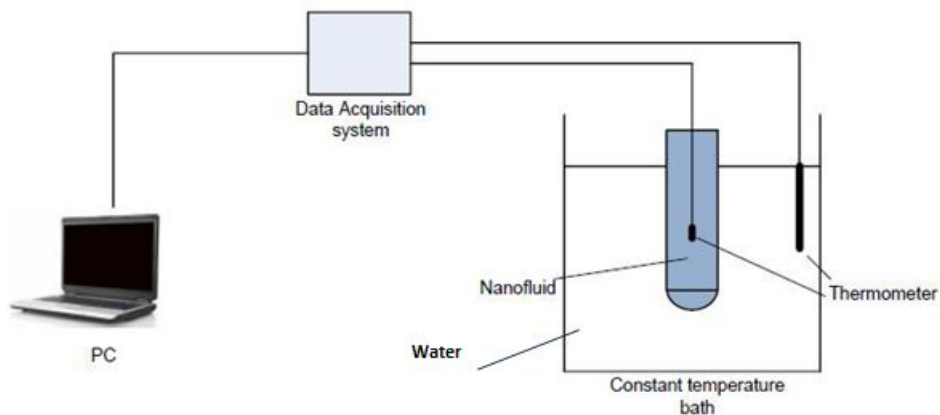
Figure 3.2: A schematic representation of the thermal conductivity experiment

$$K_s = \frac{Q}{4\pi} \frac{ln\Delta t}{\Delta T} \tag{3.1}$$

where K_s is the thermal conductivity of a tested sample, Q is the heating power, t is the heating time, and T is the temperature

In this work, heat transfer module in Comsol Multiphysics 4.2 is used to acquire temperature data in which different K values are calculated until it fits with the experimental data (Figure 3.3). Then, the thermal conductivity of the material can be found at a temperature of 30 ° C.
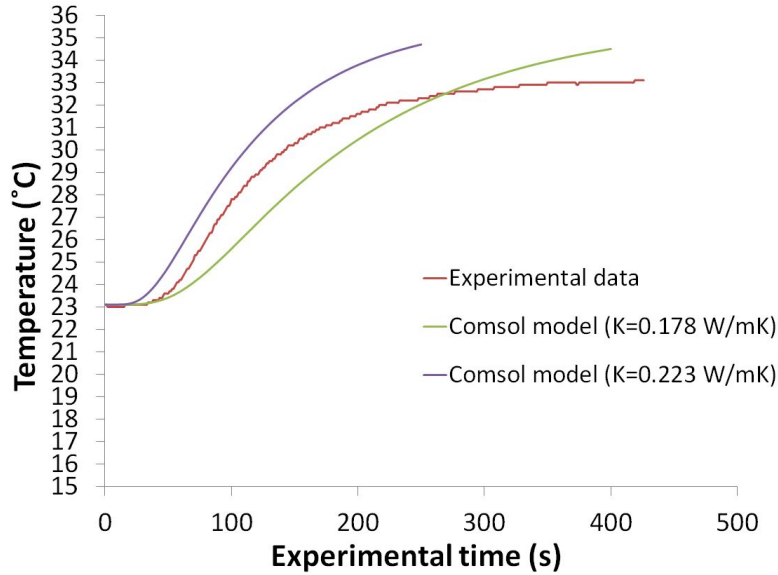
Figure 3.3: Example for temperature profile measured at the center for the 1.5% graphite-based AGL nanofluid sample and compared with different predicted K values

3.3 Dynamic Viscosity Measurement

The purpose of this experiment is to determine μ of the nanofluids using a rheometer instrument and to investigate the impact of NP additives on the rheological characteristics. The device used for dynamic viscosity measurement is a controlled strain AR2000 rheometer (TA Instruments, DE) with shear rate ranges from 1 to 2000 s^{-1}. The rheometer consists of three main parts, as can be seen in Figure 3.4. The main

28

unit needed for the geometry. (2) The electronic box. (3) Sample holder. A single experimental measurement takes approximately 11 minutes. The selection of the geometry mainly depends on the fluid being tested. The plate can be concentric cylinders or parallel plates. In the case of oils and gels, parallel plates are used with a 200 μm gap. In this rheometer, torque resolution of the instrument is 0.1nNm. During the experiment, all other parameters including the working temperature of fluid, 40° C, speed of 60 rpms, and frequency of 1 Hz are held constant. Due to pre-shearing the oil at small torque values, measurements are performed at steady-state conditions after waiting 180 s. As such, viscosity data at very small torques are discarded and not considered due to this experimental uncertainty.

The following procedures are followed:

- A sample is placed between the two plates. The bottom plate that is stationary, and moves at a speed of 60 rpm, and a top plate known as the geometry where a uniaxial compressive force at a displacement rate of 7.5 mm/s is applied and shear stress is produced on the top plate.

- The sample then comes in close contact with the two surfaces and a 1 % strain is applied.

- The built-in rheology software outputs two graphs: (1) Rheological curve: shear stress vs. shear rate. (2) Viscosity vs. shear curve

3.4 Viscosity Index Measurement

VI is another important lubricant property that defines the change in viscosity with respect to the change in temperature of oil. A high VI indicates minimal change of viscosity with temperature, and on the other hand,a low VI means a large viscosity change with temperature. A reverse-flow viscometer (Fig 3.5) is used to calculate
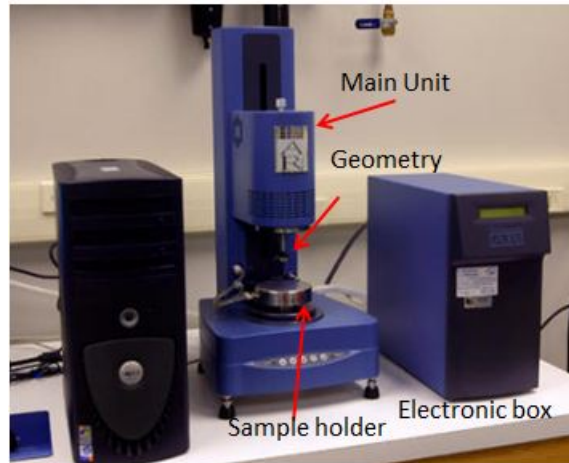
Figure 3.4: TA AR2000 Rheometer

the VI values for the nanofluids under study. First, the kinematic values γ of the nanofluids are measured at temperature of 40 ° C and 100 ° C, respectively. The viscometer is inserted into a constant temperature bath where an oil sample is injected in the bulb, the sample is allowed to flow vertically downwards until it reaches the temperature of interest. This follows measuring the efflux time, in which γ is calculated through multiplying: efflux time * size factor. This constant is dependent on the size of the tested tube. Finally, VI values can be easily calculated from the γ at both of the described temperatures.
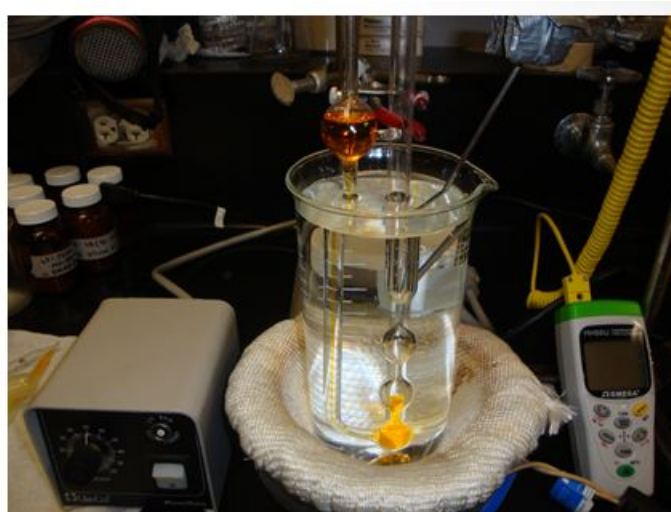
Figure 3.5: ASTM D445 capillary viscometer

3.5 STATISTICAL ANALYSIS

Results are reported as mean value $\pm$ std. All experiments are replicated five times (n=5) to reduce uncertainty in measurements or artifact of instruments. The uncertainty in the instruments are within 95% confidence. This is followed by performing a t-test to evaluate if experimental results are statistically valid, where a p value < 0.05 is considered statistically significant. All experimental results reported below are significant.

3.6 RESULTS AND DISCUSSION

3.6.1 THERMAL CONDUCTIVITY

K results for two turbine jet oil fluid samples are summarized in Table 3.2. The incorporation of BN NP materials in the oil increased K value from base oil of 0.142 (W/mK) to 0.167 (W/mK).

Table 3.2: Thermal conductivity results for turbine-based BN jet oil samples: values are mean $\pm$ std

Jet oil sample (vol%)	K (W/mK)
0% (Base oil)	0.142 $\pm$0.006
0.5% (BN)	0.147 $\pm$0.010
1% (BN)	0.167 $\pm$0.008

K results for three AGL-based BN NPs and five AGL graphite-based NPs are summarized in Table 3.3. Similarly to jet oil, increases in K values is observed for the AGL fluid. 2% BN sample reaches a high of 0.178 W/mK $\pm$0.008, which is almost a 30% increase, compared to the Base AGL sample. Graphite-based AGL nanofluid

samples have shown the highest increases in K, compared to the BN-based additives and turbine jet oil samples, reaching $0.220\ W/mK$ for the 2.5% graphite NP samples. The rest of the dispersions display different ranges of K values ranging from $0.150\ W/mK$-$0.195\ W/mK$.

Graphite particles are known to have substantial higher K values, compared to BN. As such, the increases in K values for the AGL graphite-based nanofluid results can be attributed to the incorporation of graphite particles with possibility of having more surface available in the fluid that yield excellent thermal behavior and its ability to reduce temperatures by conducting more heat, if applied as a potential lubricant in the gearbox.

Table 3.3: Thermal conductivity results for AGL based samples: values are mean $\pm$ std

AGL sample (vol%)	K (W/mK)
0% (Base AGL)	0.135 $\pm$0.012
1% (BN)	0.150 $\pm$0.008
1.5% (BN)	0.155 $\pm$0.014
2% (BN)	0.178 $\pm$0.008
0.5% (graphite)	0.163 $\pm$0.011
1% (graphite)	0.173 $\pm$0.007
1.5% (graphite)	0.178 $\pm$0.009
2% (graphite)	0.195 $\pm$0.014
2.5% (graphite)	0.220 $\pm$0.016

3.6.2 Shear-rate dependence

μ measurements in Figure 3.6 illustrate that the 0.5% jet oil-based BN nearly maintains Newtonian features even after the incorporation of the NPs with slight improvement in rheological properties, compared to base jet oil. However, the 1%

incorporation of NPs clearly has a negative impact on the rheological behavior of oil, which demonstrates non-Newtonian shear-thinning behavior. Despite measurements being performed at low shear rate conditions in the rheometer, it is clear that the incorporation of 1% jet oil additive has a dynamic viscosity dependent on shear rate. After the sudden sharp decrease in viscosity, it became constant near the end of the experiment, almost matching behavior of the other lubricants. This shows that the 1% jet oil additive is not meeting expectations of significant improvement in rheological properties for nanofluids. Based on this result, it can be theorized that the 1% jet oil additive would not perform as an optimum lubricant for the IGB at higher shear rates, due to possible rheological changes in μ that can eventually lead to film rupture, more friction, wear and high temperature responses.
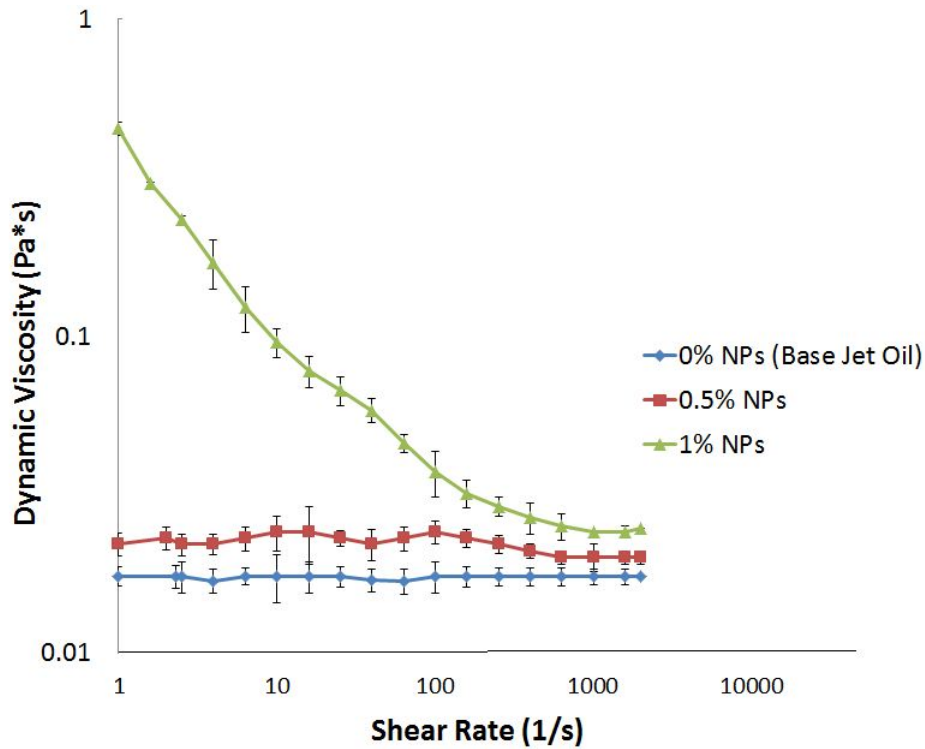
Figure 3.6: Rheometer results for turbine jet oil BN samples. values are mean $\pm$ std

Further theoretical investigation showed that the 1% jet oil sample falls into a Carreau model; a rheological model that describes shear-thinning behavior of Newtonian fluids. The mathematical expression of Carreau model is given by:

$$(\frac{\mu_\gamma - \mu_\infty}{\mu_0 - \mu_\infty}) = [1 + (\gamma\lambda)^a]^{\frac{n-1}{a}} \tag{3.2}$$

where μ_∞ is the viscosity function that approaches the constant value μ_∞ as the shear rate becomes large, μ_0 is the viscosity function that approaches the constant value μ_0 as the shear rate becomes small, a is an exponent that affects the shape of the transition region, γ is the time constant parameter for the fluid, n is a power-law like parameter that describes the slop of the rapidly decreasing portion of the viscosity curve where $n = 1$ for Newtonian fluids, $n < 1$ for pseudo-plastic fluids and $n > 1$ for dilatant fluids.

The Carreau model agrees well with the 1% experimental data and can be considered a good fit (Figure 3.7). Furthermore, model parameters are summarized in Table 3.4 where the exponent n value is 0.23, indicating a shear-thinning response. More details for this behavior of shear thinning in oil nanofluids is discussed in chapter 5.

Table 3.4: Carreau model parameters for 1% turbine jet oil sample

Parameter	Value
μ_∞	0.022
μ_0	2.48
a	4.35
n	0.23
λ	9.986

μ results for AGL-based BN and AGL-based graphite samples are summarized in Figures 3.8 and 3.9, respectively. Viscosity data at smaller shear rates are discarded,
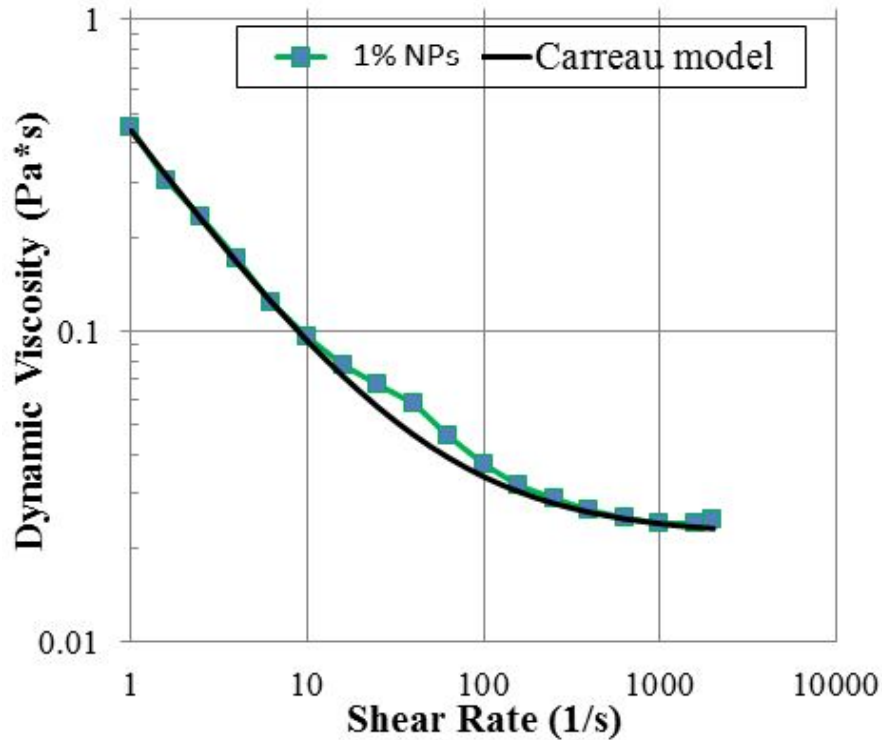
Figure 3.7: Fitting the Carreau model to rheological data

where torque values are too small to reach steady state. Compared to the rheological characteristics of jet oil from Figure 3.6, the AGL nanosamples demonstrated higher μ with Newtonian behavior across the given shear rate range. Also, these AGL-based graphite samples show significant increases of dynamic viscosity values, compared to the base AGL.

Brownian and hydrodynamic interactions of particles in fluids are known to be the main contributor for improving rheological characteristics. These hydrodynamic interactions seem to be more dominant for graphite additives in the nanofluid samples than those of BN-based samples. As the former may have more free surface available in the fluid, also the significate improvement of thermal properties of graphite reported in previous section play a role to enhance rheological characteristics.
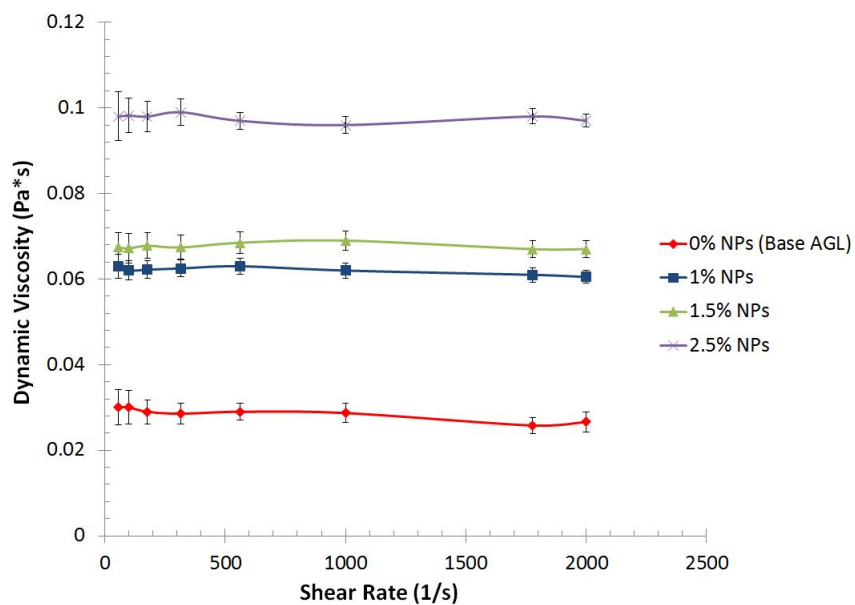
Figure 3.8: Rheometer results for AGL BN samples. Error bars represent mean ± std
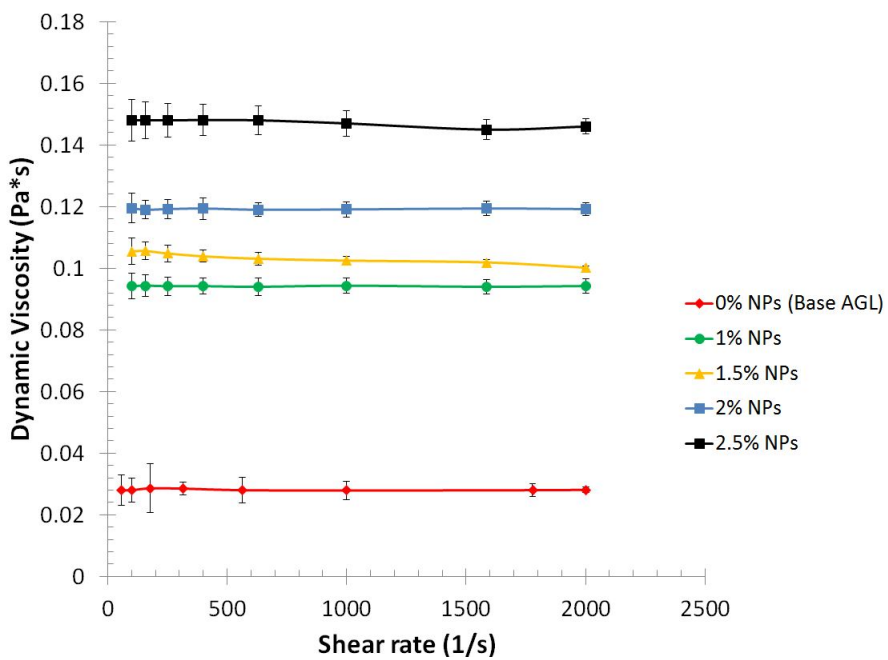
Figure 3.9: Rheometer results for AGL graphite samples. Error bars represent mean ± std

3.6.3 Viscosity Index

VI results from the reverse flow experiment are summarized in Table 3.5. The 0.5% NPs sample increased VI value from 145 to 185, compared to the controlled sample. Moreover, the VI experiment for the 1% sample could not be completed and was terminated due to phase separation of particles, which correlates with the rheometer results from Figure 3.6 that indicated drastic rheological changes in the oil sample. Furthermore, VI results of AGL-based nanofluid samples are summarized in Table 3.6 with significant VI values as high to 182. As expected, VI results for AGL-based nanofluids are higher than those obtained from jet oil that indicate less change of viscosity with respect to temperature. These high VI values can be attributed to the incorporation of particles and its ability to maintain a constant viscosity at different temperature due to Brownian and hydrodynamic interactions.

Table 3.5: Viscosity index results for turbine jet oil BN samples:values are mean ± std

Jet oil sample (vol%)	VI
0% (Base oil)	145 ±6
0.5%(BN)	185 ±9

Table 3.6: Viscosity index results for AGL graphite samples: values are mean ± std

AGL Sample (vol%)	VI
0% (Base oil)	160 ±5
0.5%(graphite)	155 ±9
1% (graphite)	161 ±6
1.5% (graphite)	166 ±4
2% (graphite)	182 ±12
2.5%(graphite)	180 ±10

3.7 THEORETICAL MODEL

The well-known classical EMT models, such as, Maxwell and Hamilton fail to predict thermophysical properties of nanofluids due to the inherent limitations of being a function of concentration only in a solid-liquid mixture with submicron-sized particles, and produce poor thermal and rheological properties (Abareshi et al., 2010; Earnshaw and Riley, 2011). Thermal and rheological behavior of non-spherical NPs in non-aqueous liquids,such as oil,is still not well understood (Yu et al., 2012). The purpose of this study is to introduce a new comprehensive nanofluid model by combining two well-known NP mechanisms that are most likely to represent the nanofluids investigated: (1)Interfacial nanolayer of particle, which is defined as solid-liquid layer around the particle surface and (2) Hydrodynamic interactions of particle during dynamics the fluid. The model is modified from the conventional EMT as a quick tool of analysis to approximately predict K and μ of the non-spherical particles.

In this study, the dynamic portion of the nanofluid model is developed utilizing the kinetic theory approach and stokes regime to propose effective thermal conductivity and viscosity models. The theoretical predictions are compared with the experimental results and are tested with external data and existing models available in literature

to confirm accuracy. The developed nanoflud model for thermal conductivity and viscosity are developed in the next two sections with assumption of modelling a single particle moving in a creep flow regime.

3.7.1 Effective Thermal Conductivity Model

An effective thermal conductivity (K_e) model is developed that takes into account a modified static part (K_s) from the conventional Hamilton-Crosser model and a new dynamic part (K_d) that encompasses the hydrodynamic interaction with Brownian motion of the fluid particle and the particle-particle interactions where:

$$K_e = K_s + K_d \tag{3.3}$$

Static Part

To consider the interfacial solid-liquid layer interface of thickness h surrounding the NP of radius r_p, length l (Figure 3.10) , an equivalent particle and volume fraction (ϕ_e) is used that becomes an approximation for non-spherical or cylindrical particles as follows:

$$\phi_e = \phi_p N = (2\pi r_e^2 + 2\pi r_e l)N = [2\pi(r_p + h)^2 + 2\pi(r_p + h)l]N \tag{3.4}$$

$$\phi_e = 2\pi r_p^2(1 + \frac{h}{r_p}) + 2\pi r_p l(1 + \frac{h}{r_p}) = \phi_p(1 + \frac{h}{r_p})^2(1 + \frac{h}{l}) \tag{3.5}$$

where N is the number of particles per volume, V, and r_e is the equivalent radius of non-spherical particle.

Using equation [3.5] in the well-known Hamilton-crosser thermal conductivity model (Wang and Mujumdar, 2007), the static part of the equation is modified as follows:

$$K_s = (\frac{K_e + (n-1)K_l + (n-1)(K_e - K_l)\phi_e}{K_e + (n-1)K_l - (K_e - K_l)\phi_e})K_l \tag{3.6}$$
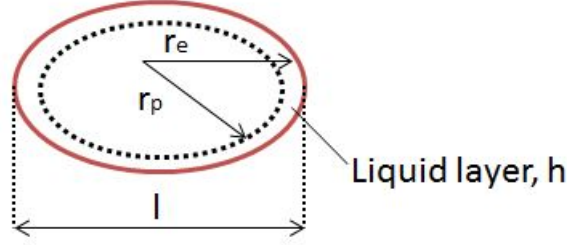
Figure 3.10: Schematic representation of nanoparticle with liquid layering

Where K_l is the thermal conductivity of the fluid, n is the empirical shape factor given by: $n = \frac{3}{\psi}$ and ψ is the sphericity.

In this work, $n=3$ for the pseudo rod-shaped particles as ψ is 1. K_e is the effective thermal conductivity of the particle and liquid layer combined and is given by:

$$K_e = (\frac{[(n-1)(1-\gamma) + \frac{\phi_e}{\phi}(1+(n-1)\gamma)}{-(\gamma-1) + \frac{\phi_e}{\phi}(1+(n-1)\gamma)})K_p \tag{3.7}$$

Where γ is the ratio of thermal conductivity of the liquid layer to that of the particle and is approximately equal to 1.

Dynamic Part

From the kinetic theory, the heat flux or the energy across the interface (q_n) between a moving particle with Brownian velocity (v), time (Δt) and in thermal equilibrium at T_1 and T_2 (Figure 3.11) can be defined as follows:

$$q_n = \frac{\Delta Q}{\Delta t A} = \frac{PN m_P (T_1 - T_2) c_v}{\Delta t A} = \frac{-m_P N C_v \frac{\Delta T}{l} l v}{A \Delta t v} \tag{3.8}$$

where l/D is the distance a particle moves without changing its direction. For simplicity, it is assumed to be equal to 1, due to creep flow. m_p is the mass of a particle, and V_p is the volume of a particle.

$\frac{\Delta T}{l} l = \nabla T, m_p = \rho V_p$, $A \Delta t = V$, C_v is the specific heat of the liquid, $\frac{N V_P}{V} = \phi$ is the concentration of particles and P is the expected probability value of a single particle to travel in one direction, which is estimated to be approximately one-sixth of total particles generated in a given sample (Koo and Kleinstreuer, 2004).

$$q_n = (\frac{-PN\rho_p V_p C_v l v}{V})\Delta T = -P\phi\rho_p C_v v l \nabla T = q_n = -K_d \nabla T \qquad (3.9)$$
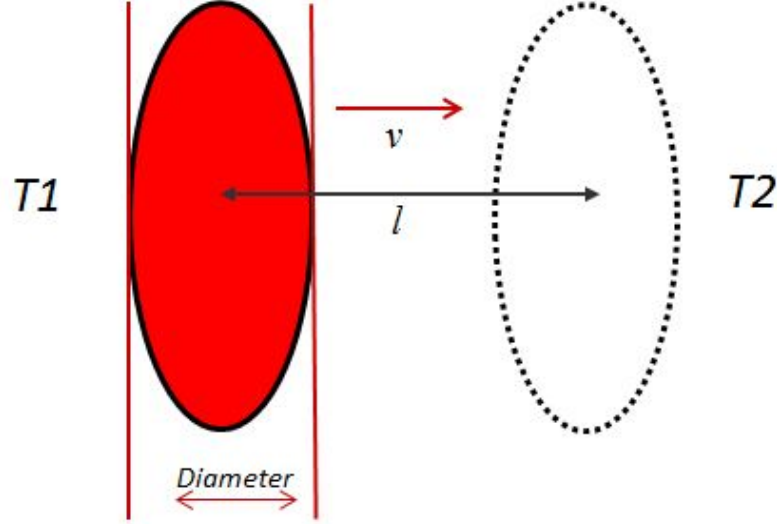
Figure 3.11: Schematic representation of a particle's Brownian motion in two different temperature gradients

Koo et al. developed a thermal conductivity nanofluid model for predicting the effective thermal conductivity. However, their work was only limited to spherical particles and the v_b used in the analysis was independent of the particle concentration, but it is more justifiable to employ the Brownian velocity as a function of particle volume fraction. In this proposed model,the Brownian motion based on effective diffusion concept is used after taking into account the equivalent volume fraction (Earnshaw and Riley, 2011):

$$v_b = \sqrt{\frac{3kT(1 - 1.5\phi_e)}{2\pi\rho_e r_e^3}} \qquad (3.10)$$

Where k is Boltzman constant, T is the temperature, ϕ_e is the effective volume fraction, ρ_e is effective density of particle and liquid layer, and r_e is equivalent radius of particle and liquid, given by $r_e = r_p + h$. v_b is substituted in equation [3.9] yielding:

$$K_d = P\phi_e\rho_l C_v \sqrt{\frac{3kT(1 - 1.5\phi_e)}{2\pi\rho_e r_e^3}} \qquad (3.11)$$

41

Model Parameters

During hydrodynamic interactions, part of the liquid surrounding a particle is affected and should be considered. The analytical solution for the dynamics of non-spherical particles is still a challenging task and such a solution is only available for spherical particles and only few researchers addressed this approach as an approximation for the movement of non-spherical particles (Leith, 1987; Hölzer and Sommerfeld, 2008; Rohini Priya et al., 2012; Yu and Choi, 2003). However, the approach used for modelling was only limited to regression analysis of existing EMT models without accurately accounting for all dynamic parameters, while others developed non-spherical nanofluid models based on the EMT, without taking into account effect of hydrodynamic interactions.

This model takes into account several important dynamic factors such as particles size, shape, temperature, velocity and interfacial nanolayer that would contribute to the improvement of lubricant properties. In this proposed model (Figure 3.12), a numerical solution using creeping flow interface in Comsol Multiphysics 4.2 is utilized as an approximation for the model to estimate the region moving with the particle (V_f). This model assumes steady-state creep flow (Re<1) as follows:

$$V_f = \frac{3.14}{6} a^2 b \qquad (3.12)$$

The numerical representations are presented in Figure 3.13 that show V_f is an ellipsoid being influenced by the particle motion for both a spherical and a non-spherical shape. Fluid bodies surrounding particles depend on the shape of the ellipsoid with dimensions a and b. This means more bodies of fluid for the non-spherical case are expected to move with the NPs than those of the spherical and as a result enhance thermophysical properties. From the creep flow, boundary conditions are estimated
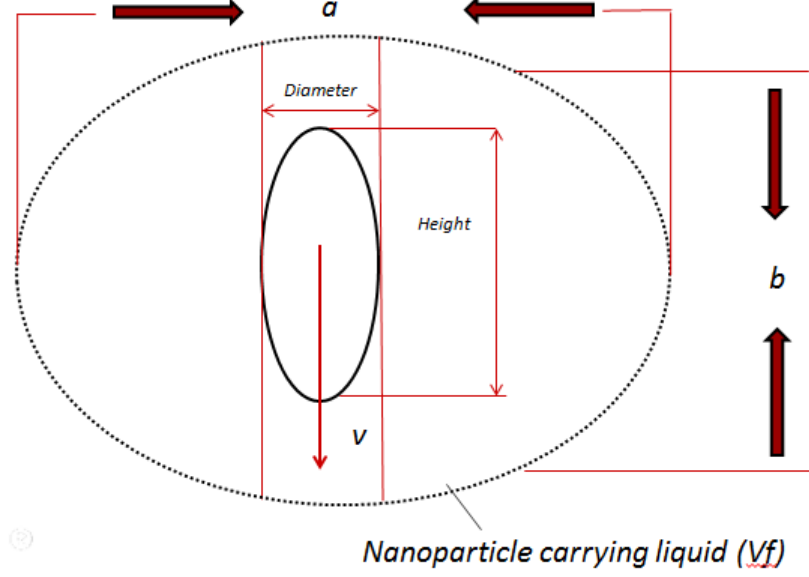
Figure 3.12: Schematic representation of the proposed mechanism: particle with surrounding fluids

to be: $vmax = 0.01vbrownian$ at $r = 0$ and $v = 0$ at $r = rmax$ and the dimensions of the ellipsoid can be determined as follows:

$$a = 4.317D + 5.275H - 0.325DH + 17.500 \tag{3.13}$$

$$b = 8.367D + 10.233H - 0.637DH + 35.611 \tag{3.14}$$

where a, b are the dimensions of the ellipsoid. D and H are the diameter and height of a particle, respectively.

Therefore equation [3.11] turns into:

$$K_d = V_f P \beta \phi_e \rho_l C_v \sqrt{\frac{3kT(1 - 1.5\phi_e)}{2\pi \rho_e r_e^3}} f(T, \phi) \tag{3.15}$$

$$K_d = 40660 P \beta \phi_e \rho_l C_v \sqrt{\frac{3kT(1 - 1.5\phi_e)}{2\pi \rho_e r_e^3}} f(T, \phi) \tag{3.16}$$

where β is the first model parameter that represents the particle-liquid interaction and a fraction of V_f travelling with the liquid. Furthermore, the effect of particle-particle interaction is considered and is assumed to be very strong and represented

43
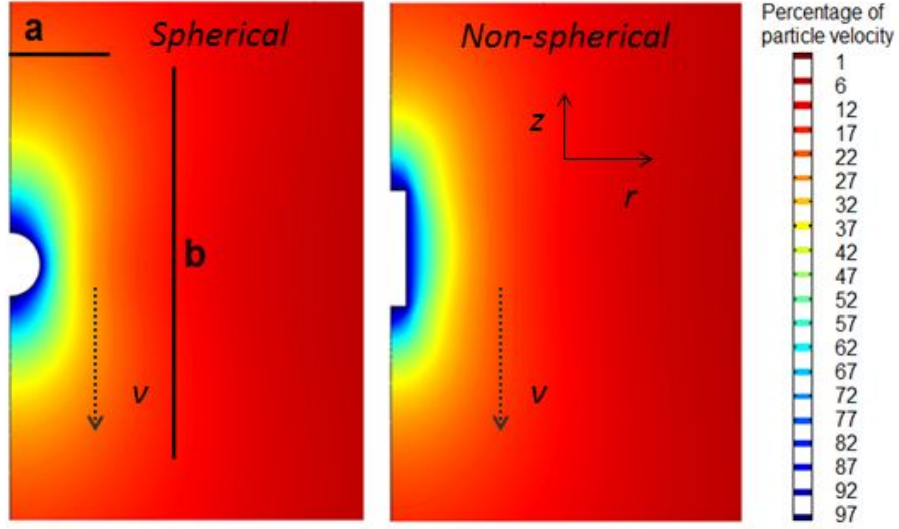
Figure 3.13: Numerical solution of Comsol model to estimate region of influence

by a fractional function $f(T, \phi_d)$, which is the second model parameter. Both these parameters were empirically developed in the literature(Das et al., 2003; Patel et al., 2003).

Estimation of model parameters

In this work, both β and f are a function of particle concentration (ϕ), where β is expected to decrease with increasing particle concentration. Also, f increases with the increase of particle concentration. we use only one parameter, α that accounts for all possible hydrodynamic interactions, given by:

$$\alpha = \beta.f \tag{3.17}$$

$$\alpha = \phi^{-C_1}.(C_2\phi T + C_3 T) \tag{3.18}$$

where C_1, C_2 and C_3 are constant parameters that are calculated by fitting the experimental data.

The final expression for dynamic thermal conductivity in non-spherical particles is given by:

$$K_d = 40660 P\phi_e\rho_l\alpha C_v\sqrt{\frac{3kT(1-1.5\phi_e)}{2\pi\rho_e r_e^3}} \tag{3.19}$$

3.7.2 EFFECTIVE VISCOSITY MODEL

Using the same approach for deriving the effective viscosity model, a modified Batchelor equation for non-spherical NPs is used as the static part in the model (Wierenga and Philipse, 1998).

$$\mu_s = 1 + \frac{r_e^2}{15 \ln r_e}\phi + \frac{36 r_e^6}{5\pi^2 \beta \ln r_e}\phi^3 \tag{3.20}$$

where r_e is the equivalent radius of the particle and β is an empirical factor(10^3-10^6)

The final form of the dynamic viscosity portion model is given by:

$$\mu_d = V_f P \phi_e \rho_l \alpha \sqrt{\frac{3kT(1 - 1.5\phi_e)}{2\pi \rho_e r_e^3}} \tag{3.21}$$

Comparing with the dynamic thermal conductivity model:

$$K_d = V_f P \alpha \phi_e \rho_l C_v \sqrt{\frac{3kT(1 - 1.5\phi_e)}{2\pi \rho_e r_e^3}} \tag{3.22}$$

Most of the work in the literature developed nanofluid models based on spherical nanoparticles dispersed in aqueous solutions (eg.water), as spherical particles are easy to be investigated both experimentally and theoretically. However, nanofluids for real-life application are mostly non-spherical due to the high aspect ratio and more promising characteristics. Section 3.7 developed a new nanofluid model based on the EMT approach that describes thermophysical properties for non-spherical NPs dispersed in oil. A new dynamic term, represented in equations [3.21] and [3.22] is developed to account for hydrodynamic interactions that include Brownian motions as well as several other parameters: temperature, particle concentration, size, and shape.

3.8 Nanofluid Model Results

3.8.1 Effective Thermal Conductivity

The relative thermal conductivity ($K_r = K_e/K_b$) is the output from the model and is used as an indicator to compare the performance or effectiveness of nanofluids relative to base fluids, where K_e is the effective thermal conductivity and K_b is the thermal conductivity of the base fluid. From equations [3.7] and [3.19], model results are summarized in Figure 3.14 that show an increase in the K_r value with particle concentration. An increasing trend is developed where theoretical results from the proposed K_r model almost agree with the experimental data having an R^2 value of 0.988. Moreover, results are compared to the existing predictions of Hamilton-Crosser model that is unsuitable for AGL nanofluids and yields lower predictions than the experimental values.

Model results for the jet oil and BN AGL samples are summarized in Figure 3.15. However, unlike the graphite-based AGL samples, there are limited number of experimental data to test the model.

To validate the accuracy of this proposed model, three external experimental data sets from Rohini (Rohini Priya et al., 2012) are fit to the proposed model and results are presented in Figure 3.16. Rohini produced non-spherical Copper oxide NPs dispersed in water as the base fluid. Results show that the theoretical predictions to a great extent closely agree with the experimental data at different temperatures. The accuracy of the model increases at higher temperatures ($R^2 = 0.971$) that demonstrates the impact of particle dynamics on thermal properties of AGL nanofluids. The proposed model is compared with existing non-spherical nanofluid models from the literature, it demonstrates more adequate K results than those presented by Choi and Rohini (Yu and Choi, 2003; Rohini Priya et al., 2012). Also, results are compared with Maxwell model to emphasize the advantageous attributes of non-spherical NPs.
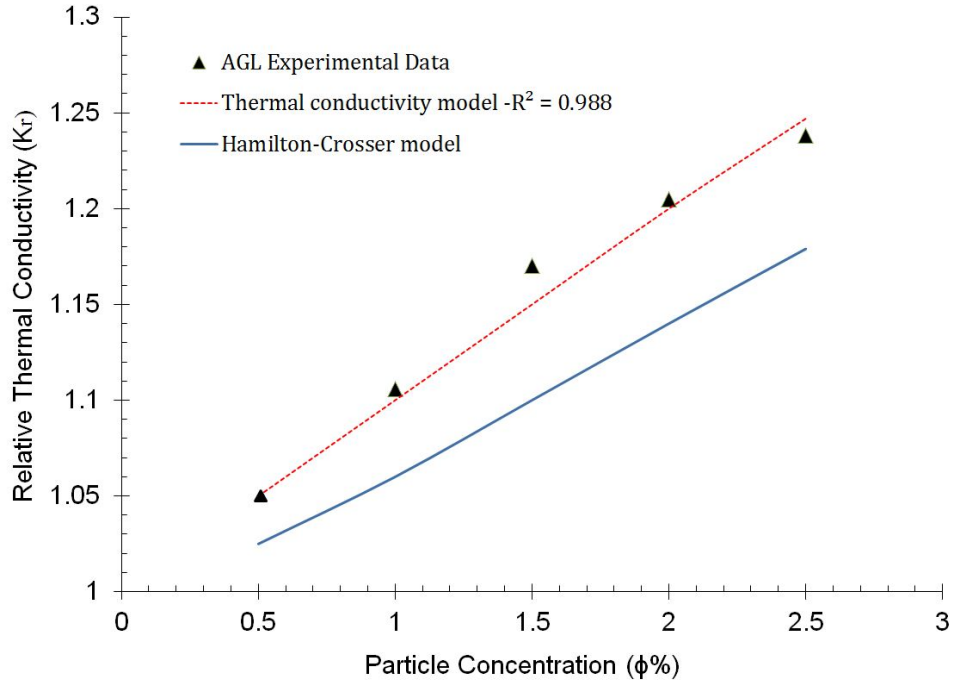
Figure 3.14: Comparison of thermal conductivity model predictions with graphite-based AGL experimental data sets

Maxwell model was originally developed to predict spherical NPs in fluids. The former under predicts the external experimental data and is not considered to be a good model for this application. Table 3.7 summarizes fitting parameters for the thermal conductivity model, where the constant parameters depend on the size and shape of the particles during hydrodynamic interactions.

Table 3.7: Thermal conductivity model fitting parameters

Fluid	particle percentage (%)	C_1	C_2	C_3
AGL	0.5-2.5	-0.97954	$2.23 * 10^{-6}$	$-1.7 * 10^{-8}$
Water	0.4-1.6	-0.89996	0.000489	$-1.5 * 10^{-6}$
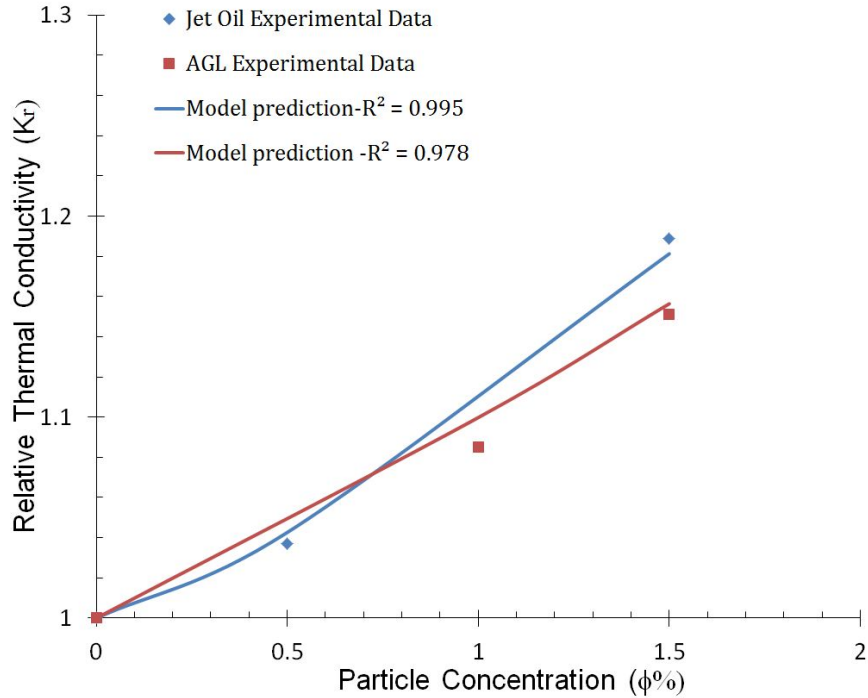
Figure 3.15: Comparison of thermal conductivity model predictions with BN-based turbine jet oil and AGL experimental data sets

3.8.2 EFFECTIVE VISCOSITY

The relative viscosity (μ_r) of AGL graphite NPs is presented in Figure 3.17. Similarly, model results using equations [3.20] and [3.21] show increases in the relative viscosity with particle concentration that closely agrees with experimental data (R^2 value of 0.981), in which an increasing trend can be observed. Similarly results are compared to the existing predictions of Batchelor model from the EMT that is clearly unsuitable for nanofluids and yields lower predictions than the experimental values.

External experimental data from the literature is fit to the proposed model (Duangthongsuk and Wongwises, 2009) that used water as base fluid. Results in Figure 3.18 demonstrate the effectiveness of the theoretical predictions compared to the experimental data produced at different temperatures and concentrations. The proposed model at $25°C$ is in agreement with the existing model from the literature presented by Duaugthongsuk. However, at $30°C$ the proposed model produces more
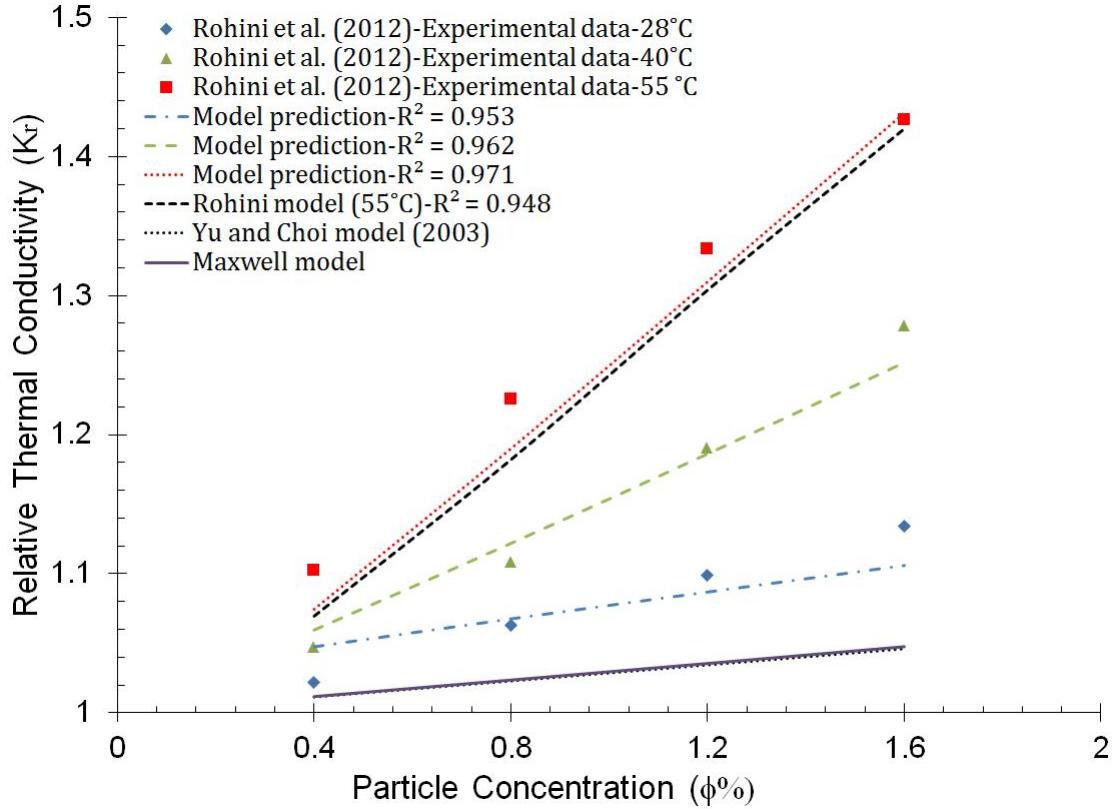
Figure 3.16: Comparison of thermal conductivity model predictions with external experimental data

suitable μ results with $R^2 = 0.975$. Similarly this indicates the importance of the hydrodynamic interactions among particles that was not introduced in Duaugthongsuk nanofluid viscosity model. Table 3.8 summarizes fitting parameters for the viscosity model, where the constant parameters depend on the size and shape of the particles.

3.9 Conclusions

This chapter demonstrates the crucial impact NPs have on thermophysical properties. Turbine jet oil and Mobil AGL nanofluid samples are experimentally investigated using offline tools to test the hypothesis of the improved characteristics of the oil samples and to select the samples with optimum thermal and rheological properties needed for online testing. Despite viscosity being measured in a rheometer with lower
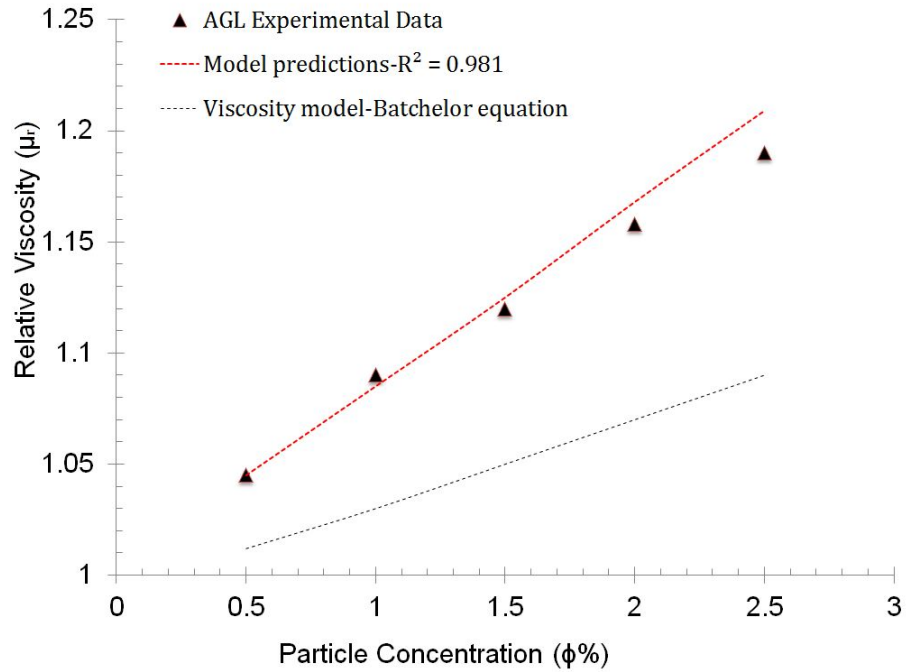
Figure 3.17: Comparison of viscosity model predictions with graphite-based AGL experimental data sets
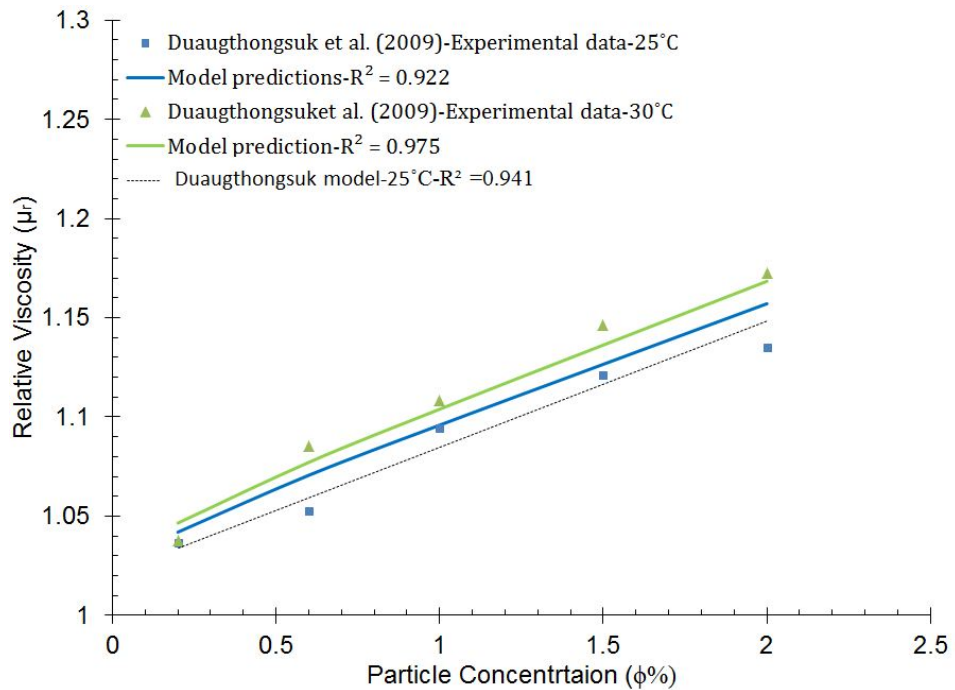
Figure 3.18: Comparison of viscosity model predictions with external experimental data sets

50

shear rate conditions than those expected in a gearbox, results provide an important understanding of viscosity of nanofluids.

The addition of BN NPs in turbine oil has improved thermal characteristics. However, shear-thinning behavior of the oil is clear due to the incorporation of NP additives. Furthermore, BN and graphite NP additives in base AGL are tested. It is shown that the incorporation of graphite-based AGL samples display significant increases in both K, and VI with with minimum change in μ, demonstrating Newtonian characteristics, compared to both turbine-based samples and AGL-based samples with BN additives. Based on these findings, four AGL samples with graphite additives are applied as new lubricants for online testing in the IGB.

A new nanofluid model is proposed that introduces two key mechanisms responsible for the enhanced properties. The proposed model has demonstrated the ability to predict K and μ of non-spherical nanofluids with R^2 value as high to 0.988. External experimental data from the literature is used to test the model. Results are found to be a good fit to the external data when using different fluids with high R^2 values (0.971 and 0.975) that can produce more adequate results than existing literature models. Overall, the model promotes importance of the flake-like morphology of NPs (eg. aspect ratio) coupled with its dynamic behavior to drastically increase fluid properties, compared to spherical NPs. More experimental data sets would still be needed to improve the proposed model accuracy and have solid conclusions. Despite the reasonable assumptions made to the model that include: creep flow and movement of NP in one direction, it has given a fundamental understanding of non-spherical NP behavior in oil lubricants. These results can be further expanded to more advanced computational studies that involve numerical simulations of AGL nanofluids in turbulent fluid flow conditions, and is beyond the scope of this work.

CHAPTER 4

A NOVEL METHODOLOGY FOR GEARBOX FEATURE EXTRACTION USING WAVELET ANALYSIS

4.1 INTRODUCTION

This chapter is two-fold. The first part focuses on a signal-based approach of wavelet analysis for feature extraction. The mathematical theory of wavelets is presented. Based on this theory, a new wavelt index is developed as a potential signal processing tool, denoted as WI. Sections 4.2-4.4 were previously summarized in (Gouda et al., 2015). Second part presents a feature selection methodology using statistical analysis on the wavelet results to prove if results are statistically valid. This is a key part because of redundancy from the continuous wavelet transform. A wavelet denoising method based on a modified thresholding is proposed to remove small wavelet coefficients caused by noise and improve wavelet index performance. Section 4.4 illustrates a detailed step by step approach for the wavelet denoising method, and a wavelet-scheme for feature extraction is summarized. Also, section 4.5 summarizes a statistical test to be performed on the wavelet power spectrum. Wavelet power of Gaussian white noise(GWN) is used to derive the null hypothesis with an 85 % confidence interval estimated about the wavelet power spectrum mean value.

4.2 WAVELET TRANSFORM

Wavelet transform is the convolution of the signal x_n with a set of wavelets of various scales (stretches) and shifts in time. The output at a given time and scale is known as the wavelet transform coefficient. The CWT is defined in the discrete form as a function of two variables and performs the following inner product operation (Heidari Bafroui and Ohadi, 2014):

$$C(\tau, s) = \frac{1}{\sqrt{|s|}} \sum_{t=0}^{T-1} x(n).\psi^*(\frac{(n-\tau)\delta t}{s}) \tag{4.1}$$

where C is the wavelet transform coefficient, x_n is the discrete input signal, s is the scale, τ is the translation or the location of the window, ψ is the mother wavelet and * stands for complex conjugate. The energy of the wavelet is normalized by $\frac{1}{\sqrt{|s|}}$, so that the wavelets have the same unit energy at every scale.

4.3 MOTHER WAVELET

The wavelet function adopted in the analysis is non-orthogonal. Numerous mother wavelets have been broadly investigated in the literature. However, Morlet has been shown to accurately represent signals in condition monitoring applications because of its similarities to the intermittent impulses, which are the symptoms of faults in machinery diagnostics applications (Rafiee et al., 2010). In this work, Morlet is chosen as the mother wavelet. A Morlet wavelet is presented graphically in Figure 4.1 as an exponential decaying cosine function that satisfies the regularity condition (Fugal, 2009).

The mathematical description of the Morlet wavelet is given in equation [4.2]. For a successful transform, the mother wavelet satisfies the admissibility condition as shown in equation [4.3] and equation [4.4] (Su et al., 2010).
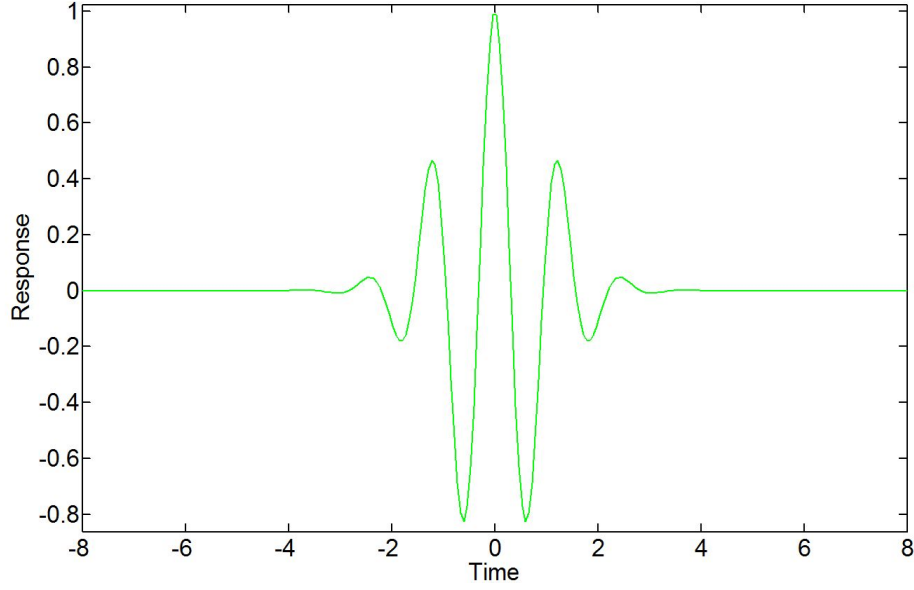
Figure 4.1: Example of a Morlet Wavelet

$$\psi(t) = \exp(\frac{-t^2}{2})\cos(5t) \tag{4.2}$$

$$\int_{-\infty}^{\infty} \frac{|\psi(|\omega^2|)}{|\omega|} d\omega \tag{4.3}$$

where $\psi(\omega)$ is the FT of $\psi(t)$. This admissibility condition implies that the Fourier transform of the mother wavelet is 0 at 0 frequency. Thus, the mother wavelet has no DC component as follows:

$$\psi(0) = \int \psi(t) dx = 0 \tag{4.4}$$

4.4 DEVELOPMENT OF A WAVELET INDEX

A wavelet index (WI) is proposed as a new tool to determine whether a CWT to detect failure is possible. Wavelet coefficients are a measure of vibrational energy distribution in the signal at a certain scale. These coefficient values can be used as an indicator to describe progression of fault in the gearbox. The proposed WI is given in

equation [4.5]. The wavelet coefficients from the convolution are first used to compute the wavelet power spectra. Then, the index is computed by summing the absolute wavelet power spectrum values, which are located at different time shifts and at a particular scale that represents the frequency of interest in the gearbox. The WI is then further normalized by the number of samples for better comparison with other index values.

$$WI_s = \sum_{n=n_1}^{n_2} \frac{|C_i(\tau, s)^2|}{N} \tag{4.5}$$

Where $|C_i(\tau, S)^2|$ is the absolute wavelet power spectrum at a given scale s and n is the wavelet energy sample at given position in τ .

To relate the WI to the actual frequencies in a physical system, the scales can be converted to a pseudo-frequency as follows:

$$F_s = \frac{F_c}{s.T_s} \tag{4.6}$$

where F_c is the central frequency of the Morlet wavelet, s is the scale and T_S is the sampling period.

4.5   Wavelet Thresholding: Denoising

Real-world vibration signals from rotating components are often corrupted with noise that can lead to loss of important information. As previously discussed in chapter 1, there are numerous linear filtering techniques used to remove noise and process the data for feature extractions such as time synchronous averaging or Fourier analysis. However, these frequency domain filtering are often ineffective to separate all the noise from signal due to spectra overlap.

It is crucial to remove noise from signals before diagnosis, while keeping true features untouched. Unlike the classical filtering methods, a key attribute of using wavelets is suppressing noise by means of thresholding the wavelet coefficients, and

have the signal information represented with small number of large wavelet coefficients. The thresholding approach is based on the hypothesis that small wavelet coefficients are caused by noise in the signal, while large absolute wavelet coefficients contain the important impulse characteristics. To do this, the absolute wavelet coefficients are compared with the variance of the wavelet coefficients. Therefore, it is crucial to chose a wavelet function that would match impulse components in the signal and yield high wavelet coefficients. There are numerous wavelet shrinkage methods presented in the literature (Guo and Zhang, 2012). The most famous is the wavelet scheme using hard and soft shrinkage, as proposed by Donoho and Johnstone(Donoho and Johnstone, 1995).In their work, Donoho and Johnstone proposed a wavelet denoising thresholding technique, in which the empirical wavelet coefficients are being threshold based on an appropriate shrinkage function (Φ) to remove the unwanted noise from the signal. Wavelets has the capability of thresholding its coefficients. The larger the value is an indication of true features, and the smaller the value can be presented as noise.

If we assume the background noise to be GWN with zero mean and unknown variance. After the transform, the noise-based wavelet coefficients has the same independent distribution. According to the statistical inference of Donoho, the distribution depends on the variance of the noise and number of data points. An appropriate threshold value, T is calculated based on the given data. If the wavelet coefficients are below this value, a reasonable estimator for the wavelet coefficient is zero. Thus, we cannot separate wavelet coefficients from noise. On the other hand, if large coefficients above T value are kept untouch, then an estimator is the wavelet coefficients itself. The proper choice of threshold depends on several factors: variance of noise (σ^2), sample size (N), and signal-to-noise (SNR) ratio. A large T value, yields fewer wavelet coefficients, resulting in over-smoothing. This can lead to the possibility of losing important information. On the other hand, with a small T value, yields

more wavelet coefficients. The optimum selected of T for noise damping performance still remains an open statistical problem. Wavelet denoising methods as presented by Donoho has been successfully implemented in numerous applications for image processing and edge detection.

However, it has two shortcomings when applied with mechanical diagnostics. First, the background noise might not be modeled as GWN due to the dyadic discretization, white noise means constant power at all the frequencies. Second, an orthogonal wavelet has to be used for the DWT damping noise capabilities. In this dissertation, a modified hard thresholding approach is proposed using non-orthogonal Morlet function instead of a dyadic DWT. High and low frequency components can appear in the signal with different features of mean and variance. The approach used here is a sample size-dependent threshold method, where T values are calculated for each signal of sample size, N.

Advantages of using wavelet thresholding denoising in this work are:

- Elimination of small wavelet coefficients caused by noise; minimizing false alarms

- Improvement of the proposed WI metric, represented by fewer number of wavelet coefficients

Based on these advantage attributes, a proposed a wavelet scheme for gearbox feature extraction is presented in Figure 4.2. The detailed mathematical steps for denoising WI approach is given as follows:

Step 1.The given input original signal,x(n) is modeled as:

$$y(n) = x(n) + GWN(0, \sigma^2) \tag{4.7}$$

where y(n) is the signal with GWN, N is the noise with zero mean and finite variance.

Step 2. Perform the CWT and compute wavelet coefficients $C(\tau, s)$ as explained in

equation [4.1].

Step 3. Compute the variance of noise, σ^2 from the given wavelet coefficients (Donoho and Johnstone, 1995).

$$\sigma = \frac{med(|C\tau, s|)}{0.6745} \tag{4.8}$$

where $med(C\tau, s)$ is the median of the absolute wavelet coefficients.

Step 4. Thresholding the coefficients using a universal threshold, T value (Narona et al., 2013).

$$T = \sigma^2 \sqrt{2log(N)} \tag{4.9}$$

where σ^2 is the variance of wavelet coefficients, N is the number of samples. In this study, thresholding is performed on different intervals of collected gearbox data to compute different T values with noise reduction capabilities

Step 5. This step attempts to remove the irrelevant wavelet coefficients caused by noise. Thresholding is performed using the following shrinkage function (Narona et al., 2013):

$$\Phi = \begin{cases} y, & \text{if } |y| \geq T \\ 0, & \text{if} |y| < \text{T} \end{cases}$$

Step 6. Reconstructing the original denoised signal, y(n) by computing the inverse continuous wavelet transform (iCWT) from the revised wavelet coefficients. Despite the redundancy of CWT, an approximate reconstruction of the signal is possible from a subset of CWT coefficients.

$$s(n) = \frac{1}{C_\psi} \sum_{n_1}^{n_2} C_i'(s, n) s^- 3/2 \tag{4.10}$$

where C_i' is the revised wavelet coefficients, and C_ψ is defined in equation [4.3].

Step 7. Compute the WI metric after eliminating irrelevant wavelet coefficients due to noise.

58

Step 8. In this last step, a statistical analysis is performed by evaluating the root-mean square error (RMSE), SNR, and correlation coefficient (R). These metrics are commonly used in the literature to evaluate wavelet denoising reduction performance (Narona et al., 2013).

$$RMSE = \sqrt{\frac{1}{N}\sum_{i=1}^{N}(std_{Originalsignal} - std_{Denoisedsignal})^2} \qquad (4.11)$$

The SNR can be determined as:

$$SNR = 10log_{10}\frac{\sum_{i=1}^{N}(Denoisedsignal)^2}{\sum_{i=1}^{N}(originalsignal - denoisedsignal)^2} \qquad (4.12)$$

The correlation coefficient is a statistical measure that illustrates resemblance of predicted signal and original signal.

$$R = \frac{\sum_{i=1}^{N}(x - \bar{x})(y - \bar{y})}{\sqrt{\sum_{i=1}^{N}(x - \bar{x})^2 \sum_{i=1}^{N}(y - \bar{y})^2}} \qquad (4.13)$$
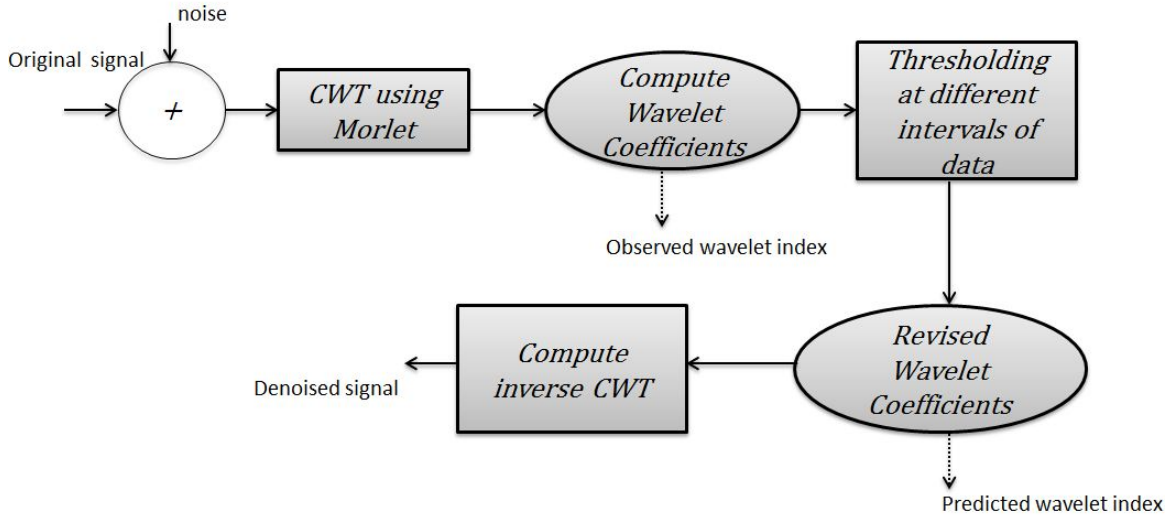

Figure 4.2: A proposed wavelet scheme for denoising the wavelet index

4.6 Statistical Test on Wavelet Power Spectrum

In this section, statistical analysis is extended to prove if wavelet power spectrum results are statistically valid through a statistical test, which should be taken into consideration to avoid misinterpretation of the data. Statistical tests using wavelets is not something new and has been extensively studied in the literature(Torrence and Compo, 1998; Ge, 2008). However, their work was limited to theoretical signals and few actual observations, here we will extend the developed statistical test for wavelets using real-world vibration data from mechanical systems. The same reasonable assumption is valid in which the wavelet power spectrum of studied samples follows a normal distribution about a mean value. Ge created the null hypothesis from the wavelet power sampling distribution of GWN for the statistical test that was found to be dependent on the covariance of wavelets at different time locations. Consequently, this significant test depends on the choice of wavelet functions, as well as, distribution of wavelet power at different time locations. The mean wavelet power spectrum (or WI) can be shown in equation [4.15], and is defined as sum of the absolute wavelet power spectrum values that are located at different time shifts and at a particular scale or frequency. Finally, the null hypothesis when only using Morlet wavelet is given by equation [4.14].

$$\frac{|C|^2}{\sigma^2} \Longrightarrow \frac{1}{2}\delta t X_k^2 (1 - \alpha) \tag{4.14}$$

$$C(\bar{s})^2 = \frac{1}{N} \sum_{n=n_1}^{n_2} |C(s,n)^2| \tag{4.15}$$

Equation [4.14] shows that the normalized wavelet power have a chi-squared normal distribution only when using Morlet wavelet function, where k is the degree of freedom (k=2, incase of Morlet), δt is the sampling time, σ^2 is the variance of input

vibration signal, and $(1 - \alpha)$ is the significance level for confidence interval, α can have different values such as 0.05, 0.01, and 0.1, and depending on the application.

The null hypothesis is accepted if a wavelet power spectrum peak is below the significant level and can be inferred due to random noise. On the other hand, the null hypothesis is rejected, if wavelet power spectrum is above this level, then one can say that the wavelet results are statistically significant with a confidence level that represent true features of the system.

CHAPTER 5

OIL NANOLUBRICANT TESTING: A NEW APPROACH

5.1 INTRODUCTION

This chapter consists of two main parts. The first is testing of nanofluids in a preliminary test-bed known as 'no-load' test stand. The second part is nanofluid testing in the TRDT test stand with load being applied. Numerous vibration and temperature data are collected during the experiments to investigate the impact of nanofluids on IGB responses. The newly developed wavelet index is applied on the raw vibration data as a metric to reflect on lubricant testing conditions. Furthermore, viscosity measurements are performed after gearbox testing to investigate changes in rheological characteristics of nanofluids.

5.2 NO-LOAD NANOFLUID TESTING

The purpose of this testing is to filter out poorly performed oil samples in the IGB based on the dynamic responses and to reduce the number of variables tested on the full-load TRDT. The no-load test stand in Figure 5.1 is capable of being used as a preliminary test bed for components before moving to the full-load test stand. Currently, the no-load test stand is set up similarly to the tail rotor drivetrain test stand. It is driven by a 5 horsepower motor and it allows for full speed testing of components without applying a torque load. It is worthy of mentioning that in the no-load there are difficulties in identifying the frequency components in the IGB due

to the free vibration, noise or other components in the drivetrain sharing similar frequencies. For the purpose of this task, as much as possible, analysis is performed as if no other vibrational information are present.

Testing is preformed on an IGB that was removed from an Apache aircraft after completing its lifetime. A design of experiment (DOE) approach is applied , where the four chosen nanofluid samples alongside a fifth control AGL sample (0%NPs) are tested for a thirty minute experimental run per sample (Table 5.1). The purpose of this DOE is to identify the dominant factor that would yield optimum responses. The concentration of NPs is the tested factor with different levels of concentrations, and vibration and temperature are the experimental responses. Each sample is tested three times, and after completing all the experimental runs of a tested sample, the gearbox is drained and flushed at least 3 times using fresh oil to ensure the removal of oil from the previous experiment. All experiments are performed in a controlled climate lab environment.
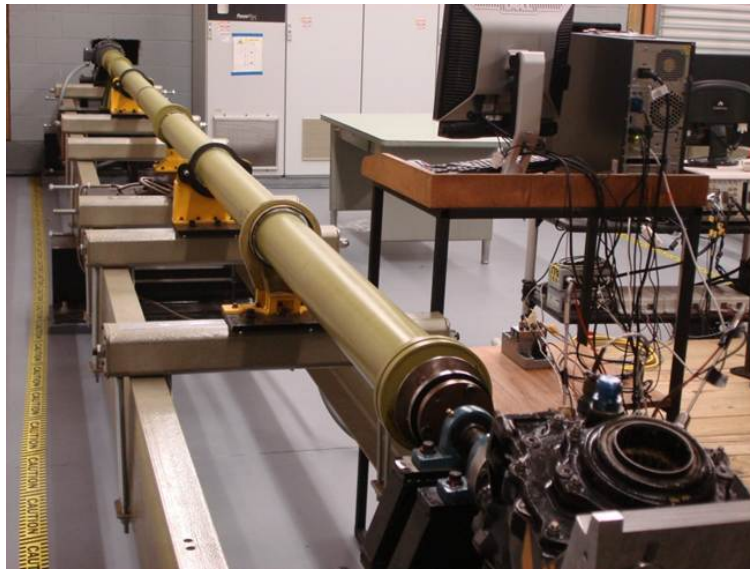

Figure 5.1: No-load test stand at USC

Table 5.1: Design of experiment on no-load test stand: 15 total of experimental runs

Experimental run	NP Concentration (vol%)
1,2,3	0% (control sample)
4,5,6	1%
7,8,9	1.5%
10,11,12	2%
13,14,15	2.5%

5.3   DATA DESCRIPTION

NI-DAQ (cDAQ-9174) is used to acquire vibration data that is collected periodically during the thirty minute experimental run (Figure 5.2). The responses are measured using sensors as illustrated in Figure 5.3; a spark type accelerometer to measure vibration from the gearbox and a K-type thermocouple that measures temperature close to the gear mesh. On the other hand, temperature data is collected continuously during the coarse of the experiment. The following sampling parameters are used:

- Total sampling period: 4 s
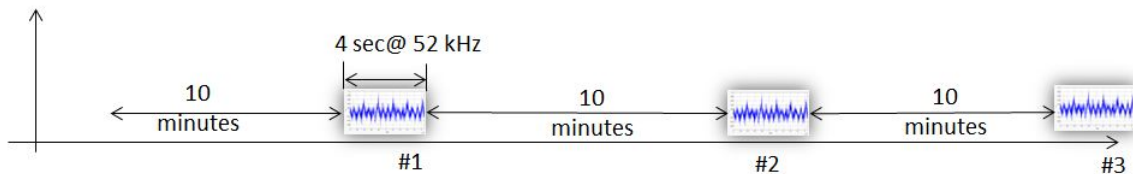
- Sampling Frequency: 52 kHz

Figure 5.2: Acquiring vibration data

Oil in the gearbox lubricates both gears and bearings with a fluid film between moving surfaces. So, it is crucial to measure bearing temperature to investigate the
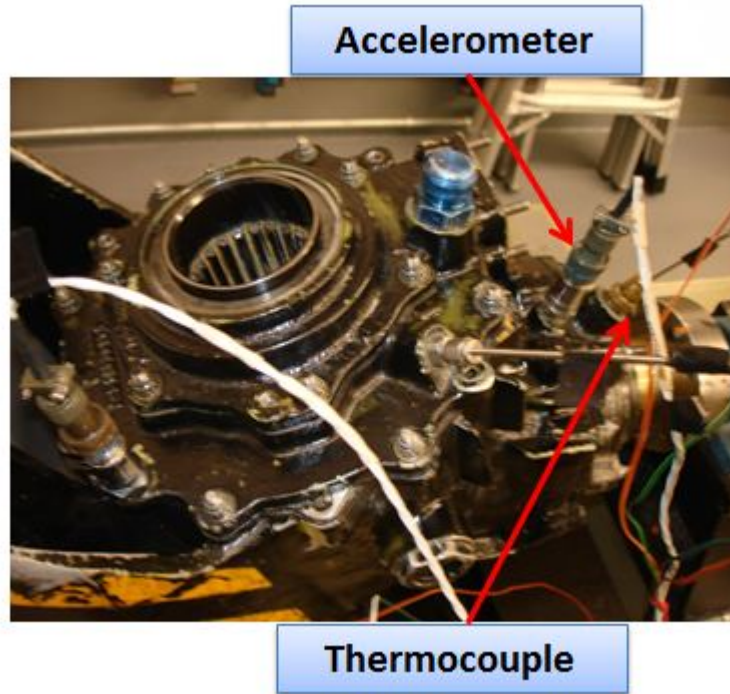
Figure 5.3: Accelerometer and thermocouple sensors on IGB

impact of nanofluids on bearings. Additional thermocouple sensors are installed near the input roller bearing (IRB) and output dublex bearing (ODB), as illustrated in Figure 5.4.

5.4 Results and Discussion

5.4.1 Temperature Analysis

Temperature readings for two experiments performed on the no-load stand are summarized in Figure 5.5. The response of the lubricants have the same trend from both experiments, almost reaching steady state after 25 minutes. A significant improvement is seen in temperature responses due to the implementation of NPs in the oil lubricant. The 1.5% and 2% NP samples demonstrate an operating temperature near $150°F$, which is approximately $35°F$ less than that of base AGL, while the 1% shows minimum improvement.

Figure 5.4: Different thermocouple sensors on IGB

As briefly mentioned in chapter 1, the lubrication mechanism between gears is the EHL, where friction is dependent on shearing of the lu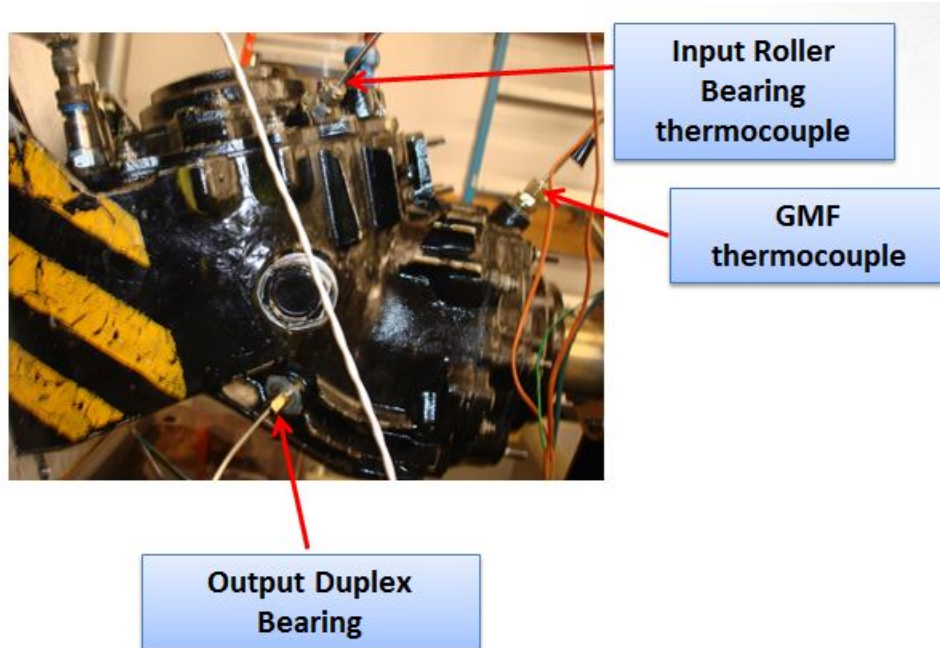bricant film. As such, the nanolubricant maintains a solid film between gear surfaces, with particles having high surface area-to-volume ratio. This means it has the capability to absorb heat generated due to friction more effectively than the base AGL, carrying it through the lubricant, and speeding heat transfer between the oil and metal contaminants. The heat dissipates away by conduction or convection, resulting in the cooling of the gearbox. Surprisingly, the 2.5% had an operating temperature higher than that of base AGL. Apparently, excessive amount of heat is generated due to incorporation of the NPs in oil. Analysis of other system dynamics in the upcoming sections are investigated. Results are connected to the nanofluid mechanism from chapter 3 to interpret the reason of the unexpected high temperature response of the 2.5% nanofluid. Overall, these temperature results are promising to improve the performance of the gearbox with the possibility of reducing friction and slowing oil break down.
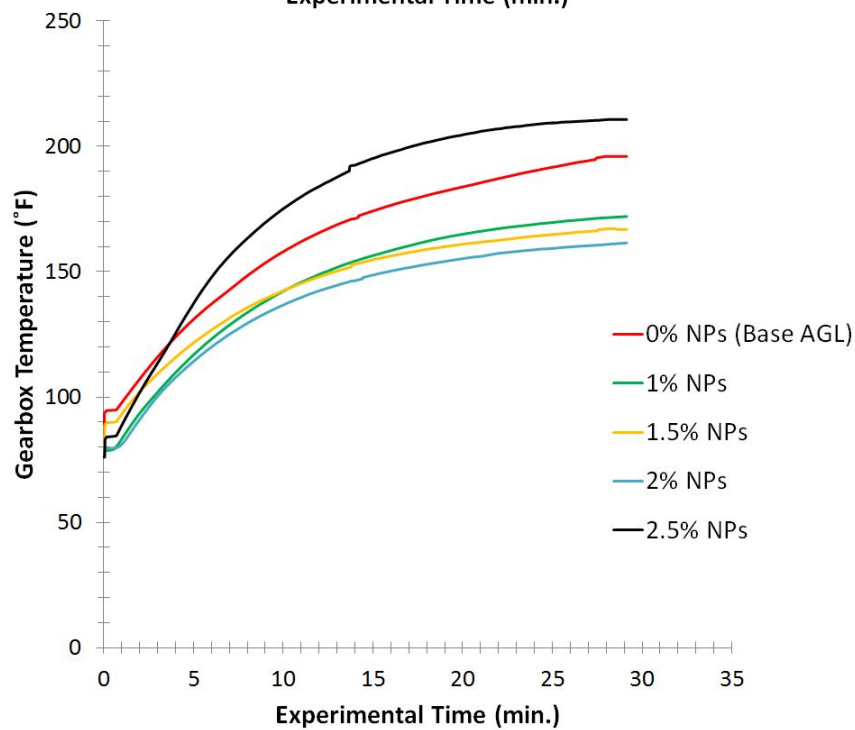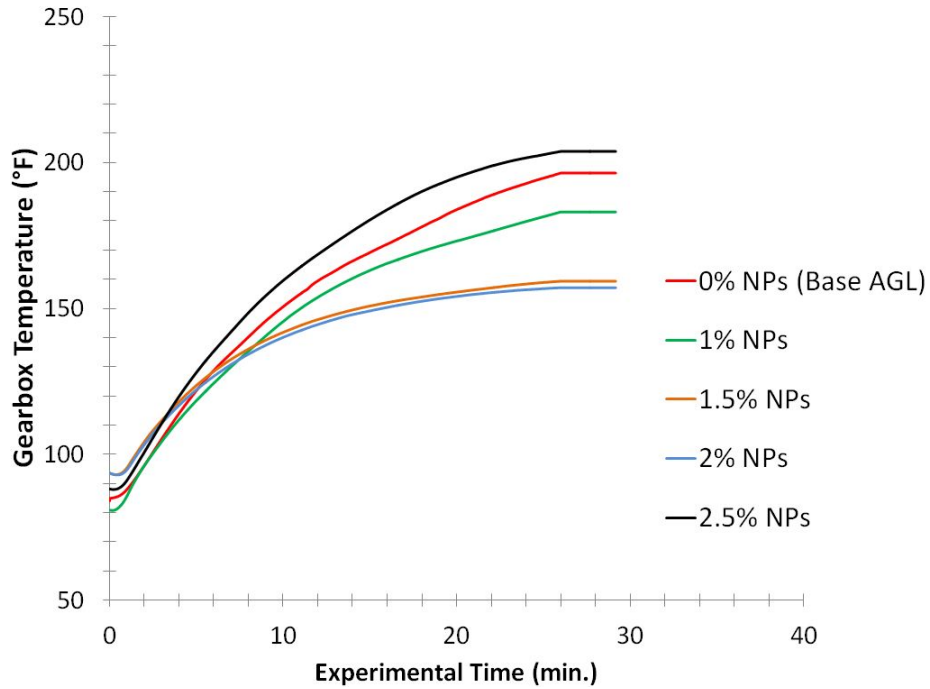
Figure 5.5: Average operating temperature of IGB on the no-load using different oil samples from no-load experiments

From the same experiments, bearing temperature plots are summarized in Figures 5.6 and 5.7. The 1.5% sample has demonstrated slight decreases in IRB and ODB temperatures, compared to AGL. The response from the 2% sample has shown the

most significant decreases in temperature. On the other hand, the 2.5% sample had minimum improvement effect on bearings, where the thermal plot demonstrated responses close to that of the AGL, indicating poor thermal characteristics.

Nanofluids also have an impact on improving bearing temperature. In the case of nanofluids, a very strong lubricant film between the surfaces is formed that absorbs heat and cools supporting bearings of the IGB.

Figure 5.6: Average bearing temperature of IGB on the no-load. Base AGL (left) and 1.5% (right)

Figure 5.7: Average bearing temperature of IGB on the no-load. 2% (left) and 2.5% (right)

68

5.4.2 Vibration Analysis

A typical waveform from the collected raw vibration data can be seen in Figure 5.8. These signals are complex and have a low SNR to extract meaningful vibration features. The data has to be further processed for better feature extractions.
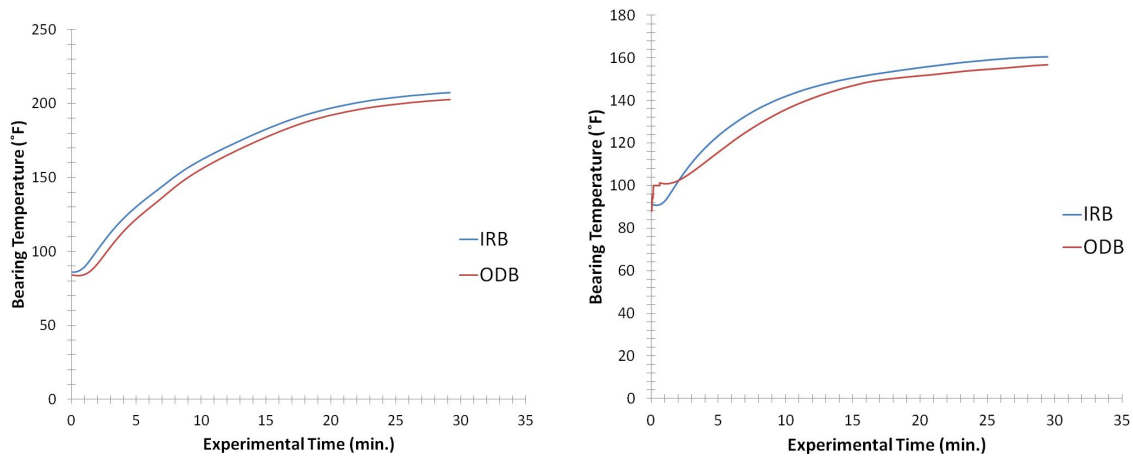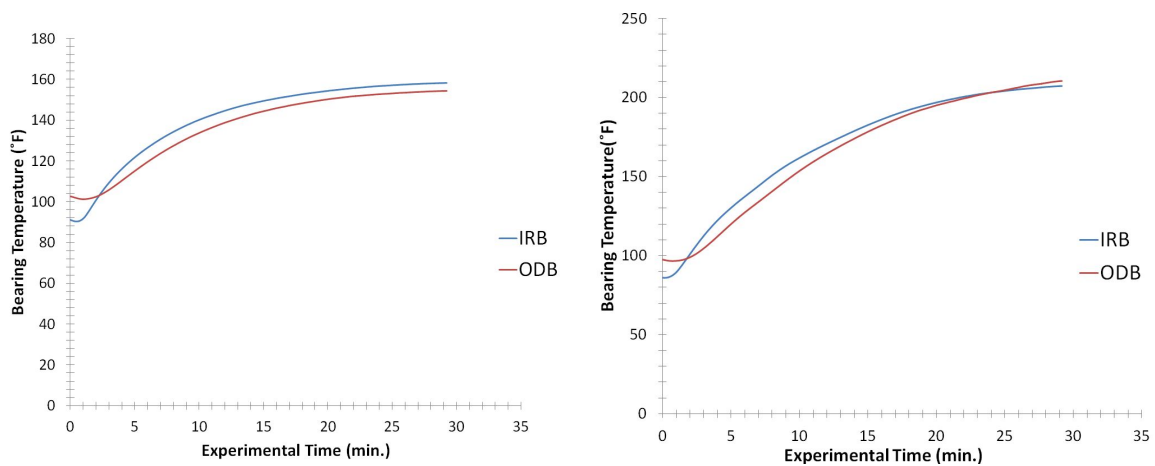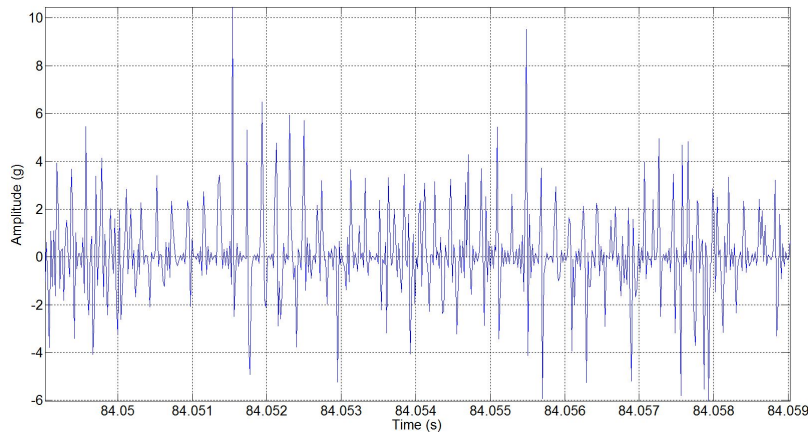

Figure 5.8: Example of waveform sample collected from Intermediate gearbox

Spectral analysis is a tool used for diagnostic capabilities in rotating machinery. A gearbox spectrum contains vital information about this complex system that include: shafts rotational frequency, bearing frequencies, GMF, harmonics, and sidebands. Other high frequency components can be excited in the spectrum such as structural resonance or noise.

Samples of the auto-power-spectrum (PS) from the oil experiments is presented in Figured 5.9 and 5.10. PS plots show the majority of energy near the GMF of IGB at 3000 HZ with the presence of other GMF harmonics, sidebands and other high frequency components. As previously mentioned due to the nature of the no-load test stand, there is a possibly of having other high frequency noise from the remaining drivetrain components in the spectrum and it is extremely challenging to distinguish true vibrational properties.

For a qualitative description of the system, cumulative sum of numerous PS samples taken at different time-locations of no-load testing are summarized in Figures

69
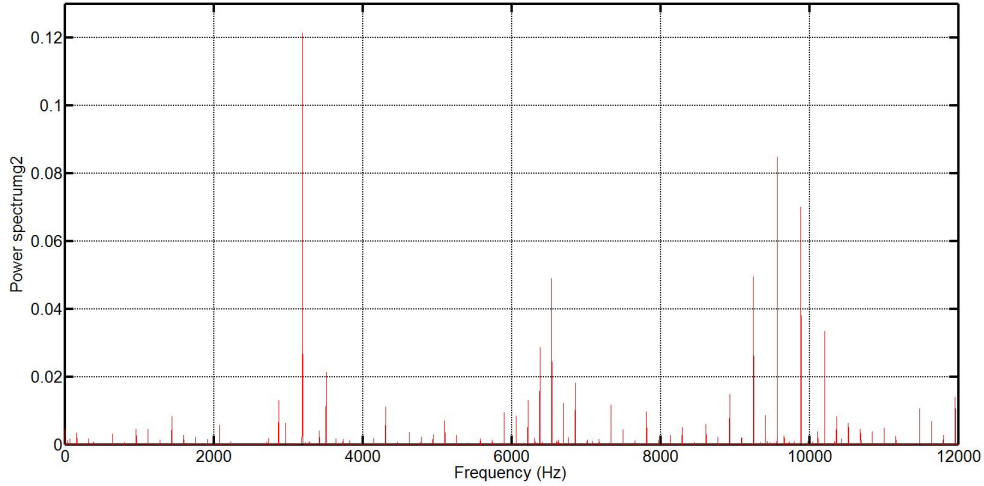
Figure 5.9: Example of power-spectrum (Base AGL)
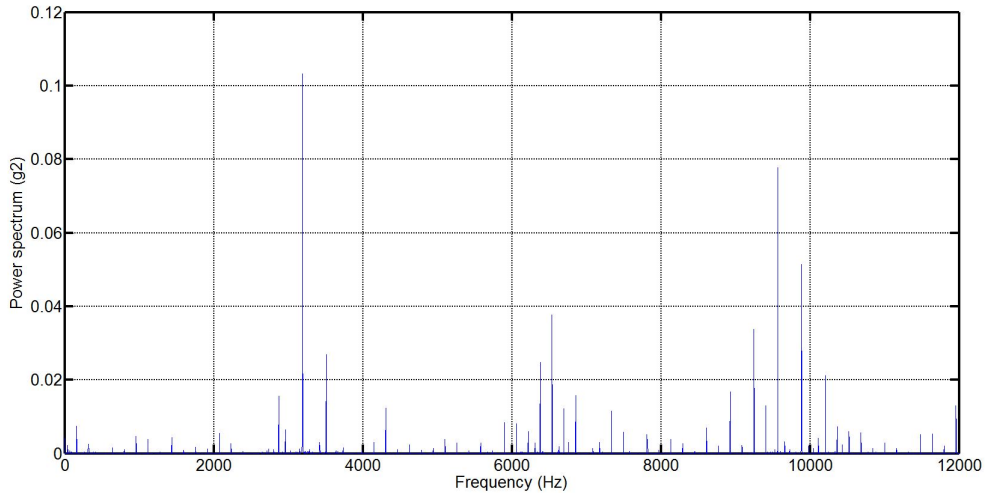
Figure 5.10: Example of power-spectrum (2% nanofluid sample)

5.11-5.13. A trend develops from these different samples. Nanofluid show almost little to no impact impact on improving vibrations of low-frequency bearing components that approximately range from 500 Hz-29000 Hz. However, differences in frequency response for the tested lubricants appear at high gear mesh harmonics (>3000 Hz), where the 2% NP sample displays overall less vibrational energy, compared to all tested samples, and the 2.5% NP sample has the highest energy response.

It can be theorized that the damping effect in vibration at high gear mesh frequency harmonics is attributed to the impact of nanofluids. It lubricates gears

through a solid fluid film, where the NPs act as a filler or bundles between surfaces, having the capability to absorb load and reduce vibration effects. These key vibrational characteristics that represent the actual physical system (eg. misalignment, wear, or friction) start to appear due to interactions between gear surfaces and are picked up by the gearbox spectrum.
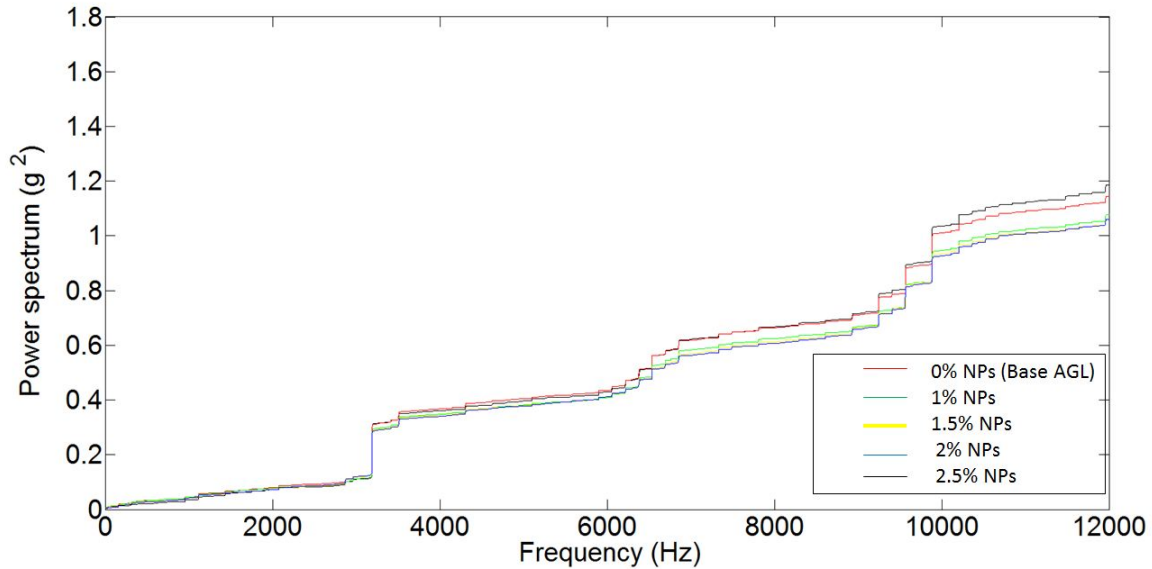
Figure 5.11: Cumulative sum of PS plot after 10 minutes
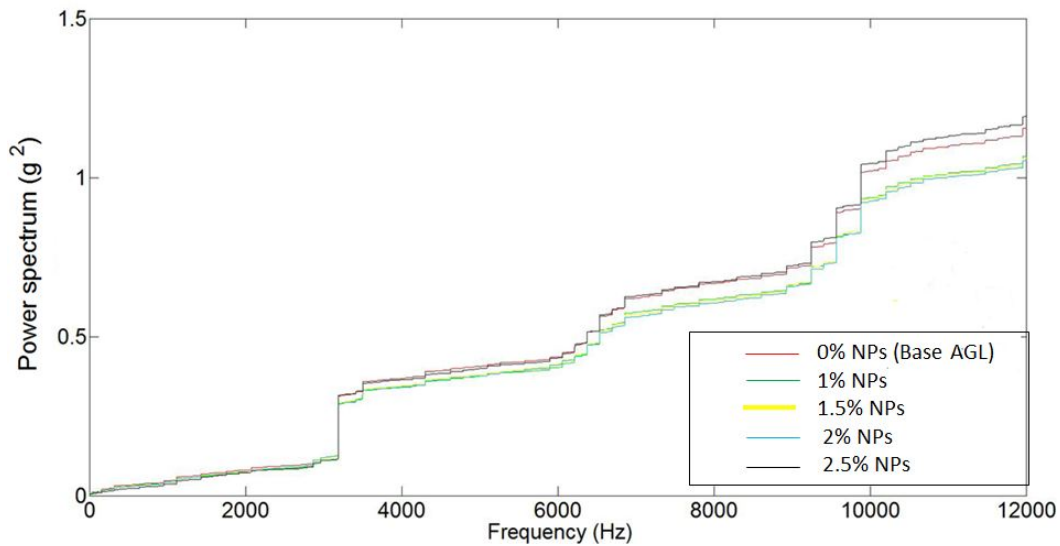
Figure 5.12: Cumulative sum of PS plot after 20 minutes

71
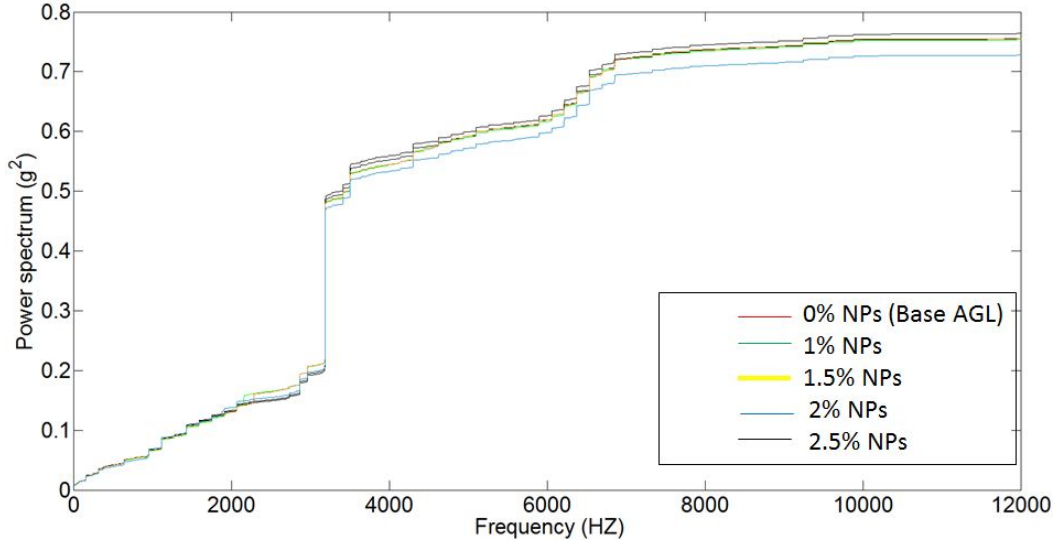
Figure 5.13: Cumulative sum of PS plot after 30 minutes

Wavelet analysis is performed to validate spectral results an to capture periodic impulses that are still buried in noise. Impulses are localized in time, therefore, it is preferable to perform the analysis at finer time granules. The sampling period of four seconds collected on the no-load test stand are cut-off into smaller window samples of 0.01 seconds to accurately capture transients in signals.

Wavelet plots at different temporal locations are summarized in Figures 5.14 and 5.15. Additional frequency bands in the ranges of 1000 Hz-2800 Hz from the 2.5% nanofluid samples are repeated. These transient characteristics can also be seen from the base AGL samples, but with a slightly less distribution. On the other hand, the 2% nanofluid samples have less vibrational distribution near bearing frequencies. These frequency components represent second, third, and fourth energies of ball pass frequency. Moreover, the repeated wavelet peak distributions near GMF harmonics from the base AGL and the 2.5% nanofluid samples progress with more intensity, compared to distribution from the 2% sample.

These impulses can occur due to poor lubrication between gears or on the inner-race or outer-race of a bearing. As a gear or roller spin through a defect an impulse can appear that can be the start of a possible fault in the system and have to be

detected in its very early stages. It can be theorized that the nanofluid properties near surface become important in reducing vibration effects through maintaining a strong lubricant film during friction. The high surface-area-to volume ratio of the particles increases the capability of the lubricant to absorb loads effectively.
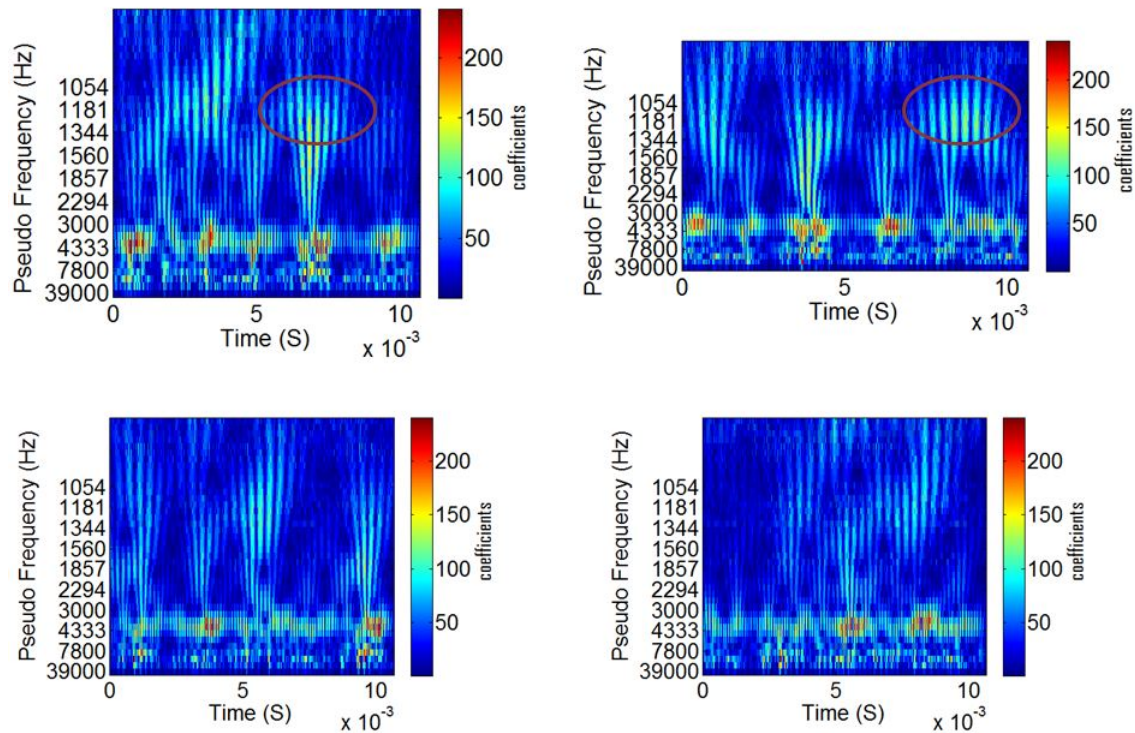
Figure 5.14: Wavelet plots during gearbox testing.2.5% nanofluid (top) and base AGL (bottom). Circles represent regions of additional frequency components

The proposed WI is applied on the truncated experimental data at different time intervals and for different lubricants and computed at a frequency where majority of energy appears, 3400 Hz. Results are summarized in Figure 5.16. As the concentration of NPs increase, WI values demonstrate a decreasing trend for 0.5%, 1%,1.5%, and 2% samples due to the incorporation of the nanolubricants. However, WI yields the highest value for the 2.5% sample, which is an indication of more transient characteristics.
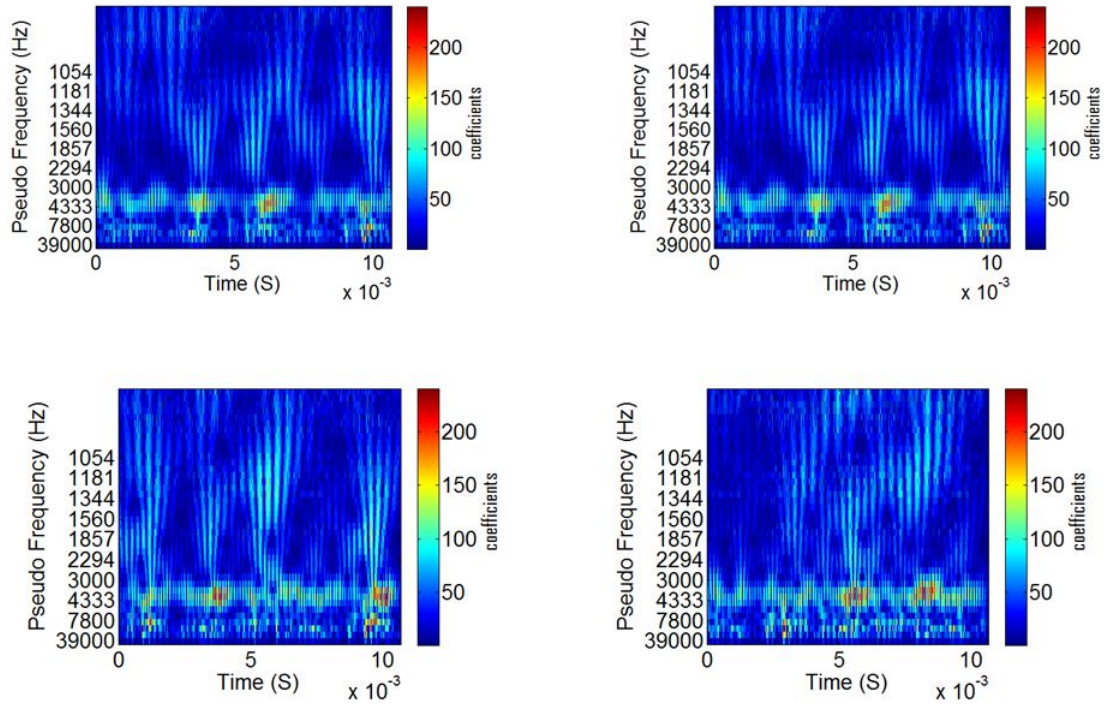
Figure 5.15: Wavelet plots during gearbox testing. 2% nanofluid (top) and base AGL (bottom)

These wavelet results agree with the conventional spectral analysis and validate the importance of nanofluids to reduce vibration effects by maintaining a strong lubricant film between surfaces that tend to reduce vibration sources at high gear mesh frequency harmonics
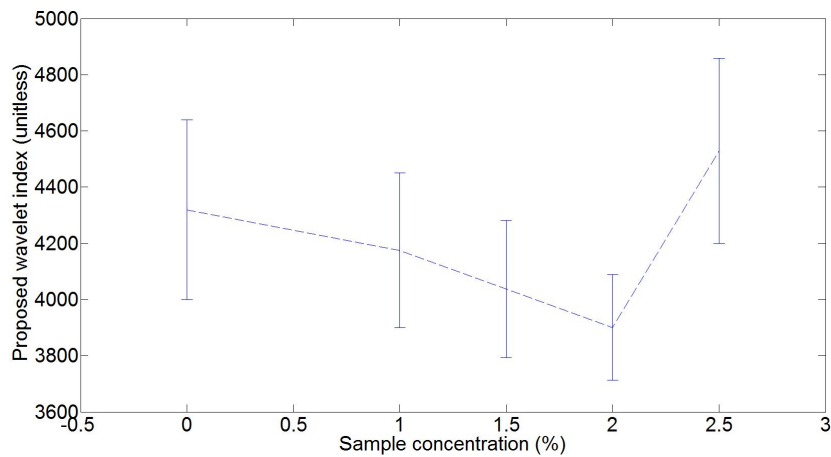
Figure 5.16: Proposed wavelet index for tested lubricants on no-load test stand. Error bars represent mean ± std

74

5.4.3 Viscosity Analysis

Nanofluids are expected to be applied in real-life applications with flow conditions and so viscosity plays a key role in performance and is affected by many factors. Shear-rate and temperature are two of them that impact rheological characteristics of nanofluids. In this section, we will investigate these effect on the tested nanofluids. Rheometer measurements are performed under lower shear rate conditions than the real gearbox. However, viscosity results give an important understanding of impact of NP additives in oil on the rheological characteristics, predicting the expected behavior of tested lubricant in a gearbox.

Shear-rate dependence

After gearbox testing, the dynamic viscosity of used oil are measured in the rheometer and results are summarized in Figure 5.17. Results illustrate that nearly all nanofluids had a Newtonian plateau with slight decreases in dynamic viscosity values even after gearbox testing. However unlike the initial results of fresh oil from Figure 3.9, the 2.5% nanofluid sample clearly demonstrated a shear thinning behavior due to the NPs. These results seem to be consistent with findings in the literature that showed low viscosity NP dispersions are approximated as Newtonian fluids, where as high viscosity NP dispersions ($> 3\%$) demonstrate non-Newtonian flow (Zhou et al., 2010).

From a colloidal suspension point of view, Newtonian fluids are changed to non-Newtonian fluids due to complex interactions between the fluid and particles. Recalling nanofluid model results from chapter 3 that concluded key mechanism for increasing thermophysical properties is the hydrodynamic interactions between fluid and particles. Therefore it can be hypothesized that under high shear rates, aggregations are formed in the relatively high concentration 2.5%, leading to an inhomogeneous network structure of NPs that negatively impact fluid properties and possibly to disrupt dynamic interactions of the particles. This means that nanofluid sample would form an ineffective lubricant film between gears and bearings. Mechanical fric-

tion may start to occur, and this explains high temperature and vibration responses from onboard sensors that are presented earlier in this chapter. Low concentration nanofluids have small shear-rate dependence and can be approximated as Newtonian fluids. However, relatively high concentration of particles in nanofluids often show non-Newtonian behavior due to shearing of NP additives.
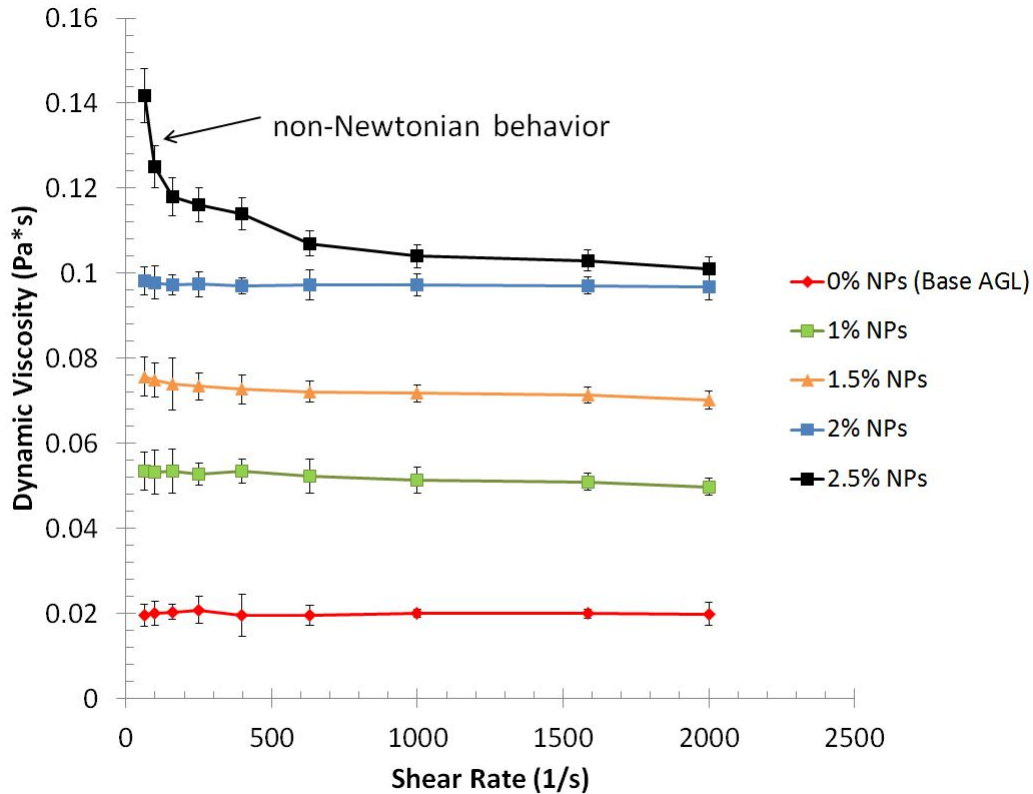
Figure 5.17: Rheometer results for tested AGL nanofluid samples. Error bars are mean $\pm$ std, n=5

Temperature dependence

The nanofluid model from chapter 3 illustrated that temperature dependence of nanofluid viscosity is vital, as it influences hydrodynamic interactions. As a result, temperature dependence on the absolute viscosity and relative viscosity ($\mu_r = \mu/\mu_b$) of nanofluids are investigated. A TA AR2000 rheometer with a temperature sweep feature is used to measure relation between apparent viscosity and temperature. The following controlled variables are used:

- Temperature ranges from $8°C$-$56°C$

- 1% strain applied to allow flow of material

- Speed of motor is 60 rpm

The relation between viscosity of nanofluids and temperature is summarized in Figure 5.18. As expected for for all liquids, viscosity of nanofluids decrease with the increase of temperature. However, the change of dynamic viscosity with temperature is slightly greater for the largest concentration Np sample, compared to all tested fluids.
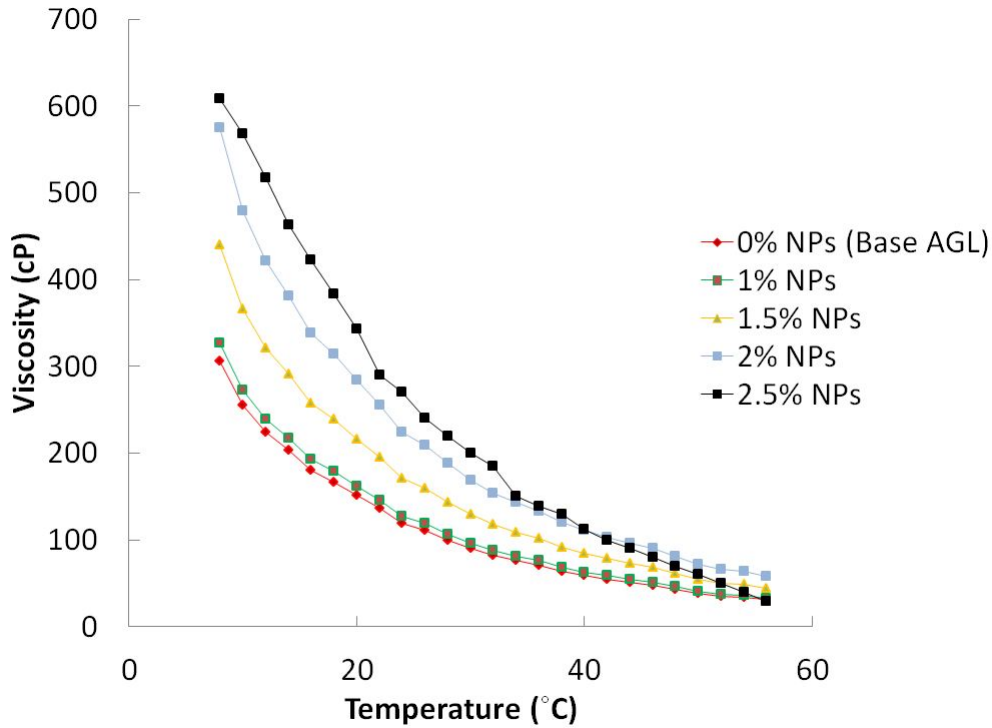
Figure 5.18: Relation between dynamic viscosity of nanofluids and temperature

The viscosity-shear rate results presented is a motive to explore more on the relation between relative viscosity, μ_r and temperature of nanofluids. Relative viscosity is computed and is plotted against temperature for all nanofluid samples in Figure 5.19. According to this graph, relative viscosity for the 1%, 1.5%, and 2% is almost

constant against temperature with values around 1.5 ± 0.04, 1.79 ± 0.02, and 2.24 ± 0.07, respectively. However, the relative viscosity of the 2.5% nanofluid sample decreases with increasing temperature. These relative viscosity trends with temperature are consistent with results in the literature (Zhou et al., 2010).
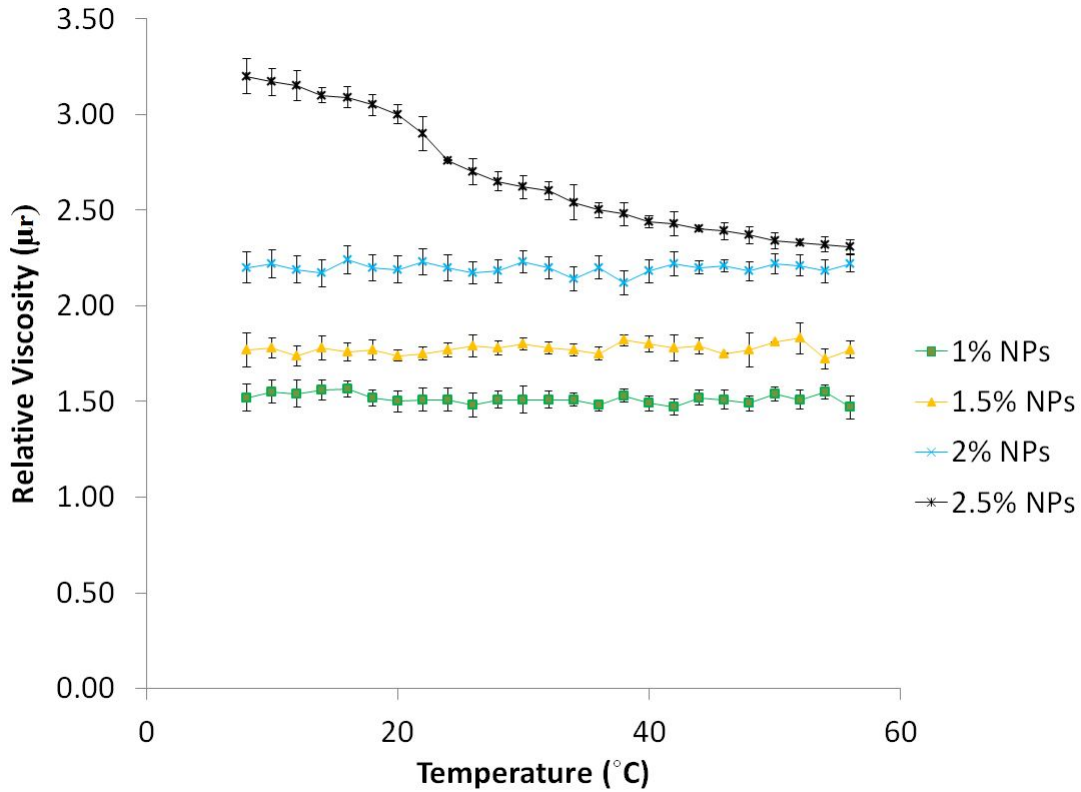
Figure 5.19: Relation between relative viscosity of nanofluids and temperature. Error bars are mean ± std, n=5

From these findings, it is clear that most of the studied nanofluids can be approximated to be independent of temperature, which means that changes in rheological behavior is mainly due to the base fluid (BF) rather than the incorporation of NPs. Moreover, the 2.5% nanofluid sample has a relative viscosity dependent on temperature, which means the movement and dynamics of NPs is dominant more than BF effects. Another interesting observed effect is that nanofluids either demonstrate Newtonian rheological characteristics with relative viscosity temperature indepen-

dence (1%, 1.5%, and 2%) or have non-Newtonian rheological characteristics (2.5%) with temperature dependence of relative viscosity.

5.5 Preliminary Gearbox Testing Conclusions

Preliminary gearbox testing is successful as an intermediate or optimization step to test the performance of the nanolubricant samples and in achieving its objective before the main TRDT testing. The following conclusions are drawn:

- Initial vibration and temperature results indicate the promising features of the nanolubricants.

- 2% nanofluid sample yielded optimum results and the 2.5% yielded unsatisfactory results.

- High viscosity AGL nanofluids are possibly more susceptible to rheological changes in the gearbox due to high shearing of NPs.

- Viscosity results provides a fundamental understanding of particle-fluid interactions and can be linked to online gearbox responses

- AGL nanosamples demonstrate both Newtonian and non-Newtonian rheological characteristics that can be empirically correlated to temperature of relative viscosity of nanofluids.

The 2% sample is further tested in the IGB of the full-load TRDT test stand alongside a base AGL sample for comparison purposes.

5.6 Full-load Nanofluid Testing

The same IGB from preliminary testing is used on the main TRDT to minimize the number of variables (Figure 5.20). On the main test stand, we investigate the

effectiveness of nanofluids in a full-scale mechanical system with coupling effects from other drivetrain components. A single test run on the TRDT is 4 hours long where the torque is ramped up from 0 ft-lb to 1223 ft-lb during the experimental run with a 10 minute survey at a constant load step of 111ft-lb (Table 5.2). These specific conditions of speed, time of test and torque match those of flight regimes as requested by AED (Goodman, 2011). In this work, a total of four IGB experiments are performed that sums to a total of 16 testing hours.

- 4 hrs base AGL; 1 experiment

- 12 hrs nanofluid; 3 experiments
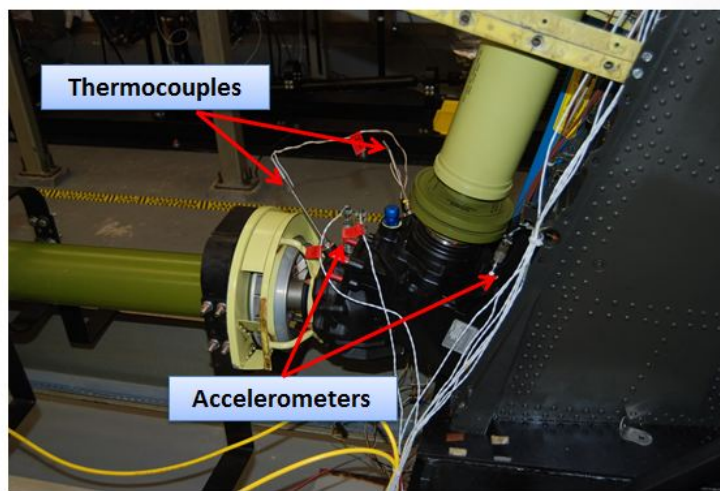
Figure 5.20: IGB on full-load test stand

Table 5.2: Load profile of AH-64 TRDT test stand

Time (hrs)	Output Torque(ft-1b)	hp
00:00-00:10	111	30
00:10-01:00	371	100
01:00-01:10	111	30
01:10-02:00	734	198
02:00-02:10	111	30
02:10-03:00	979	264
03:00-03:10	111	30
03:10-04:00	1223	330
04:00-04:10	111	30
> 04:10	0	0

5.7 DATA DESCRIPTION

As briefly mentioned in the introduction chapter, data is collected from two DAQ sources: MSPU and NI. MSPU is the source for vibration-based CIs. NI collects raw data for validating, improving or creating new CIs. In this section, we investigate both MSPU-CIs and results from analysis of raw data. The following are the DAQ parameters for the collected data.

- **Experiments 1 and 2**. Vibration data is sampled and collected during survey with parameters: total sampling period (4 s), sampling rate (F_s=48 kHz), and number of samples (N)=192000 samples. Moreover, temperature data is collected continuously.

- **Experiments 3 and 4**. Vibration data is sampled and collected every 2 minutes: total sampling period (0.17 s), sampling rate (F_s=48 kHz), and number

of samples (N)=8192 samples. Moreover, temperature data is collected continuously.

5.8   Results and Discussion

5.8.1   Temperature Analysis

Thermal plots are illustrated in Figures 5.21-5.23, where the nanofluid sample approximately operates $45°F$ cooler than different responses obtained from base AGL. This reduction in temperature is crucial that validates no-load results and shows potential of this nanofluid to enhance oil performance. It is worthy of mentioning that the thermal plots illustrate the effect of loading on the IGB temperature where the increases in temperature regions correspond to the loading periods and the areas of decreases in temperatures correspond to the cooling regions during the MSPU survey.

This new finding indicates the ability of nanolubricants to improve existing CI temperature response.
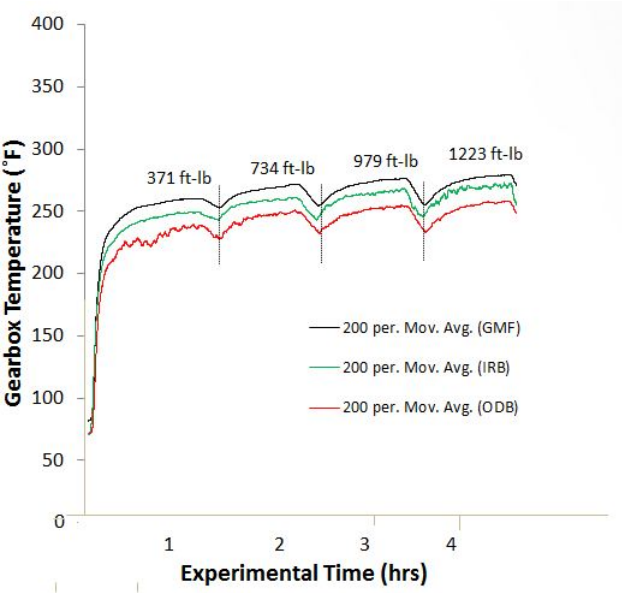
Figure 5.21: Experiment 1. IGB temperature response of base AGL response from full-load test stand
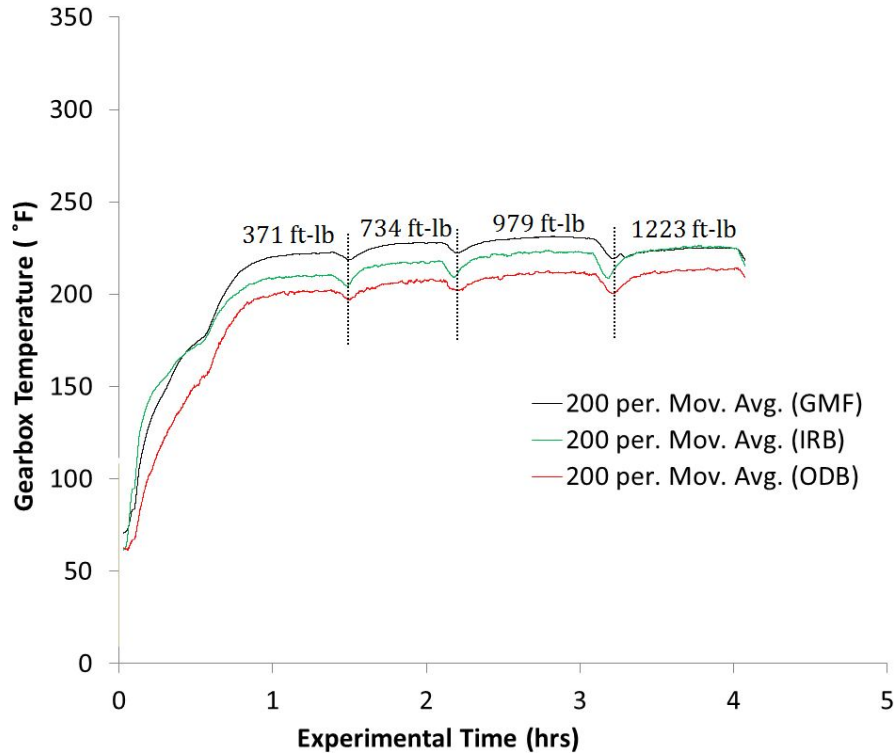
Figure 5.22: Experiment 2. IGB temperature of nanofluid response from full-load test stand

5.8.2 Vibration Analysis

Two key MSPU-CIs extracted from the vibration signatures are presented in Figure 5.24. The nanolubricant sample has a noticeable impact on those CIs, the intensity of FM4 CI is less than that obtained from the base AGL through the coarse of the experiments. FM4 CI of the nanofluid is fluctuating near 4, and the FM4 CI of the base AGL is near 3-3.4.

The second CI is the FM0, which almost trends in a similar way as the presented FM4. FM0 CI of the nanofluid is hovering near a value of 10 and the FM0 CI of the base AGL is almost constant at 12.

FM0 CI is an indicator sensitive to major wear or vibrational characteristics at the gear meshes, while FM4 is more sensitive to minor wear or localized vibrational char- acteristics at the gear meshes. As interactions occur between gear surfaces, friction-
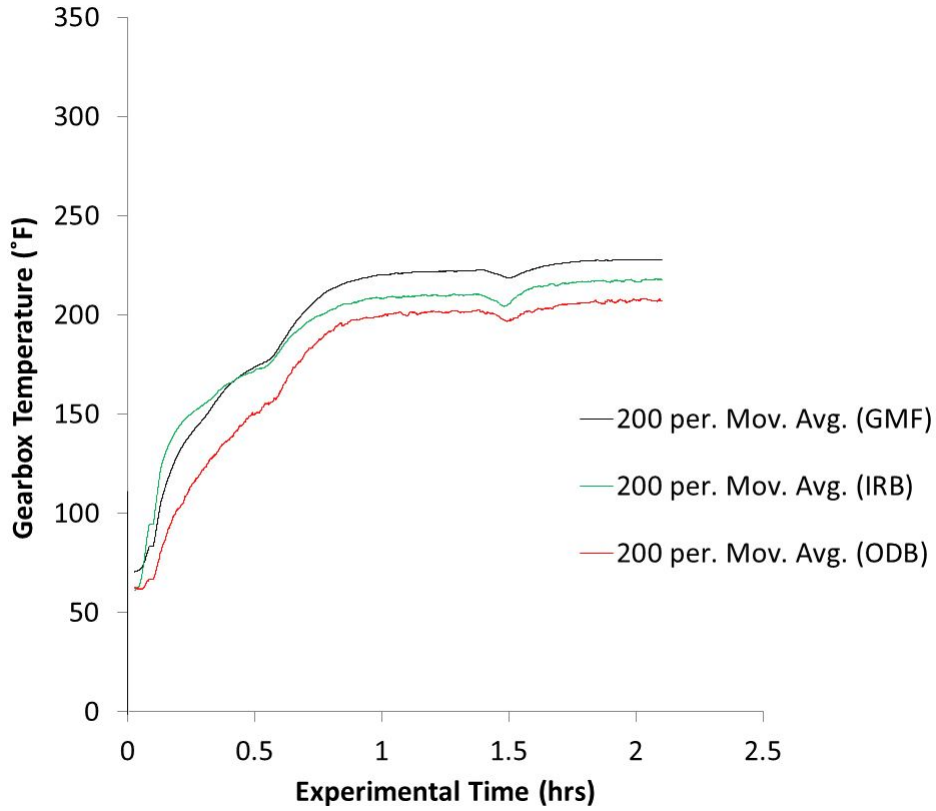
Figure 5.23: Experiment 3. IGB temperature of nanofluid response from full-load test stand

induced vibrations is strongly dependent on shearing of lubricant film. As such, CI responses from nanofluid experiments subside, compared to those obtained from base AGL.
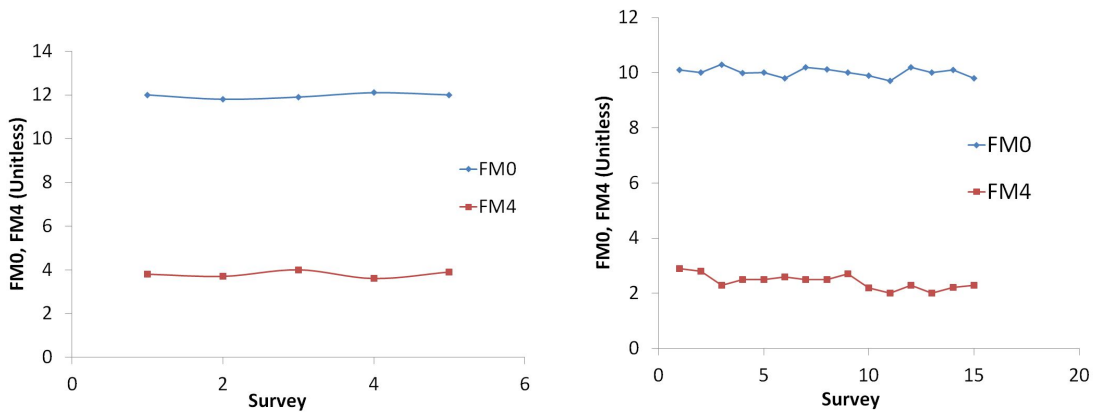
Figure 5.24: Condition indicator results. Base AGL (left) and 2% (right)

Raw vibration data is used to validate MSPU results, and produce a new CI from nanofluid experiments. This is achieved through the following frequency-domain analysis and wavelet analysis.

FFT samples taken periodically throughout the IGB experimental runs are summarized in Figure 5.25. The majority of vibrational energy for base AGL and the nanofluid plots is located at the first GMF of 3000 Hz with a few sidebands, and other GMF harmonics at 6000 Hz and 9000 Hz. Furthermore, the spectrum contains few energies for 1st, 2nd, and 3rd harmonics of ball pass frequency input at frequencies of 794, 1588, and 2382, respectively. Vibration amplitudes of the nanosample experiment at different frequencies is less in magnitude across the bandwidth of the spectrum.
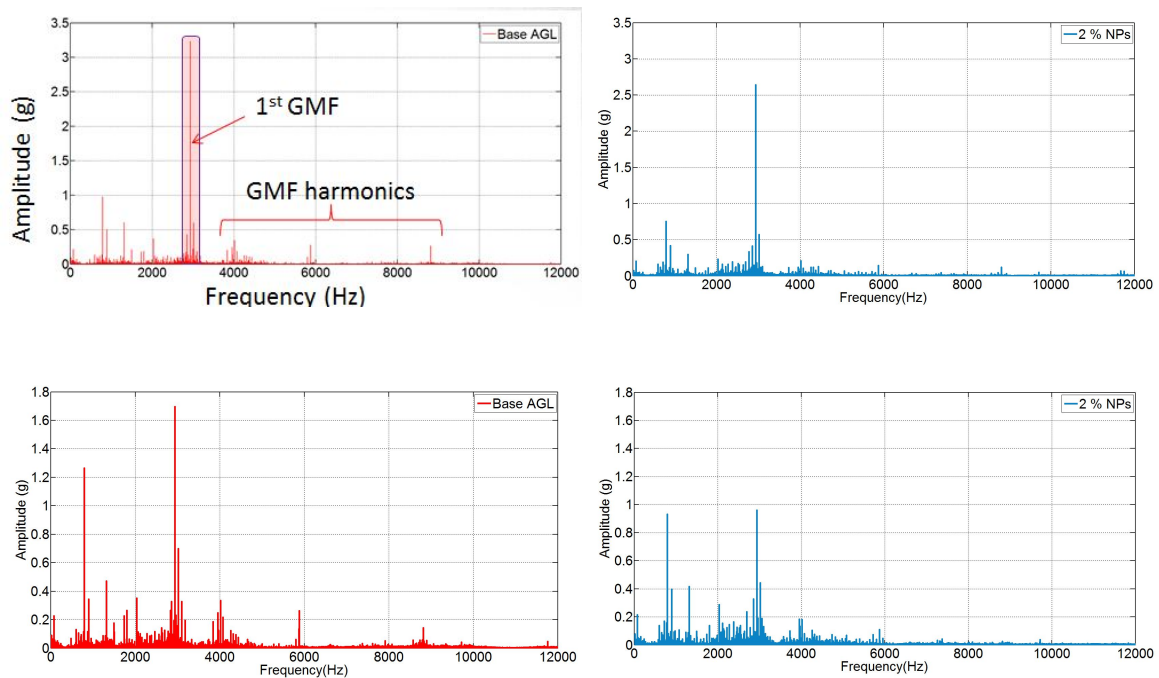
Figure 5.25: Progress of FFT spectrum for experiments 1 and 2 of gearbox testing after 2 hrs (top) and after 4 hrs (bottom)

Moreover, an accurate representation for the spectral results are illustrated in Figures 5.26-5.29. The cumulative sum of the FFT energies from the different lubricant experiments are presented. From these repeated spectral results, it is clear that

each lubricant has its own frequency response distribution, where Nanofluids have an overall less vibrational energy distribution across the spectrum.

Similar to the preliminary interpretation discussed earlier in the chapter, the impact of nanofluids becomes more clear at higher frequencies. Starting at approximately 1000 Hz, the two frequency response start to diverge apart. Most of energy in FFT gearbox spectrum is located at the fundamental GMF and sidebands. These energies are more likely to represent vibrations sensitive to physical phenomena of friction, temperature, and gear mesh near the surfaces. In this EHL regime, load is carried by the pressure within the fluid, nanolubricants are effective to damp these high vibration effects induced from the gearbox due to their enhanced thermophysical properties near the surface. On the other hand, for a bearing component, important information due to wear or improper lubrication are short in time and are represented as impulses. As such, most of these vibration information are undetectable in the FFT to conclude impact of nanofluids on bearings.
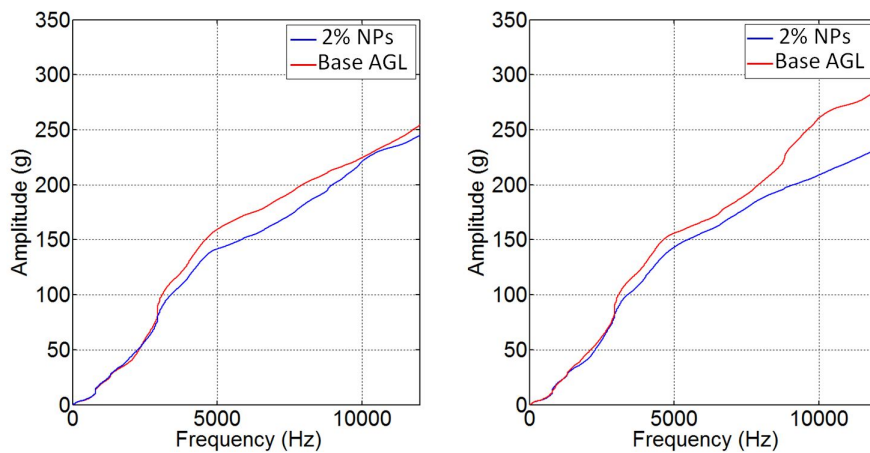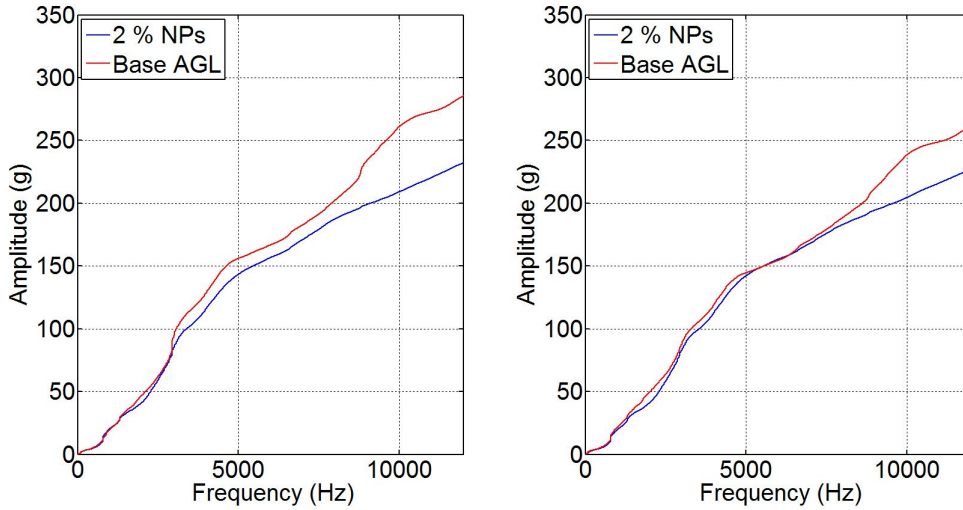
Figure 5.26: Cumulative sum of FFT energies. After 1 hr (top) and two hrs (bottom) from experiments 1 and 2
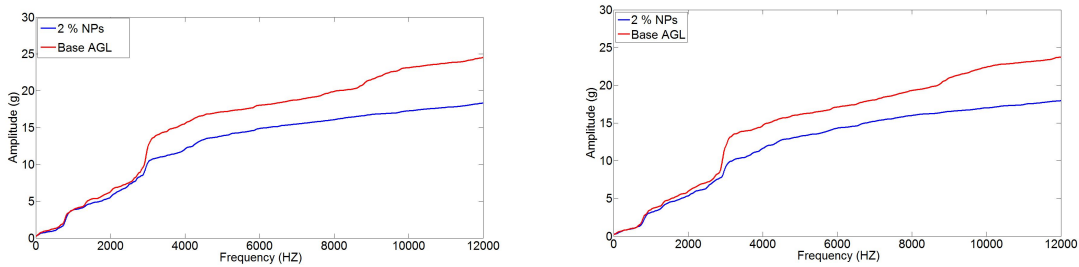
Figure 5.27: Cumulative sum of FFT energies. After 10 minutes from experiments 1 and 3
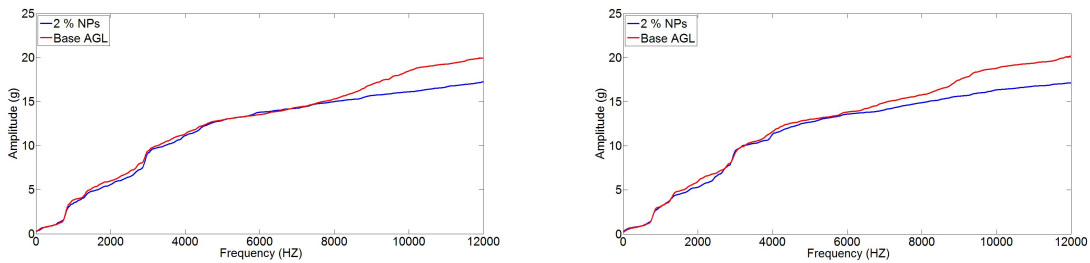
Figure 5.28: Cumulative sum of FFT energies. After 1 hr from experiments 1 and 3

Motivated by the above mentioned discussion, wavelet analysis is performed on different short-time locations to investigate impact of nanofluids on gearbox components through extracting repeated periodic impulses or transient characteristics. Moreover, the proposed WI is applied on the data and is compared to conventional CI results to illustrate its effectiveness as a potential tool for feature extraction.
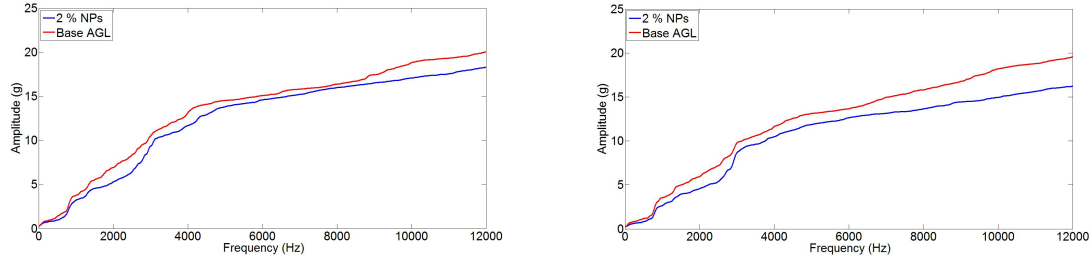
Figure 5.29: Cumulative sum of FFT energies. After 4 hrs from experiments 1 and 4

Numerous wavelet plots during the first two experiments are illustrated in Figures 5.30-5.33. All wavelet results show majority of vibrations from first GMF harmonic and from bearing components. At the first 1 hr of running, significant transient impulses near frequency components of 795 Hz-1050 Hz appear from the base AGL experiment. However, these energies are clearly reduced from the nanofluid experiment. After 3 hrs of running and near the end of the experiment, a similar trend can be seen for base AGL with apparent distribution of impulses across different frequency bands in the wavelet spectrum, and major distribution near GMF. On the other hand, distribution of vibrational energy from the nanosample becomes only located at selected frequency bands of the first GMF and sidebands with less intensity.
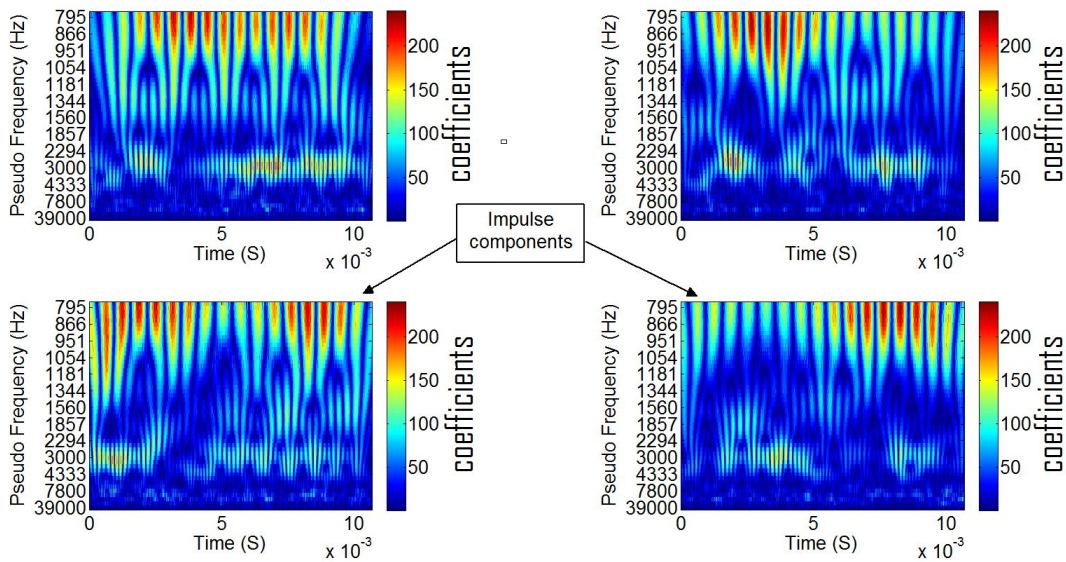
Figure 5.30: Experiment 1. Wavelet plots during gearbox testing. Base AGL (1 hr)
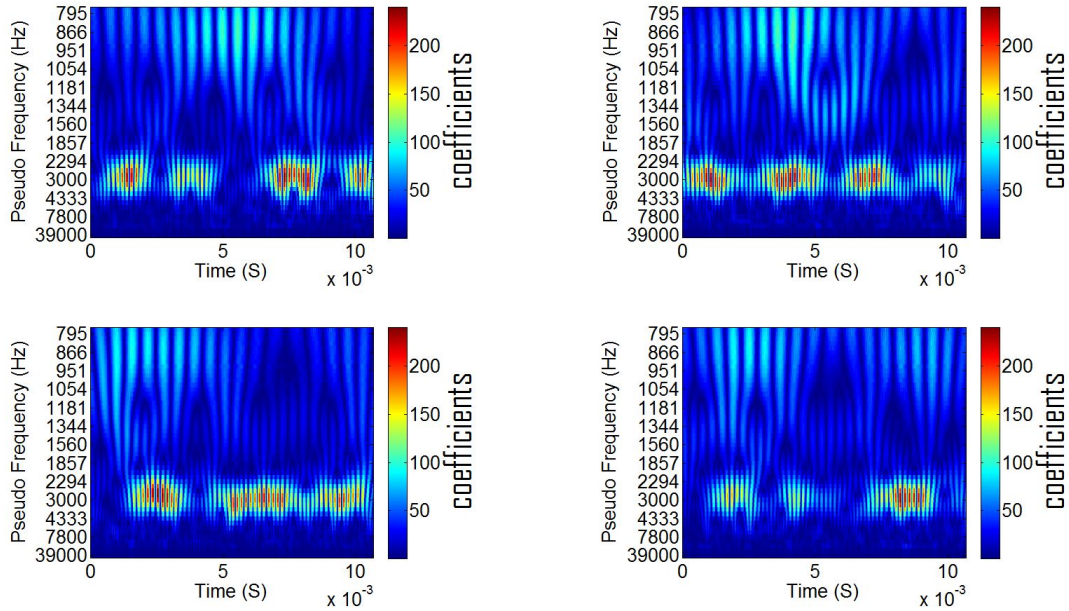
Figure 5.31: Experiment 2. Wavelet plots during gearbox testing. Nanofluid (1 hr)
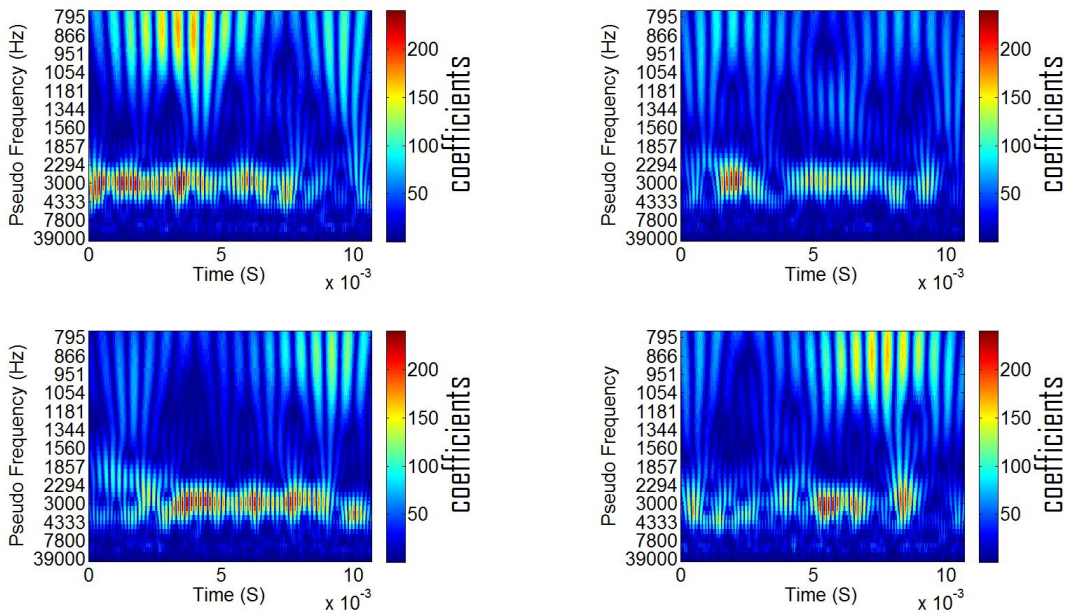
Figure 5.32: Experiment 1. Wavelet plots during gearbox testing. Base AGL (3 hrs)

Wavelet plots during the third and fourth experiments of the nanofluids are summarized in Figures 5.34-5.36 that show similarity to the results of the second nanofluid experiment. After 10 minutes, there are slight vibrational distributions across the wavelet spectrum. It is not until 1 hr into the experiment, impulse components are
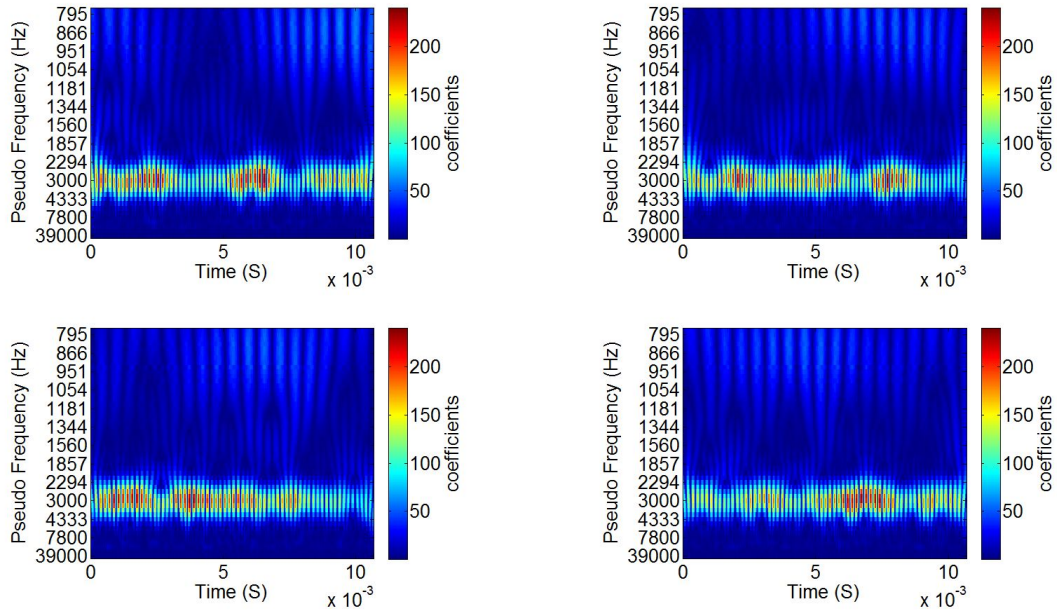
Figure 5.33: Experiment 2. Wavelet plots during gearbox testing. Nanofluid (3 hrs)

minimal near bearings and majority of energy is located near GMF and harmonics.

Moreover, after 3 hrs of running, all vibrations are only present near the fundemental

GMF and sidebands.
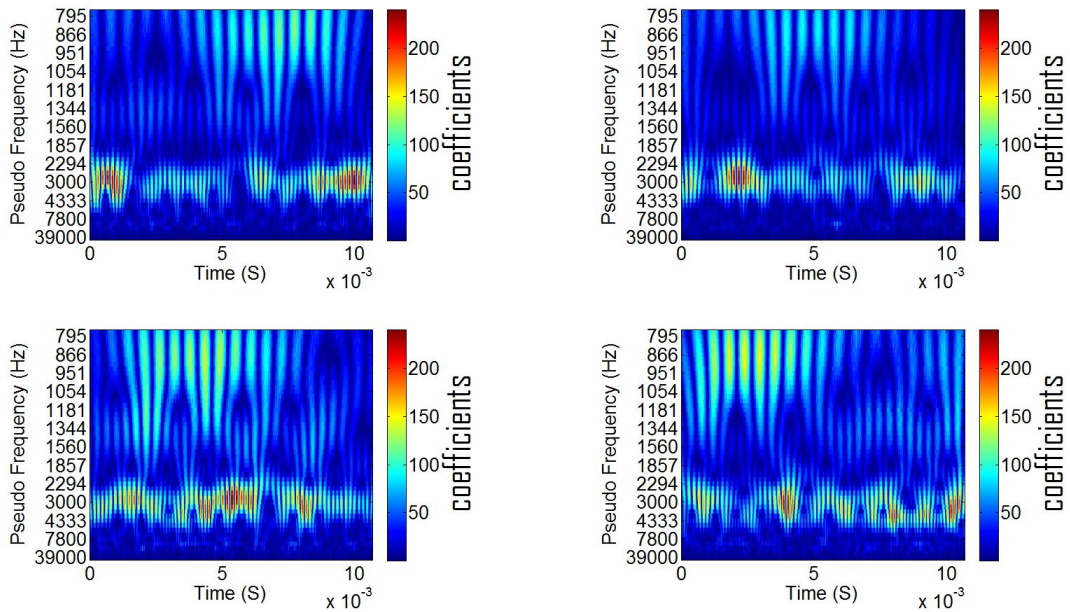
Figure 5.34: Experiment 3. Wavelet plots during gearbox testing. Nanofluid after 10
minutes
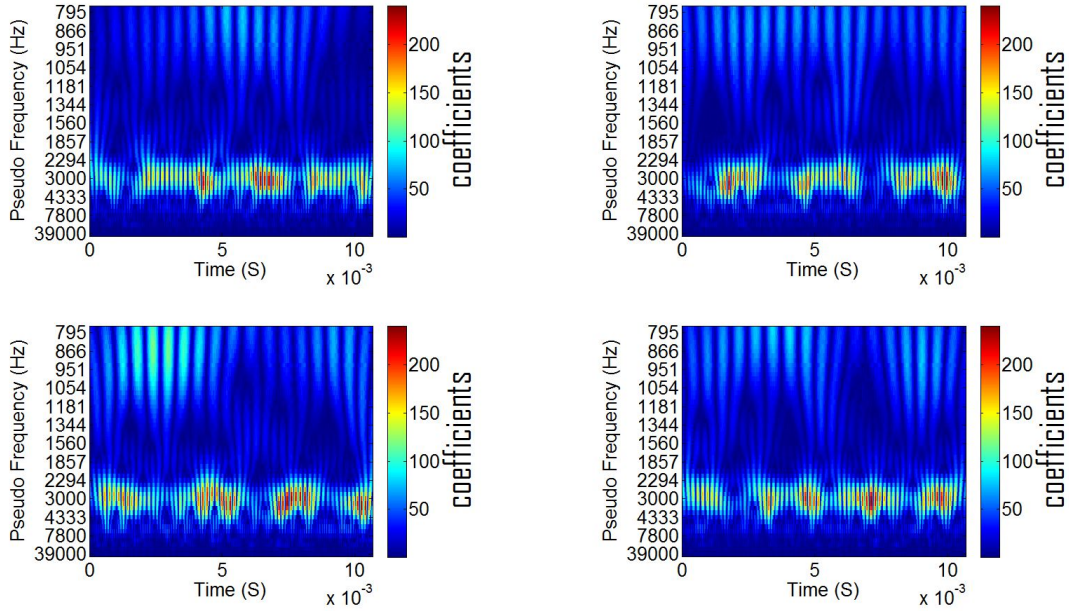
Figure 5.35: Experiment 3. Wavelet plots during gearbox testing. Nanofluid after 1 hrs

To accurately match feature extraction process in the 4 hr run, the proposed WI is computed during survey after each load step. Results are summarized in Figures 5.37-5.38. WI values are computed where majority of energies are distributed. Based on the results, a significant difference in WI values is observed between both tested lubricants. For bearing energies at 850 Hz , WI extracted from the base AGL experiment has larger values, compared to those extracted from the nanolubricant. Also, WI extracted near GMF frequency from nanofluid experiment has a constant trend with less variations in the data. Comparing these wavelet results to the MSPU CIs from Figure 5.24, WI as a potential CI shows capability of capturing transient characteristics that remain undetectable from the conventional vibration methods and illustrates potential improvement in performance of nanolubricants using wavelet as a tool. Overall, the distribution of impulse components across the entire wavelet spectrum from nanofluid experiments subside and only focus on vibration at the fundamental GMF and its sidebands. On the other hand, impulse components from

91
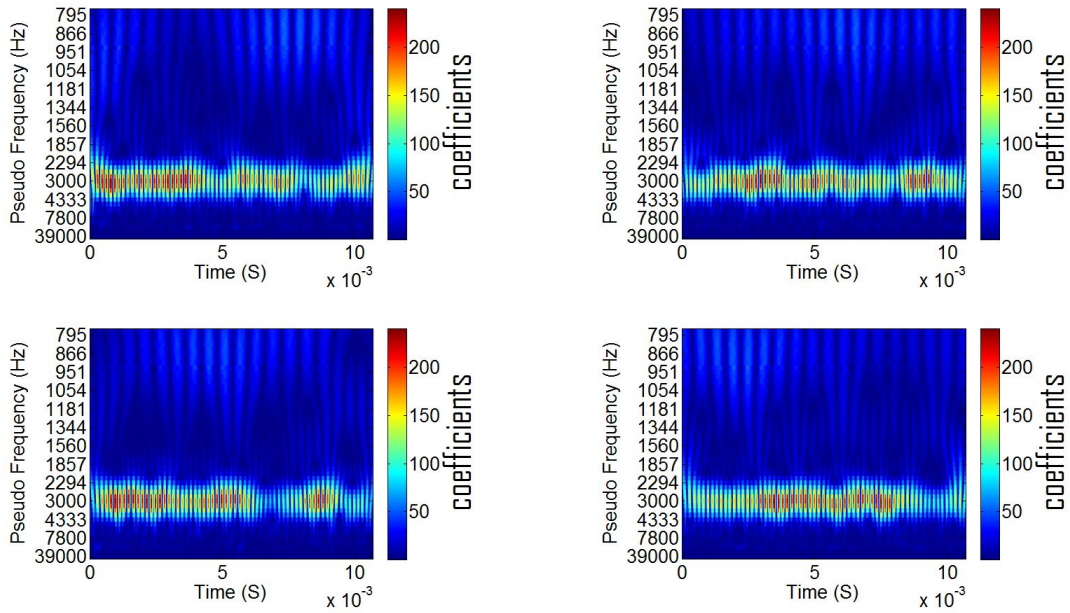
Figure 5.36: Wavelet plots during gearbox testing. Nanofluid after 3 hrs. Experiment 3 (top) and experiment 4 (bottom)

base AGL experiment are more distributed at different frequency bands across the spectrum.

This wavelet analysis shows how more transient characteristics are extracted from the base AGL experiment than nanofluid responses. Similarly to previous interpretations, it is theorized that nanofluids can protect gear and bearing components from friction, high temperatures or vibration characteristics due to maintaining a solid lubricant film between gear surfaces.

5.9 Conclusions

In this chapter, a new approach of applying nanofluids as potential lubricant for the IGB is possible. Gearbox testing is demonstrated on two different test stands for optimization purposes that shows lower viscosity nanolubricants (2% graphite-based AGL) yielding optimum responses and performing better than higher viscosity nanolubricants. This short-term testing of nanolubricants has shown potential performance
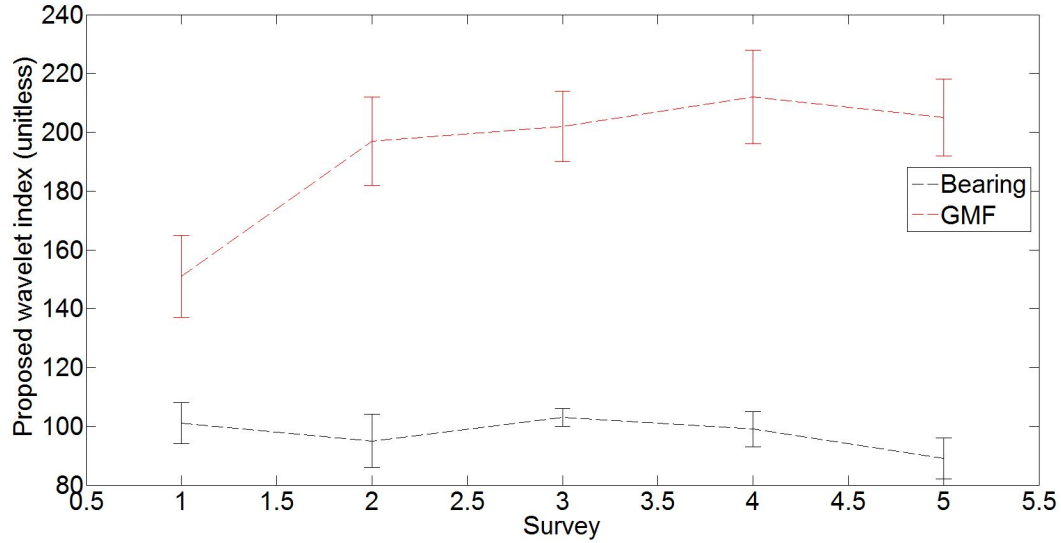
Figure 5.37: Wavelet index of Base AGL during loading profile. Error bars are mean ± std
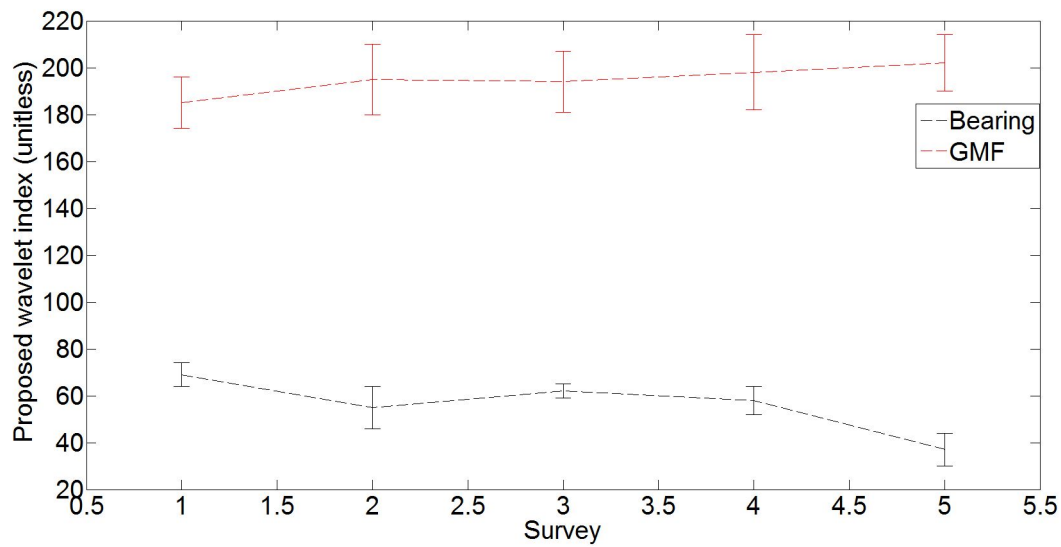
Figure 5.38: Wavelet index of nanolubricant during loading profile. Error bars are mean ± std

benefits in a full-scale mechanical system. Moreover, a possible empirical correlation between temperature, vibration, and the lubricant can lead to further development of diagnostic algorithm or a predictive nanofluid tool for CBM. However, these long-term benefits as a tool on the real helicopter may require more hours of testing. The following conclusions from this study are presented as follows:

- A significant contribution in this study from a condition monitoring perspective is the improvement of temperature response as a CI due to the nanolubricants. This improvement show that temperature can add value by giving an early warning of lubricant performance rather than depending on vibration as the only source of dynamic information.

- Improvements in existing vibration-based CIs and spectral results due to the implementation of nanolubricants.

- Wavelet analysis is used as a tool to validate vibration-based CIs and to advance gearbox performance through its impulse feature extraction capabilities from gearbox lubricant testing

- High concentration of AGL nanofluids is prone to drastic rheological changes upon shearing. This is demonstrated by both online gearbox responses and off-line viscosity measurements.

CHAPTER 6

A WAVELET-BASED INDEX FOR FAULT DETECTION AND ITS APPLICATION IN CONDITION MONITORING OF HELICOPTER DRIVE-TRAIN COMPONENTS [1]

6.1 INTRODUCTION

The first part of this chapter demonstrates results of advanced signal processing based on wavelet analysis for feature extraction. The wavelet-based index is applied on a TGB experiment to detect a possible fault. This gearbox has demonstrated severe grease lubrication conditions, where gear wear remains undetectable by conventional vibration tools. Second, this chapter presents statical analysis to prove that wavelet results are statistically valid. First, The proposed wavelet denoising method is adapted on different TGB signals for the purpose of improving WI through reducing redundant wavelet coefficients. Predicted WI is evaluated and compared to the observed WI. Second ,a statistical test established from the GWN is applied on numerous samples from the TGB experiment with an appropriate significant level and confidence interval to statistically validate autocorrelation distribution of the wavelet power.

6.2   AH-64 TGB Experiment with Output Seal Leak

The TGB is a right-angled grease lubricated gearbox mounted on the vertical stabilizer as previously presented mentioned. The TGB constitutes a critical component on the AH-64D drive-train helicopter and its function is to transmit torque to the blades. This gearbox contains a set of pinion and output spiral bevel gears with a gear ratio of 2.591:1 and a gear mesh frequency (GMF) of 1333.20 Hz. The TGB is comprised of two sections: main gear compartment and static mast, as explained in Figure 6.1. The output seal is located at the end of the static mast. It was hypothesized among maintenance crew that the static mast was sealed completely from the main gearbox chamber.
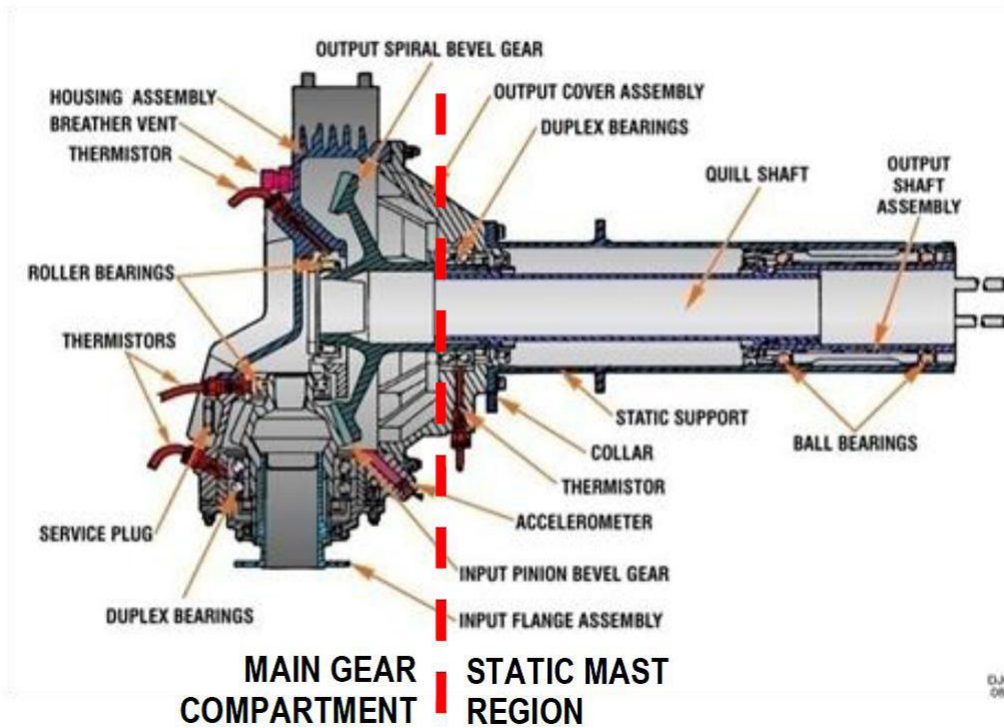
Figure 6.1: TGB internal components

In the field however, TGB is known to be susceptible to grease leaking from its output seal (Goodman et al., 2009). Motivating this study was the fact that the Army

replaced the entire TGB at the first sight of grease leaks. This natural occurring field-fault has contributed to the aircraft not being available for flight operations.

A test plan was initiated to create a worst case scenario through a seeded fault TGB experiment. The original objective of the test was to demonstrate whether the aircraft would continue to operate with a leaking output seal until the scheduled phase maintenance of 250 hours. A secondary objective was to identify the failure mode of the gearbox. A leak was induced in the output seal that allowed grease to drain from the static mast.

During the first few days of testing, large volumes of grease were observed leaking from the static mast. The test was stopped for an inspection that showed the main gearbox to be under-serviced with grease. Grease was added to the gearbox following standard military procedures to compensate for the loss. The test was resumed and grease ejection was observed from the static mast again. At that point, it was suspected that the addition of grease to the main gearbox would interfere with the original objective of the experiment: output seal leak. Adjustments were made to the original test plan by disallowing any addition of grease to the gearbox. After 490 hours of testing, it was concluded that there were large amounts of grease movement from the main gearbox compartment to the static mast (Figure 6.2). Seeded fault testing of TGB led to the discovery of a natural fault: a previously unbeknownst phenomenon at that time of grease transfer between the two compartments. This caused gear surface starvation and eventually led to severe wear due to loss of grease at the input gear teeth (Figure 6.3). Several vibration signatures were recorded as gear failure approached.

The data for this wavelet analysis was acquired from the NI-DAQ system. This data represents the discrete vibration time-series in which numerous samples were collected and analysed during the coarse of the experiment. The vibration survey for both DAQ systems were taken simultaneously at a steady state with the following

parameters: total sampling period (0.17 S), sampling rate (F_s=48 kHz), and number of samples (N) = 8192 samples
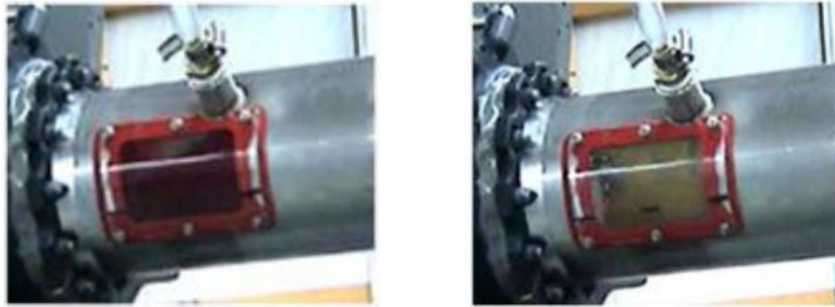
Figure 6.2: Movement of grease through static mast of TGB: after 120 minutes (left) and after 145 minutes(right)

Figure 6.3: Earlier stage of testing (left)and after failure (right)

6.3 TGB Output Seal Leak Results

6.3.1 Progress of Gearbox Failure Using Spectral Analysis

Progress of PS plots of the TGB during the last four days of testing is summarized in Figure 6.4 and Figure 6.5. Prior to the day of failure, inspection of the first three PS plots in Figure 6.4 (left and right) and Figure 6.5 (left) are almost the same. There is only a slight monotonic increase of vibrational power at the first and second harmonics of the GMF of 1333.20 Hz. It is not until the day of failure in Figure

6.5 (right) when the PS plot shows significant increases in both the third and fourth harmonics of the GMF.

The conventional PS did not give indications of increases in vibrational power to warning values except on the day of failure, which validates the inherent limitations of the CIs extracted from this method in detecting early faults.

Figure 6.4: Progress of PS during gearbox testing. 3 days before failure (left) and 2 days before failure (right)
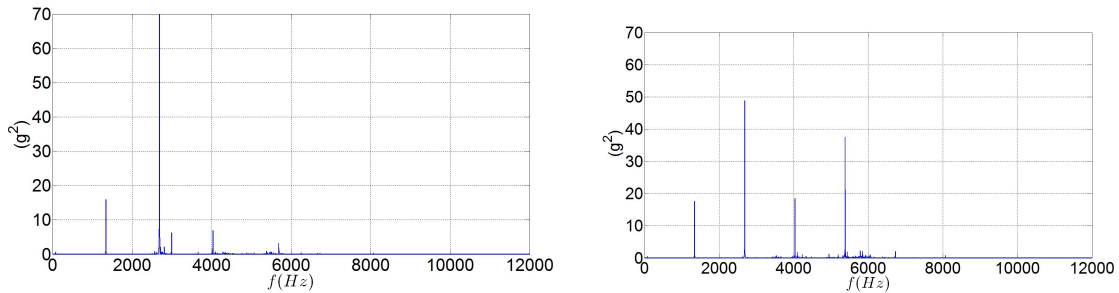
Figure 6.5: Progress of PS during gearbox testing. 1 day before failure (left)and the day of failure (right)

6.3.2 TGB CI RESULTS

TGB CIs were expected to have high sensitivity to gear wear, especially at the day of failure. However, FM0, ER, DA2, and SLF CIs in Figure 6.6 display little to no variation and remain almost flat the entire time of the experiment. None of these CIs showed alarming levels, except the input DA1 CI. It has an increase trend in its value from 6 g to 16 g during the final hours of testing. Despite this increasing trend

of the DA1 CI, it is still considered a non-warning value below the threshold limit set by AED, as previously discussed.

The x-axis in Figure 6.6 is the discrete time samples. It represents the life time of the gearbox experiment, which is 480 hours. The samples have been distributed over different hours and days depending on the time of the test. Actual numbers are not represented on the scale for conciseness. The Y-axis is divided into two portions: primary and secondary to have all the CIs plotted.
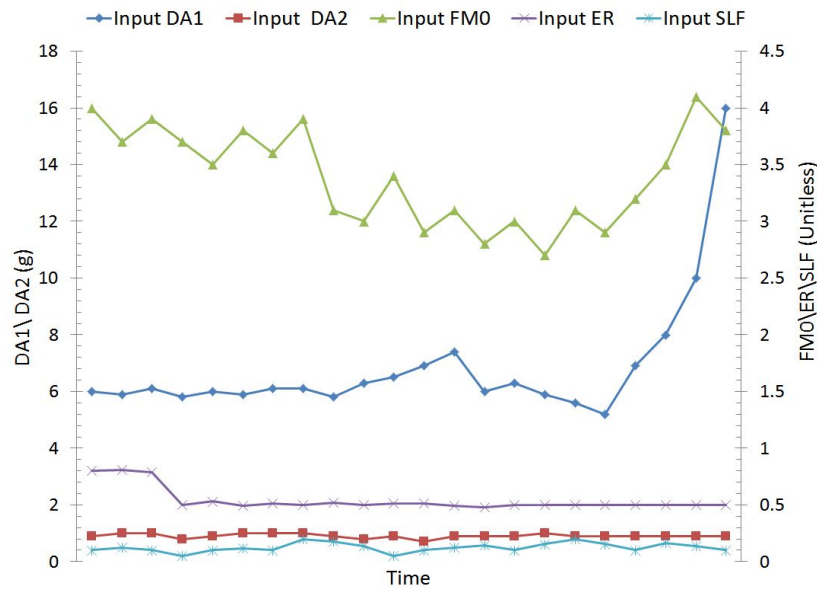
Figure 6.6: TGB CI responses over the whole period of testing

6.3.3 Progress of Gearbox Failure Using Wavelet Analysis

The results of this section are plotted using the wavelet toolbox in Matlab. CWT plots for different samples collected on the last couple days of testing are presented in Figure 6.7 and Figure 6.8 and as the extent is limited to feature extraction purposes only, the convolution is performed from scales 1:50 to have a complete picture of the scalogram. Unlike the Fourier power spectrum from Figure 6.4 and Figure 6.5, the wavelet plots start to demonstrate increases in vibrational energy where transients

at key harmonics in Figure 6.7 (bottom) start to appear at least two days before failure. Progress of the fault significantly builds up '1 day before failure' in Figure 6.8 (top) where distributions of vibrational energy at the second, third, and fourth GMF harmonics become clear.
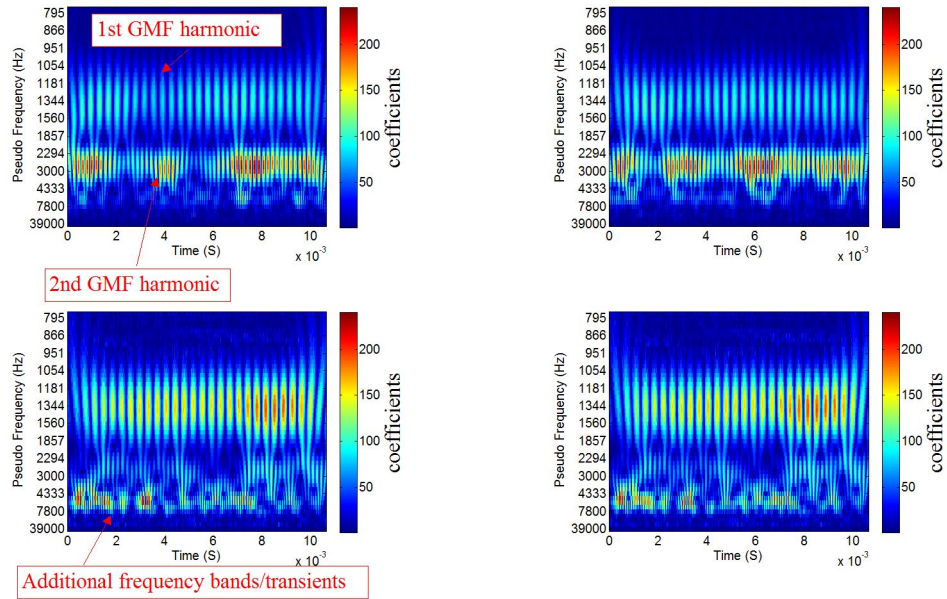
Figure 6.7: Progress of CWT during gearbox testing. 3 days before failure (top) and 2 days before failure(bottom)
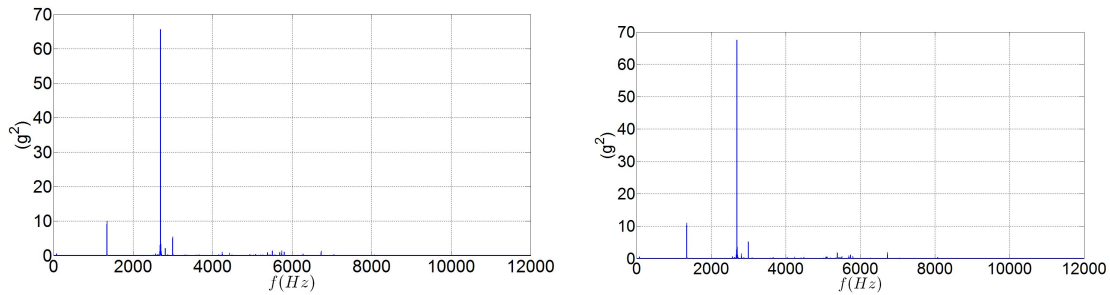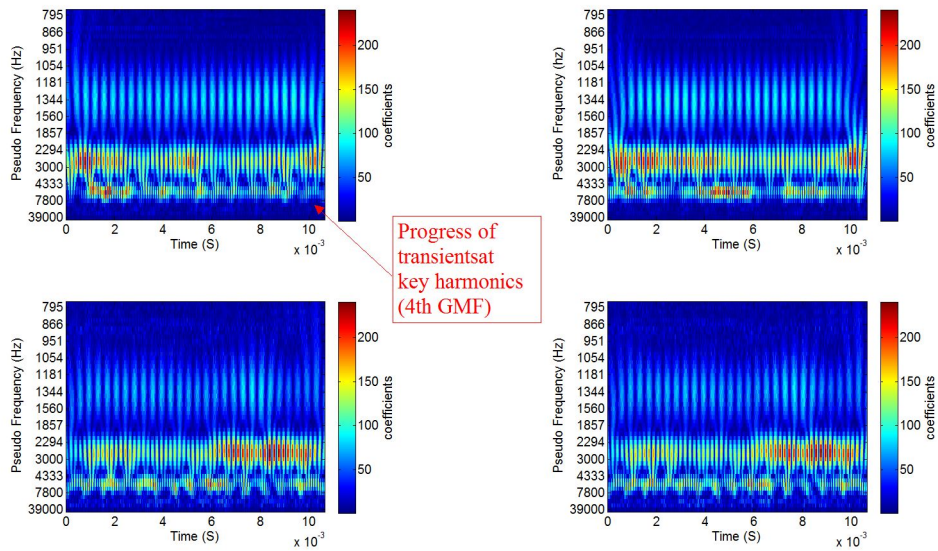

Figure 6.8: Progress of CWT during gearbox testing. 1 day before failure (top) and the day of failure (bottom)

Application of the WI is demonstrated using different sets of the experimental data. In most machinery gearboxes, excitation near the second harmonic and higher commonly promotes heavy gear wear (Scheffer and Girdhar, 2004). For diagnostic purposes, these transients are detected by the wavelets earlier than the conventional vibration methods at a region of a single frequency where the majority of transient characteristics are expected to be dominant. Consequently, the proposed WI is computed near the second and fourth GMF at 2666 and 5330 Hz, respectively and are summarized in Table 6.1. Where the large coefficients are an indication of more impulse components in the signal.

Table 6.1: Average WI value from all acquisitions taken on a single day

Day of experiment	WI at second GMF	WI at fourth GMF
Three days before failure	1477	211
Two days before failure	131	950
One day before failure	8162	5647
The day of failure	10380	6758

6.3.4 COMPARISON WITH TIME-FREQUENCY ANALYSIS

We will now show a comparison of a set of time-frequency distributions comparable to the CWT scalograms, previously obtained from wavelet analysis for the days immediately preceding part failure. These time-frequency representations in Figure 6.10 utilize a reduced interference distribution with a Zhao-Atlas-Marks kernel function for elimination of cross-terms (Zhao et al., 1990). One of the primary faults of this gearbox study is a degraded set of gear teeth. This affects the gear mesh frequencies and distribution of energy in the first through fourth harmonics, which also represent aperiodic pulses or transients. These pulses are harder to see and diagnose with the

constant sampling period typical of time-frequency analysis, when compared to the wavelet results.
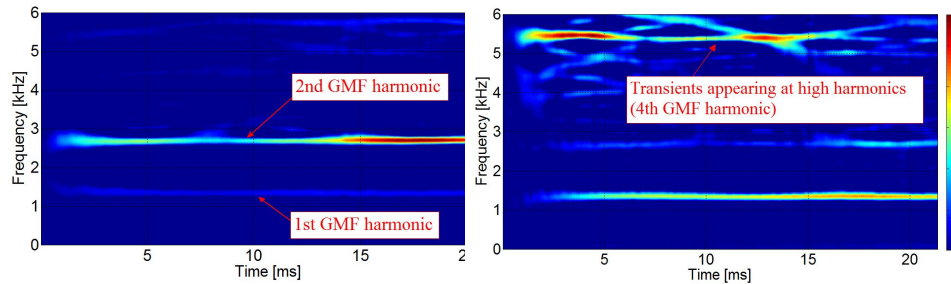
Figure 6.9: Progress of time-frequency analysis during gearbox testing. 3 days before failure (left) and 2 days before failure(right)
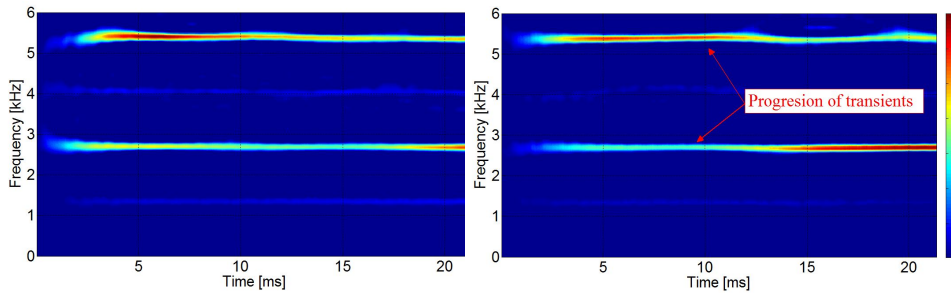
Figure 6.10: Progress of time-frequency analysis during gearbox testing. 1 day before failure(left)and the day of failure(right)

Where time-frequency plots in Figure 6.10 may present the progress of fault, it is not showing a complete distribution of energy at different frequencies like those from the wavelet approach in Figure 6.7 and Figure 6.8. The major downside of time-frequency distribution in rotating machinery applications can be collecting a kernel function that removes cross-terms and sometimes impacting valid component signals. However, one potential advantage of time-frequency would be the ability for utilizing cross-distributions such as from two separate sensor locations. On the other hand, several potential advantages are presented by the use of wavelet analysis and subsequent pseudo-frequency summing methods for the application being sought. The increased time resolution with acceptable frequency characteristics offered by the

variable time sampling period of wavelet analysis may provide a better fit for the type of fault looking to be diagnosed.

6.3.5 Comparision of WI with traditional MSPU CIs

The proposed WI is compared in Figure 6.11 with TGB CIs to validate the usefulness of the wavelet approach. Most of the conventional time-domain and frequency-domain CIs showed little to no change during the entire experimental lifetime of the gearbox. Input DA1 CI is the only indicator that reacted to the fault. However, DA1 only shows increases in the overall vibrational energy that indicates warning of an occurring event without providing information on the component that was failing; DA1 has limited value for diagnostic purposes. As for WI, an increasing trend is significantly observed at '1 day before failure' almost matching DA1 CI. The WI shows potential to identify the gear failure lubrication, being more sensitive to transients that appear in high frequency harmonics, and outperforming the rest of the CIs that include: SLF, FMO, ER, and DA2.

Wavelet analysis is presented as a promising approach for an additional feature in the MSPU of the AH-64 helicopter. The results propose a new index with useful characteristics in its sensitivity to gear wear and may facilitate in earlier fault detection for the TGB. This proposed WI shows its ability to react to vibrational energy through the derived wavelet coefficient where the the index can be physically interpreted as transient characteristics of gear teeth degradation.

6.4 Wavelet Denoising Results

The modified denoising approach proposed in chapter 4 is applied on different sample intervals of the TGB experiment. A comparison between original and predicted signals can be shown in Figure 6.12. Moreover, CWT plots of the original and recon-
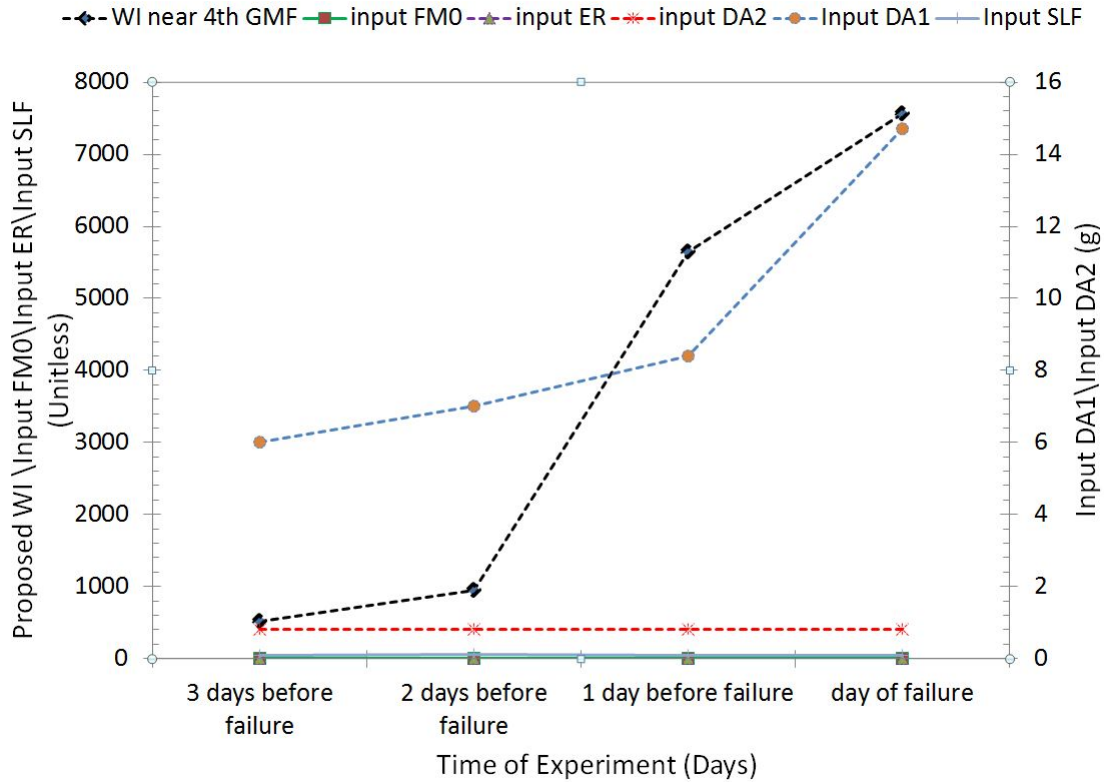
Figure 6.11: Comparison between averaged conventional TGB CIs and averaged WI during the last four days of testing

structed signal are presented in Figures 6.13-6.14. CWT using orthogonal wavelets is possible, however, the use of these wavelet types is not a good fit for the application being sought, as the vibrational distribution is scattered all over the spectrum and may not represent the true features of the system. The use of orthogonal functions yield a signal with features that may not identical to the original signal. On the other hand, wavelet plot using Morlet gives better results, in which noise seems to be reduced with less wavelet coefficient distribution at key gear mesh frequency harmonics, compared to the wavelet plot of original signal.

To quantify results in Figure 6.12, statistical metrics are calculated to evaluate reduction in noise performance between original signal and predicted signal. These metrics are the RMSE, SNR, and correlation coefficient. Results are summarized in Tables 6.2-6.3. From these tables, improved SNR values for different intervals are
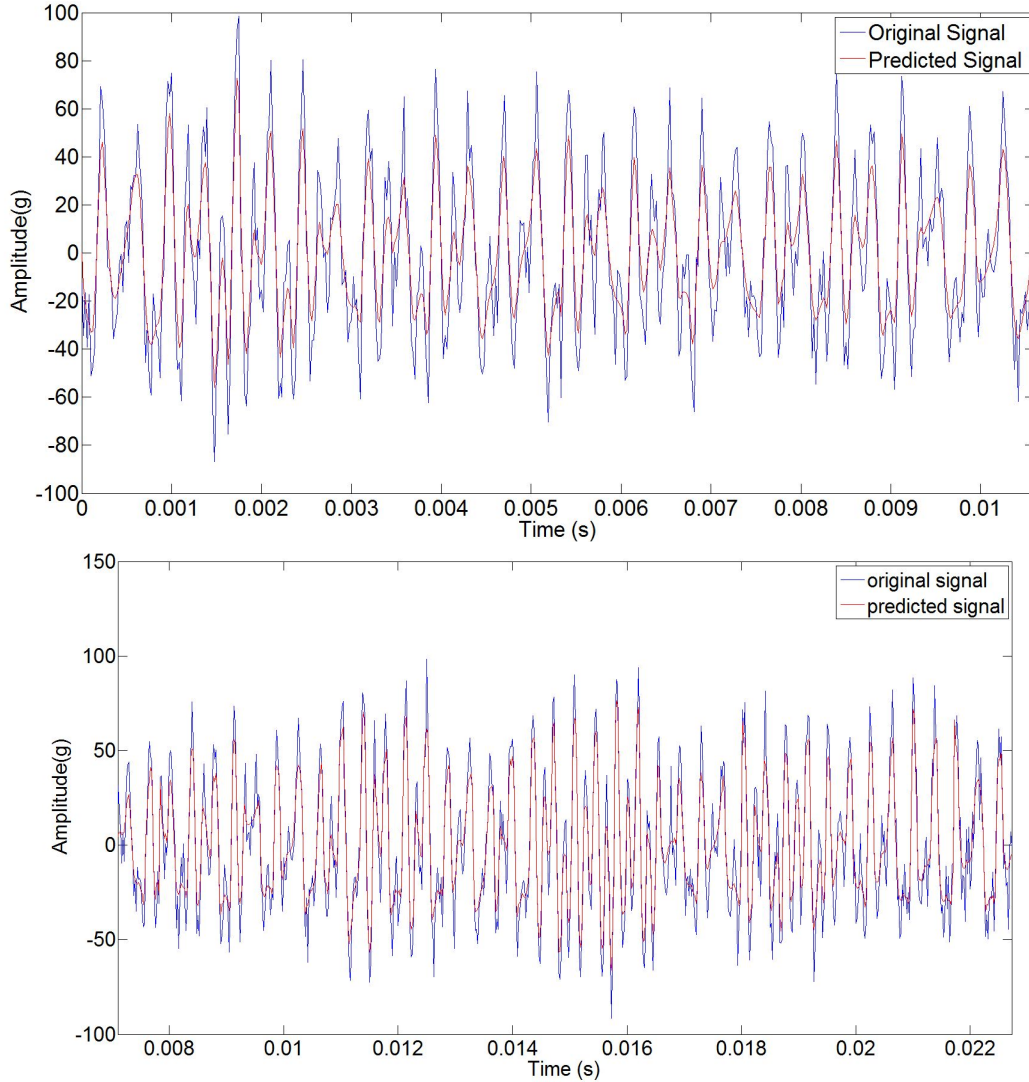
Figure 6.12: Comparison between original signal and predicted signal using different thresholds from the denoising method. N=512 (top)and N=2048(bottom)

between 72 dB and 79 dB from the proposed denoising method and are between 59 dB to 67 dB from the classical denoising approach. Moreover, ranges of the RMSE from Table 6.2 is less with higher correlation coefficient values that indicate a good fit. From these estimators, it can be shown the proposed denoising method based on Morlet has the capability to provide improved results for the WI than the classical approach of Donoho that solely uses orthogonal functions.
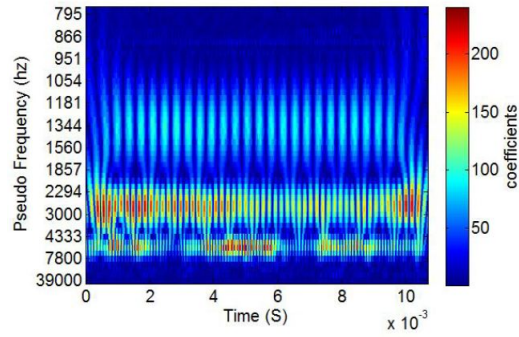
Figure 6.13: CWT wavelet plot of original signal. 1 day before failure
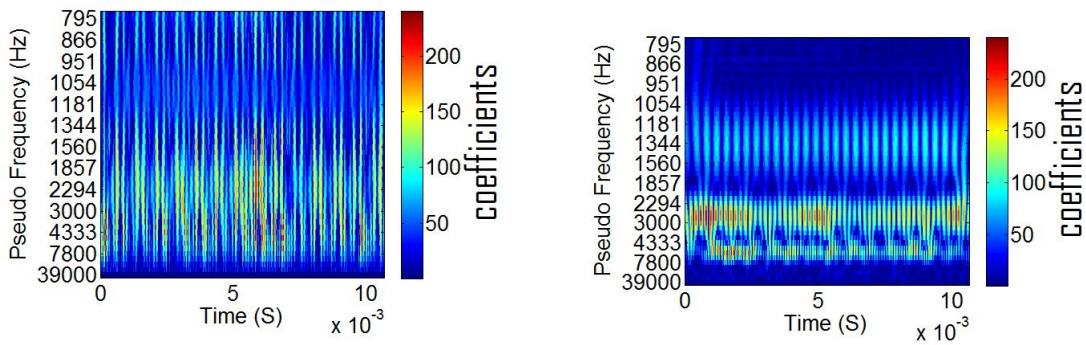
Figure 6.14: Example of CWT wavelet plots from predicted signals. 1 day before failure. Donoho's method(left) using haar orthogonal wavelet and the proposed denoising method based on Morlet(right)

Table 6.2: Statistical metrics between original and predicted signals from various sample sizes of TGB data using proposed denoising method (1 day before failure)

SNR	RMSE	corr. coeff.
72.5874	0.0985	0.9325
73.3489	0.0871	0.9465
75.9654	0.0823	0.9568
77.5268	0.0731	0.9598
79.2567	0.0524	0.9652

Table 6.3: Statistical metrics between original and predicted signals from various sample sizes of TGB data using Donoho denoising method (1 day before failure)

SNR	RMSE	corr. coeff.
59.8521	0.9025	0.6689
60.0569	0.7737	0.6718
64.2143	0.3921	0.7125
65.875	0.2569	0.7256
67.0258	0.1052	0.7426

A comparison between observed and predicted WI, extracted from the fourth GMF during TGB testing is presented in Figure 6.15. It can be shown that the predicted WI trends with less wavelet coefficient distribution, compared to the observed WI. Moreover, variability from the predicted WI represented with error bars at the given data points are reduced. This means the denosing method has significantly contributed in improving statistical performance of WI by eliminating small wavelet coefficient values in signals caused by noise and representing it with fewer wavelet coefficients close to the distribution of the mean. As such, predicted WI is more likely to reflect actual physical characteristics of vibration.

6.5 STATISTICAL SIGNIFICANCE TEST RESULTS

Different SNR samples from TGB data are applied to demonstrate the statistical significance of wavelet power at a given scale. In this section, TGB data samples from the day before failure are used in the statistical test(N=512, 2048, 4096). Results are summarized in Figure 6.16, where each distribution represent a horizontal slice of wavelet power spectrum or WI, as previously explained in section 4.5 of chapter 4. From the first drawn observation in Figure 6.16, the estimated effect is shown to be
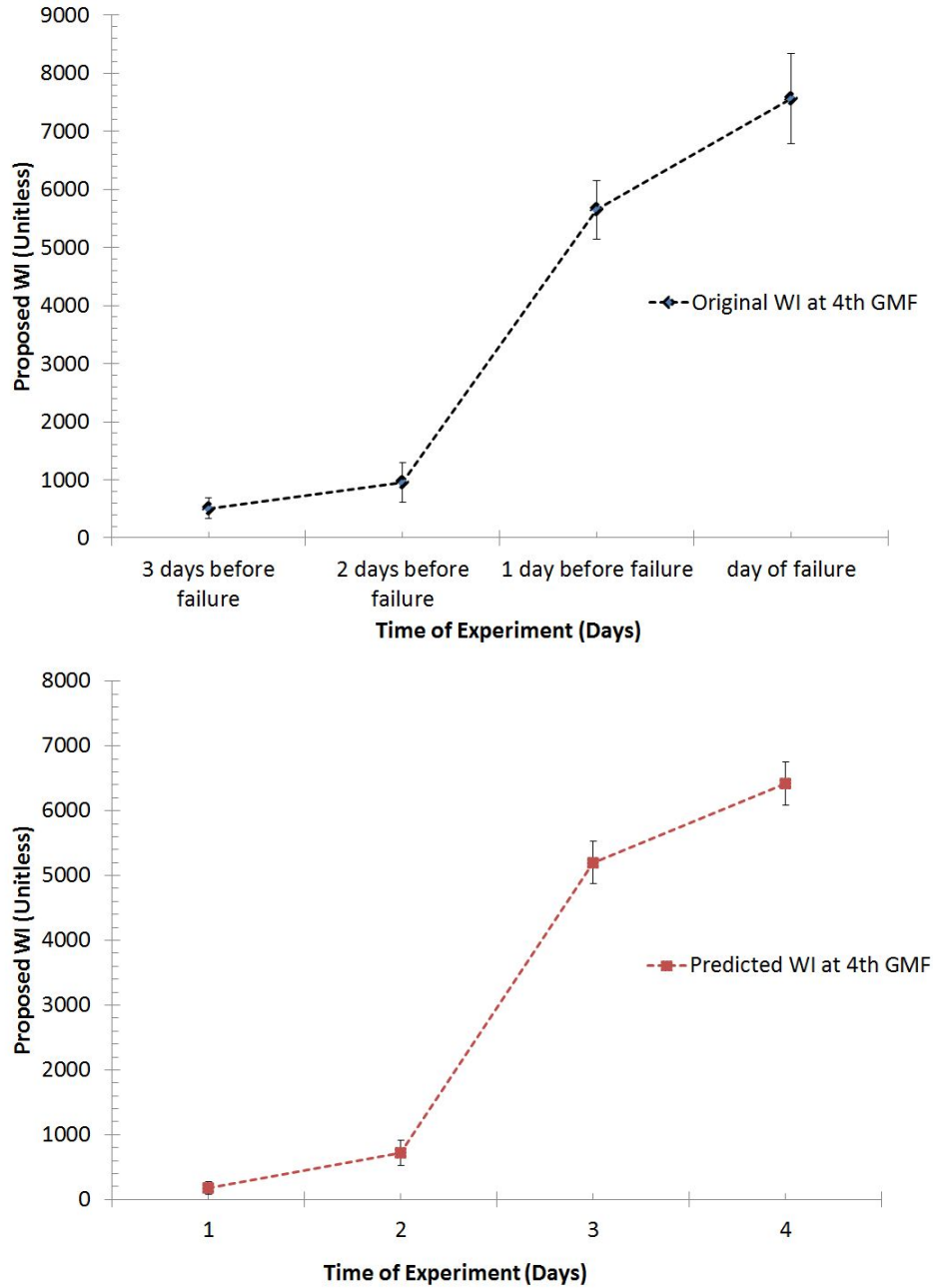
Figure 6.15: Comparison between observed and predicted wavelet index at fourth GMF from TGB experiment.Error bars represent mean $\pm$ std

within the significant level. This means that it would be possible to increase sample size for better statistical performance. In this work, vibration signals have a sampling rate of 48 kHz, Morlet wavelet is used in the analysis with chi-squared distribution (k=2). Also, since significant test is applied on real-world vibration samples, which

means the theoretical α values of 0.05, 0.1, or 0.01 might be too strict due to the nature of the low SNR of the data. As such, a fair assumption is made here by choosing a lower and less rigid significant level of 15%, which is equivalent to an 85% confidence level.

It is shown that for all three slices of WI from these different samples, wavelet peaks above the significant level of 85% confidence interval are considered to be statistically significant, reflecting actual features. On the other hand, wavelet spectra peaks below the significant level are considered to be noise fluctuations. It can be inferred from these sample observations that this significant test succeeded to distinguish true features from noise with 85% confidence.

6.6 CONCLUSIONS

The research efforts in this chapter provide potential to improve diagnostic capabilities for lubrication gear related failures in the Apache helicopter. Some important concepts utilizing wavelet analysis have been discussed through the evaluation of a new condition indicator used for fault detection. Conclusions drawn are as follows: (1) The proposed wavelet index has the capability to outperform some of the traditional signal processing techniques that are commonly used onboard the AH-64 aircraft.(2) Although CWT carries alot of redundancy, it is found to be effective in detecting the fault in a military gearbox where convolution provides the wavelet coefficients at frequency bands that are indicative of major changes in the signal.(3) Morlet wavelet is a good fit for vibration analysis of rotating machinery, matching transient signals from the gearbox.(4) Time-Frequency analysis may provide diagnostics of the gearbox, however, wavelets has more flexibility and accuracy for the application being addressed.

The work in this chapter also represents an empirical method of reducing noise in the wavelet index. A modified denoising technique based on Morlet wavelet is proposed. Results are satisfactory and show the capability of this technique to more effectively reduce noise from gearbox data, compared to the classical Donoho method. Noise reduction performance have been evaluated using well-known statistical metrics of RMSE, SNR, and correlation coefficient. Empirically WI has shown a significant reduction in overall wavelet coefficients at key GMF harmonics. These coefficients would probably represent actual vibrational characteristics with minimum noise. Despite, excellent characteristics of the traditional denoisng technique using orthogonal wavelets in numerous other applications, it is clearly not a good fit for CWT feature extraction from mechanical systems. Future work can include classification of wavelet index to accurately represent a model between sensitivity of true positive and false positive.

Statistical tests on few observations is possible, especially when studying non-stationary time series signals. It is shown that this significance test depends on the distribution of wavelet power time-series. Conclusions are only drawn from the observation samples tested, in which statistical test yield an 85% confidence interval with the ability to distinguish real properties of the system from those due to noise. Findings in this work prove that the proposed wavelet index drawn from these samples would be statistically valid. Results also show that smoothing the wavelet power spectrum by increasing the number of samples can enhance confidence of significant wavelet power, in which the estimation of 85% confidence interval of different samples can become closer to the true mean. However, more statistical analysis on larger training and testing data sets for classification would be needed to further increase statistical performance of the wavelet power.
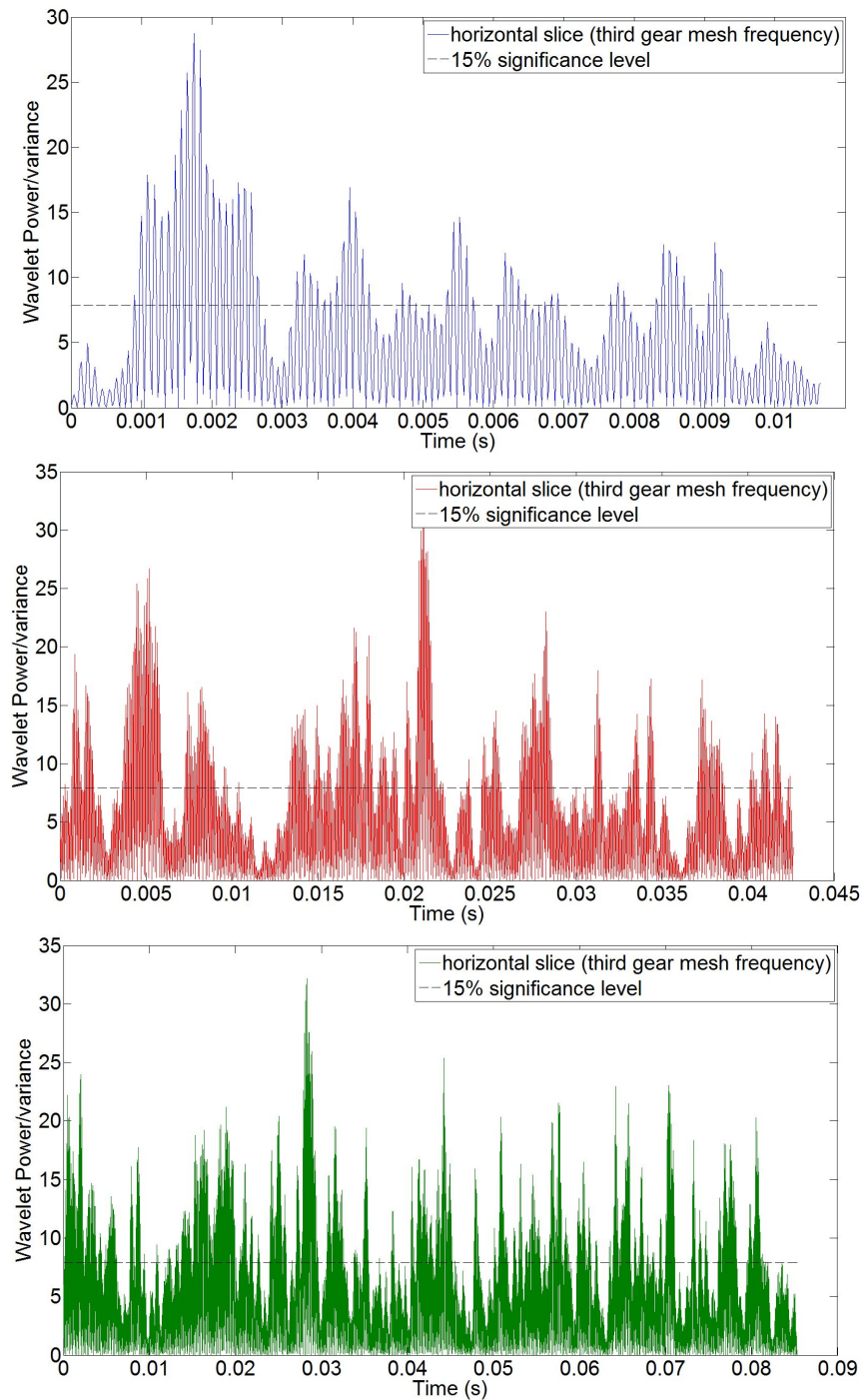
Figure 6.16: Wavelet power of different horizontal slices and the 85 % confidence interval. Top (N=512 samples), middle (N=2048 samples), bottom (N=4096 samples)

Chapter 7

Summary and Conclusions

7.1 Summary

This dissertation was motivated to address a crucial research question on how to minimize lubricant leaks in Apache helicopter drivetrain gearboxes through increasing performance. In this work, nanofluids were proposed as a potential lubricant for the intermediate gearbox (IGB) of the Apache helicopter. Moreover, an advanced signal processing approach based on wavelet analysis was utilized to develop a new condition indicator (CI) as a performance metric during gearbox lubrication conditions. First, a detailed fluid study was conducted on different oil nanofluid samples to craft the hypothesis of enhanced thermophysical properties using off-line oil analysis measurements. It was shown there were crucial effects of nanoparticles (NP) additives on oil. Next, these nanolubricant samples were investigated in the IGB on a test stand that emulates the exact operating condition of a real helicopter. Results yielded promising characteristics of the proposed lubricant based on gearbox responses. Finally, a signal processing study was addressed to create a wavelet index (WI), applied on a tail rotor gearbox (TGB)undergoing severe lubrication conditions. This WI has shown its capability to effectively capture gear wear fault from the TGB through transient characteristics extracted from vibration data. WI has also applied on the IGB data to illustrate performance of nanofluids on gearbox. Then, a wavelet denoising analysis was proposed to improve the statistical performance of WI by removing unwanted noise from signals. Finally, a statistical test based on distributions

of wavelet power spectrum and gaussian white noise estimated a threshold line that helped to distinguish meaningful wavelet peaks from those due to noise.

In the first study, turbine jet oil and Mobil Aviation Gear Lubricant (AGL) oil nanofluid samples were experimentally investigated using offline tools to measure important thermophysical properties, such as thermal conductivity, dynamic viscosity, and viscosity index. Moreover, a modified nanofluid model using the effective medium approach was derived that takes into account both the morphology and hydrodynamic interactions of non-spherical NPs in oil.

Graphite-based AGL samples displayed most significant increases in the measured fluid properties, compared to both turbine-based samples and boron nitride-based AGL samples and were recommended as the possible lubrications for gearbox testing. Interestingly, high concentration turbine jet oil demonstrated non-Newtonian characteristics due to the incorporation of NPs and as a result were not considered for gearbox testing. The proposed nanofluid model has indicated not only relevance of the two key fundamental mechanisms for the samples being studied, but also were extremely important for significant interpretation, when linked with gearbox responses. Despite the reasonable assumptions made in the model, it has given a necessary understanding of non-spherical nanoparticle behavior in oil lubricants, which can be further expanded to more rigorous computational studies that involve turbulent fluid flow conditions.

In the second study, a new approach of applying nanofluids as potential lubricant for the IGB was presented. Testing was demonstrated on two different test stands for optimization purposes: preliminary no-load test stand and the full-load tail rotor drivetrain (TRDT) test stand. Numerous gearbox responses that include: temperature and vibration were collected during experiments. Moreover, vibration data was thoroughly investigated using signal processing techniques to illustrate effectiveness of nanofluids.

Initial preliminary testing results for the 2% nanofluid sample have shown improvements in both vibration and temperature responses due to the incorporation of the NPs, while the 2.5 % yielded unsatisfactory results. Second, high viscosity AGL nanofluids are possibly prone to rheological changes in the gearbox due to high shearing of NPs. Third, AGL nanosamples either demonstrated Newtonian flow with relative viscosity temperature independence or non-Newtonian flow with relative viscosity temperature dependence.

Full-load testing was performed on the 2% nanofluid sample for further investigations. It was shown that there were improvements in the onboard vibration-based CIs, temperature CIs and spectral results due to the implementation of nanolubricants. A significant contribution in this study from a condition monitoring perspective is the improvement of temperature response as a CI due to the nanolubricants. This improvement show that temperature can add value by giving an early warning of lubricant performance, rather than depending on vibration as the only source of dynamic information. Wavelet analysis was used to validate vibration-based CIs and to advance gearbox performance through its impulse feature extraction capabilities from gearbox lubricant testing. Overall these results proved there is a strong correlation between temperature, vibration, and the lubricant, which can evolve to further development of diagnostic algorithm or a predictive tool for condition-based maintenance (CBM).

In the final third study, a new CI based on wavelet analysis was developed and applied on TGB vibration data undergoing severe lubrication conditions near the input gear. The proposed WI has the capability to outperform some of the traditional signal processing techniques that are commonly used onboard the Apache aircraft by extracting more vibration information from high-order spectra. This information can be physically interpreted as gear teeth degradation.

Wavelet denoising using a thresholding approach based on Morlet wavelet was proposed. Results were satisfactory and showed the capability of this technique to reduce noise effects from gearbox data, compared to classical approaches that soley apply the discrete wavelet transform and orthogonal wavelets. The proposed denoising method has shown a significant improvement in WI with less variability that may take less computational time to produce, due to reduction in the overall wavelet coefficients at key gear harmonics. The predicted wavelet coefficients from denoising would probably represent actual vibrational characteristics with minimum noise. Moreover, a statistical test applied on the wavelet power sampling distribution has distinguished actual features that represent real properties from those due to noise with a 85% confidence interval, indicating wavelet results from the tested samples are statistically valid.

The third study can be viewed as an extension to the previous two fluid studies, as the wavelet index adds value and can be considered a performance metric that provides important vibration information during lubricant leaks from the drivetrain gearbox.

This work provides an interdisciplinary approach aiming to utilize new approaches with an end result of increasing the Apache gearbox performance that would lead to achieving CBM objectives (eg. extension of time between overhauls). The general conclusions from this dissertation are:

- Qualification of graphite-based AGL nanofluids with optimum thermophysical properties as prospective gearbox lubricants

- Application of nanofluids in a real mechanical system is possible that leads to improvement of CIs.

- Development of a new CI based on wavelet analysis that can provide the user with a better understanding of gearbox vibrational characteristics to properly identify a gearbox event.

Overall, results of this dissertation establish a step forward towards the adaption of new CBM tools.

7.2 Recommendations for Future Work

This work was applied on a specific case study that represents a real-world mechanical system. Results of this dissertation can show promise in other helicopter fleets. However, more research through testing hours are still needed before nanofluids or wavelets are deployed as CBM tools on real helicopters. The following recommendations for future work is proposed.

First, throughout the optimization process of nanofluid testing, it was concluded that high viscosity NP concentrations in oil were prone to drastic rheological changes. Although, during off-line analysis, the 2.5% NP additive yielded highest thermophysical properties. It was theorized that complex interactions develop during shearing in a mechanical system and this assessment agrees with what other nanofluid researchers in the literature have predicted. It would be strongly recommended to pursue further testing on low concentration AGL graphite-based nanofluids ranging from 0.5%-2% for better gearbox performance.

Second, this dissertation studied and focused on vibration, temperature and the lubricant's viscosity as gearbox responses. For a complete picture of gearbox performance, studying the effect of nanofluids on power efficiency would be an important factor to add value. Moreover, measuring reduction in friction or wear between gear surfaces would be significant. This work revealed indirectly possible reduction in

117

friction due to improvements in dynamic responses of the gearbox, especially temperature.

Third, this work presented a very important conclusion of a possible correlation between temperature, vibration, and the tested lubricant. With more data available, recommendations can be aimed to the development of a nanofluid prediction model through data fusion among different attributes. The benefits can be massive, leading to a significantly richer source of information as an integrated sensor suite. Data fusion of different CIs is a part of the new CBM research outlook, envisioned as a smart predictive tool for prognostics or predicting remaining useful life of a component.

Finally, wavelet was presented as a possible approach for gearbox feature extraction on the Apache helicopter. In general, a deployment of a signal processing tool on the Apache helicopter requires other challenging steps besides feature extraction, which was the main contribution in this work. For further development of WI as a condition monitoring tool, more gearbox testing and data collection under different faulted conditions. This would be followed by statistical analysis that include training the data, eventually achieving long-term goals for feature selection through adjusting WI thresholds with maximizing true positives and minimizing false positives.

Bibliography

Abareshi, M., E. K. Goharshadi, S. Mojtaba Zebarjad, H. Khandan Fadafan, and A. Youssefi (2010). Fabrication, characterization and measurement of thermal conductivity of fe< sub> 3</sub> o< sub> 4</sub> nanofluids. *Journal of Magnetism and Magnetic Materials 322*(24), 3895–3901.

Abdel Bayoumi, Amber McKenzie, K. G. and J. McVay (2012). Impact of lubrication analysis on improvement of ah-64d helicopter component performance. *American Helicopter Society 68th Annual Forum Conference Proceedings, Fort Worth, TX*.

Archard, J. (1957). Elastic deformation and the laws of friction. *Proceedings of the Royal Society of London. Series A. Mathematical and Physical Sciences 243*(1233), 190–205.

Bartelmus, W. (2014). New focus on gearbox condition monitoring for failure prevention technology. *Key Engineering Materials 588*, 184–191.

Bendjama, H., S. Bouhouche, and M. S. Boucherit (2012). Application of wavelet transform for fault diagnosis in rotating machinery. *International Journal of Machine Learning and Computing 2*(1), 82–87.

Boulahbal, D., M. F. Golnaraghi, and F. Ismail (1999). Amplitude and phase wavelet maps for the detection of cracks in geared systems. *Mechanical systems and signal processing 13*(3), 423–436.

Chen, J., Y. Zi, Z. He, and J. Yuan (2012). Compound faults detection of rotating machinery using improved adaptive redundant lifting multiwavelet. *Mechanical Systems and Signal Processing*.

Coats, D., K. Cho, Y.-J. Shin, N. Goodman, V. Blechertas, and A. Bayoumi (2011). Advanced time–frequency mutual information measures for condition-based maintenance of helicopter drivetrains. *Instrumentation and Measurement, IEEE Transactions on 60*(8), 2984–2994.

Crook, A. W. (1961). The lubrication of rollers iii. a theoretical discussion of friction and the temperatures in the oil film. *Philosophical Transactions of the Royal Society of London. Series A, Mathematical and Physical Sciences 254*(1040), 237–258.

Das, S. K., N. Putra, P. Thiesen, and W. Roetzel (2003). Temperature dependence of thermal conductivity enhancement for nanofluids. *Journal of Heat Transfer 125*(4), 567–574.

Dempsey, P. J., J. A. Keller, and D. R. Wade (2008). Signal detection theory applied to helicopter transmission diagnostic thresholds. In *Proceedings of the American Helicopter Society 65 th Annual Forum on Disc.*

Donoho, D. L. and I. M. Johnstone (1995). Adapting to unknown smoothness via wavelet shrinkage. *Journal of the american statistical association 90*(432), 1200–1224.

Duangthongsuk, W. and S. Wongwises (2009). Measurement of temperature-dependent thermal conductivity and viscosity of tio< sub> 2</sub>-water nanofluids. *Experimental Thermal and Fluid Science 33*(4), 706–714.

Dyson, A. (1970). Frictional traction and lubricant rheology in elastohydrodynamic lubrication. *Philosophical Transactions of the Royal Society of London. Series A, Mathematical and Physical Sciences 266*(1170), 1–33.

Earnshaw, R. C. and E. M. Riley (2011). *Brownian Motion: Theory, Modelling and Applications.* Nova Science Publishers.

Eastman, J. A., S. Phillpot, S. Choi, and P. Keblinski (2004). Thermal transport in nanofluids 1. *Annu. Rev. Mater. Res. 34*, 219–246.

Fugal, D. L. (2009). *Conceptual wavelets in digital signal processing: an in-depth, practical approach for the non-mathematician*. Space & Signals Technical Pub.

Gao, R. X. and R. Yan (2006). Non-stationary signal processing for bearing health monitoring. *International Journal of Manufacturing Research 1*(1), 18–40.

Ge, Z. (2008). Significance tests for the wavelet cross spectrum and wavelet linear coherence. In *Annales Geophysicae*, Volume 26, pp. 3819–3829. Copernicus GmbH.

Girondin, V., K. M. Pekpe, H. Morel, and J.-P. Cassar (2013). Bearings fault detection in helicopters using frequency readjustment and cyclostationary analysis. *Mechanical Systems and Signal Processing*.

Goodman, N. (2011). *Application of data mining algorithms for the improvement and synthesis of diagnostic metrics for rotating machinery*. Ph. D. thesis, University of South Carolina.

Goodman, N., A. Bayoumi, V. Blechertas, R. Shah, and Y.-J. Shin (2009). Cbm component testing at the university of south carolina: Ah-64 tail rotor gearbox studies. In *Proc. of AHS SpecialistsŠ Meeting on Condition Based Maintenance*.

Gouda, K. M., J. A. Tarbutton, M. A. Hassan, D. Coats, and A.-M. E. Bayoumi (2015). A wavelet–based index for fault detection and its application in condition monitoring of helicopter drive–train components. *International Journal of Manufacturing Research 10*(1), 87–106.

Grabill, P., T. Brotherton, J. Berry, and L. Grant (2002). The u. s. army and national guard vibration management enhancement program(vmep)- data analysis and statistical results. In *AHS International, 58 th Annual Forum Proceedings-*, Volume 1, pp. 105–119.

Guo, Q. and C. Zhang (2012). A noise reduction approach based on steinŠs unbiased risk estimate. *Sci Asia 38*, 207–11.

Hamrock, B. J., B. O. Jacobson, S. R. Schmid, B. Jacobson, and B. Jacobson (1999). *Fundamentals of machine elements*. WCB/McGraw-Hill Singapore.

Heidari Bafroui, H. and A. Ohadi (2014). Application of wavelet energy and shannon entropy for feature extraction in gearbox fault detection under varying speed conditions. *Neurocomputing 133*, 437–445.

Hölzer, A. and M. Sommerfeld (2008). New simple correlation formula for the drag coefficient of non-spherical particles. *Powder Technology 184*(3), 361–365.

Kankar, P., S. C. Sharma, and S. Harsha (2011). Fault diagnosis of ball bearings using continuous wavelet transform. *Applied Soft Computing 11*(2), 2300–2312.

Koo, J. and C. Kleinstreuer (2004). A new thermal conductivity model for nanofluids. *Journal of Nanoparticle Research 6*(6), 577–588.

Lebold, M., K. McClintic, R. Campbell, C. Byington, and K. Maynard (2000). Review of vibration analysis methods for gearbox diagnostics and prognostics. In *Proceedings of the 54th meeting of the society for machinery failure prevention technology, Virginia Beach, VA*, pp. 623–634.

Leith, D. (1987). Drag on nonspherical objects. *Aerosol Science and Technology 6*(2), 153–161.

Lim, M. H. and M. Leong (2013). Detection of early faults in rotating machinery based on wavelet analysis. *Advances in Mechanical Engineering 2013*.

Lin, J. and M. Zuo (2003). Gearbox fault diagnosis using adaptive wavelet filter. *Mechanical systems and signal processing 17*(6), 1259–1269.

Liu, G., X. Li, B. Qin, D. Xing, Y. Guo, and R. Fan (2004). Investigation of the mending effect and mechanism of copper nano-particles on a tribologically stressed surface. *Tribology Letters 17*(4), 961–966.

Lokesha, M., M. C. Majumder, K. Ramachandran, and K. F. A. Raheem (2011). Fault diagnosis in gear using wavelet envelope power spectrum. *International Journal of Engineering, Science and Technology 3*(8), 156–167.

Mobley, R. K. (2002). *An introduction to predictive maintenance.* Butterworth-Heinemann.

Narona, N. H., S. Mukherjee, and V. Kuamr (2013). Wavelet based non linear thresholding techniques for pre processing ecg signals. *International Journal of Biomedical and Advance Research 4*(8), 534–544.

Nooli, P. K. (2011). *A versatile and computationally efficient condition indicator for AH-64 rotorcraft gearboxes.* Ph. D. thesis, UNIVERSITY OF SOUTH CAROLINA.

Patel, H. E., S. K. Das, T. Sundararajan, A. S. Nair, B. George, and T. Pradeep (2003). Thermal conductivities of naked and monolayer protected metal nanoparticle based nanofluids: Manifestation of anomalous enhancement and chemical effects. *Applied Physics Letters 83*(14), 2931–2933.

Peng, D.-X., Y. Kang, C.-H. Chen, and S.-K. C. F.-c. Shu (2009). The tribological behavior of modified diamond nanoparticles in liquid paraffin. *Industrial Lubrication and Tribology 61*(4), 213–219.

Rafiee, J., M. Rafiee, and P. Tse (2010). Application of mother wavelet functions for automatic gear and bearing fault diagnosis. *Expert Systems with Applications 37*(6), 4568–4579.

Randall, R. B. (2011). *Vibration-based condition monitoring: industrial, aerospace and automotive applications.* John Wiley & Sons.

Rapoport, L., V. Leshchinsky, I. Lapsker, Y. Volovik, O. Nepomnyashchy, M. Lvovsky, R. Popovitz-Biro, Y. Feldman, and R. Tenne (2003). Tribological properties of ws< sub> 2</sub> nanoparticles under mixed lubrication. *Wear 255*(7), 785–793.

Ren, X., W. Shao, W. Yang, and F. Su (2006). Extraction of gearbox fault features from vibration signal using wavelet transform. In *Journal of Physics: Conference Series*, Volume 48, pp. 490. IOP Publishing.

Rizvi, I. H., A. Jain, S. K. Ghosh, and P. Mukherjee (2013). Mathematical modelling of thermal conductivity for nanofluid considering interfacial nano-layer. *Heat and Mass Transfer 49*(4), 595–600.

Rohini Priya, K., K. Suganthi, and K. Rajan (2012). Transport properties of ultra-low concentration cuo–water nanofluids containing non-spherical nanoparticles. *International Journal of Heat and Mass Transfer 55*(17), 4734–4743.

Scheffer, C. and P. Girdhar (2004). *Practical machinery vibration analysis and predictive maintenance.* Elsevier.

Schwarz, U., S. Safran, and S. Komura (2002). Mechanical, adhesive and thermodynamic properties of hollow nanoparticles. *arXiv preprint cond-mat/0201109*.

Song, B. Y., Q. X. Yang, F. Zhang, and D. Z. Su (2010). Rheological properties of aircraft grease containing nano-additives. *Key Engineering Materials 419*, 53–56.

Staszewski, W., K. Worden, and G. Tomlinson (1997). Time–frequency analysis in gearbox fault detection using the wigner–ville distribution and pattern recognition. *Mechanical systems and signal processing 11*(5), 673–692.

Su, W., F. Wang, H. Zhu, Z. Zhang, and Z. Guo (2010). Rolling element bearing faults diagnosis based on optimal morlet wavelet filter and autocorrelation enhancement. *Mechanical Systems and Signal Processing 24*(5), 1458–1472.

Taylor, R., S. Coulombe, T. Otanicar, P. Phelan, A. Gunawan, W. Lv, G. Rosengarten, R. Prasher, and H. Tyagi (2013). Small particles, big impacts: A review of the diverse applications of nanofluids. *Journal of Applied Physics 113*(1), 011301.

Toms, L. A. and A. M. Toms (2008). *Machinery Oil Analysis: Methods, Automation and Benefits: a Guide for Maintenance Managers, Supervisors & Technicians.* Society of Tribologists and Lubrication Engineers.

Torrence, C. and G. P. Compo (1998). A practical guide to wavelet analysis. *Bulletin of the American Meteorological society 79*(1), 61–78.

Večeř, P., M. Kreidl, and R. Šmíd (2005). Condition indicators for gearbox condition monitoring systems. *Acta Polytechnica 45*(6).

Wang, C., R. X. Gao, R. Yan, and A. Malhi (2009). Rolling bearing defect severity assessment under varying operating conditions. *International Journal of Manufacturing Research 4*(1), 37–56.

Wang, C., W.-X. Ren, Z.-C. Wang, and H.-P. Zhu (2013). Instantaneous frequency identification of time-varying structures by continuous wavelet transform. *Engineering Structures 52*(0), 17 – 25.

Wang, X.-Q. and A. S. Mujumdar (2007). Heat transfer characteristics of nanofluids: a review. *International journal of thermal sciences 46*(1), 1–19.

Wierenga, A. M. and A. P. Philipse (1998). Low-shear viscosity of isotropic dispersions of (brownian) rods and fibres; a review of theory and experiments. *Colloids and Surfaces A: Physicochemical and Engineering Aspects 137*(1), 355–372.

Xie, H., H. Gu, M. Fujii, and X. Zhang (2006). Short hot wire technique for measuring thermal conductivity and thermal diffusivity of various materials. *Measurement Science and Technology 17*(1), 208.

Yu, L., D. Liu, and F. Botz (2012). Laminar convective heat transfer of alumina-polyalphaolefin nanofluids containing spherical and non-spherical nanoparticles. *Experimental Thermal and Fluid Science 37*, 72–83.

Yu, W. and S. Choi (2003). The role of interfacial layers in the enhanced thermal conductivity of nanofluids: a renovated maxwell model. *Journal of Nanoparticle Research 5*(1-2), 167–171.

Zakrajsek, J. J. (1989). An investigation of gear mesh failure prediction techniques. Technical report, DTIC Document.

Zhao, Y., L. E. Atlas, R. J. Marks, et al. (1990). The use of cone-shaped kernels for generalized time-frequency representations of nonstationary signals. *Acoustics, Speech and Signal Processing, IEEE Transactions on 38*(7), 1084–1091.

Zhou, S.-Q., R. Ni, and D. Funfschilling (2010). Effects of shear rate and temperature on viscosity of alumina polyalphaolefins nanofluids. *Journal of Applied Physics 107*(5), 054317.

Zhu, J., D. He, and E. Bechhoefer (2013). Survey of lubrication oil condition monitoring, diagnostics, and prognostics techniques and systems. *Journal of Chemical Science and Technology*.

Appendix A

Permission to Reprint Journal Paper

This is an email agreement between the author and Liz Harris, journal manager at Inderscience Publishers that gives permission to Kareem M. Gouda to use and reprint the article described in the footnote of chapter 6 in his dissertation.

GOUDA, KAREEM

From:	Liz Harris <liz@ielan.com>
Sent:	Tuesday, March 31, 2015 10:22 AM
To:	GOUDA, KAREEM
Subject:	FW: IJMR 10010X GOUDA proof of paper for confirmation

Dear Author

Inderscience will allow you to use this paper in your Ph.D dissertation as long as you acknowledge the original source of publication.

Kind regards

Liz Harris
Journal Manager
Inderscience

Sign up to our Newsletter for highlights from our journals and related industry events:
http://www.inderscience.com/newsletter

---

rom: GOUDA, KAREEM [mailto:gouda@email.sc.edu]
Sent: Tuesday, March 31, 2015 12:07 AM
To: Indersicenceproofs
Subject: RE: IJMR 10010X GOUDA proof of paper for confirmation

Dear Sir/Madam

I have a published paper at the international journal of manufacturing research (IJMR). I would like to have the acceptance from Inderscience to have this material released for my PhD dissertation work. How can I get the copy right released?

Best,
Kareem Gouda

Paper reference as follows:

Gouda, K.M.,Tarbutton, J.A., Hassan, M.A., Coats, D. and Bayoumi, A-M.E. (2015) 'A wavelet-based index for fault detection and its application in condition monitoring of helicopter drive-train components', *Int. J. Manufacturing Research*, Vol. 10, No. 1, pp.87–106.

1